Escola de Camins
Escola Tècnica Superior d'Enginyeria de Camins, Canals i Ports
UPC BARCELONATECH

INFLUENCE OF SEAGRASS MEADOWS ON HYDRODYNAMICS: A MODELLING APPROACH

TREBALL FINAL DE MÀSTER

Treball realitzat per:
Nicole Rusek

Dirigit per:
Vicente Gracia Garcia
Juan Pablo Sierra Pedrico

Màster en:
Coastal and Marine Engineering and Management (CoMEM)

Barcelona, 30 June 2020

Departament d'Enginyeria Civil i Ambiental

ERASMUS +: ERASMUS MUNDUS MOBILITY PROGRAMME

Master of Science in

COASTAL AND MARINE ENGINEERING AND MANAGEMENT

CoMEM

INFLUENCE OF SEAGRASS MEADOWS ON HYDRODYNAMICS: A MODELING APPROACH

Universitat Politècnica de Catalunya
30 June 2020

Nicole Rusek

The Erasmus+: Erasmus Mundus MSc in Coastal and Marine Engineering and Management is an integrated programme including mobility organized by five European partner institutions, coordinated by Norwegian University of Science and Technology (NTNU).

The joint study programme of 120 ECTS credits (two years full-time) has been obtained at two or three of the five CoMEM partner institutions:

- Norges Teknisk- Naturvitenskapelige Universitet (NTNU) Trondheim, Norway
- Technische Universiteit (TU) Delft, The Netherlands
- Universitat Politècnica de Catalunya (UPC). BarcelonaTech. Barcelona, Spain
- University of Southampton, Southampton, Great Britain
- City University London, London, Great Britain

During the first three semesters of the programme, students study at two or three different universities depending on their track of study. In the fourth and final semester an MSc project and thesis has to be completed. The two-year CoMEM programme leads to a multiple set of officially recognized MSc diploma certificates. These will be issued by the universities that have been attended by the student. The transcripts issued with the MSc Diploma Certificate of each university include grades/marks and credits for each subject.

Information regarding the CoMEM programme can be obtained from the programme coordinator:

Øivind A. Arntsen, Dr.ing.
Associate professor in Marine Civil Engineering
Department of Civil and Environmental Engineering
NTNU Norway
Mob.: +4792650455 Fax: + 4773597021
Email: oivind.arntsen@ntnu.no

CoMEM URL: https://www.ntnu.edu/studies/mscomem

CoMEM Thesis

This thesis was completed by:
Nicole Rusek

Under supervision of:
Dr. Vicente Gracia Garcia, Universitat Politècnica de Catalunya (UPC)
Dr. Juan Pablo Sierra Pedrico, Universitat Politècnica de Catalunya (UPC)

As a requirement to attend the degree of
Erasmus+: Erasmus Mundus Master in Coastal and Marine Engineering and Management (CoMEM)

taught at the following educational institutions:

Norges Teknisk- Naturvitenskapelige Universitet (NTNU)
Trondheim, Norway

Universitat Politècnica de Catalunya, (UPC). BarcelonaTech.
Barcelona, Spain

University of Southampton,
Southampton, Great Britain

At which the student has studied from August 2018 to July 2020.

Abstract

The economic pressures that have been placed on the Spanish coastline have resulted in coastal management strategies and policies that lack of consideration of the long-term costs and preservation of the natural environment. This has brought about the need to explore alternative solutions to the artificially constructed protection measures of the past. Restoration and better management of seagrass meadows along the Mediterranean coast has been proposed as a possible solution to the current problem. Sufficient evidence needs to be provided regarding their wave attenuation and erosion prevention capabilities before seagrass can be promoted as an effective coastal management strategy. This thesis presents a modeling study that aims to evaluate the wave attenuation aspect using a numerical modeling approach. The SWAN (Simulating WAves Nearshore) wave model is first calibrated using a set of flume experiments and is then applied to a case study on the Catalan coast. The results indicate that the seagrass *Posidonia oceanica* does have an influence on hydrodynamics. Although no change in wave period was observed, it was concluded that the presence of the seagrass reduces the wave heights that end up reaching the shoreline. It is anticipated that this study is a starting point for a more comprehensive model at the Baix Camp location and other locations before seagrass meadows are promoted as an effective approach to coastal management.

Acknowledgements

First of all, I would like to thank my professors and mentors: Vicenç, Joan Pau, Iván and Carlos, for their invaluable guidance. I really appreciate all of the advice you have given me as well as the incredible amount of patience you've shown me throughout this journey especially during these unprecedented times.

I also would like to thank everyone else that I have been fortunate enough to meet through the CoMEM program. Øivind, Sonja, César, Genoveva, Ivan and Sergio for their warm welcomes to Trondheim, Barcelona and Southampton and answering any questions I had along the way. You have all shared your knowledge but also your cultures with me and I have done my best to soak it all up. My professors at each of the Universities (UPC, SOTON, NTNU) who challenged me at every turn and provided me with the materials and tools necessary to succeed. My fellow CoMEM colleagues who have taught me more than they know and have helped me laugh through even the most stressful moments. I couldn't have asked for a better group to share this experience with.

Finally, I would like to thank my family for their presence and immeasurable support over the last two years. I feel tremendously privileged for this opportunity and I couldn't have crossed the finish line without the kind words I received from each and every one of you. In particular, I would like to thank my husband Daniel for being my endless source of serenity or motivation, depending on which I needed more of on any given day. Thanks to all of you, I am who I am and where I am today.

Table of Contents

1 Introduction 1
1.1 Context 1
1.2 Motivation and objectives 3
1.3 Structure of work 3
2 Seagrass meadows 5
2.1 Submergence ratio 5
2.2 Plant density and flexibility 8
2.3 Meadow length 12
3 Physical model 14
3.1 Experimental setup 14
3.1.1 Facility description 14
3.1.2 Beach sediment and geometry 14
3.1.3 Sensors: type and location 15
3.2 Artificial seagrass meadow 19
3.3 Tests 22
4 SWAN model 23
4.1 Description of SWAN 23
4.2 Vegetation module 24
5 Model calibration 27
5.1 Model strategy 27
5.1.1 Input grids 27
5.1.2 Boundary conditions 28
5.1.3 Physical processes 28
5.1.4 Vegetation module 28
5.2 Methodology 30
5.3 Results 34
6 Application to the Baix Camp seagrass meadow 40
6.1 Seagrass cartography and bathymetry 40
6.2 Wave climate 42
6.3 Modeling strategy 43

6.4 Results 45
6.4.1 Present wave climate and seagrass distribution 45
6.4.2 Without seagrass 46
6.4.3 With seagrass 47
6.4.4 Comparison 48
7 Discussion 53
8 Conclusions 57
References 58
Appendices 61

1 Introduction

1.1 Context

Coastlines have been traditionally managed with engineered hard structures or artificial beach nourishment. While these techniques have been an effective approach in the past, they are not the most sustainable options for coastal protection looking ahead into the future. The global coastal engineering community has been turning its attention to nature-based solutions (NBS) in order to improve coastal resilience. The idea is that NBS are less destructive to the natural environment, oftentimes even work to enhance it, and tend to have lower construction and maintenance costs than hard structures. Using natural elements in engineering is not a straightforward task as there are many knowledge gaps and uncertainties regarding their behavior. Scientists and engineers have been studying various NBS to try to minimize these unknowns in order to promote more widespread implementation. Spain has invested in a project of this type named COBALTO which was designed to study a specific type of seagrass, *Posidonia oceanica*, that is endemic to the Mediterranean Sea and lives at depths from 1-40 m depending on water clarity (Telesca et al., 2015). Ultimately, COBALTO will evaluate the influence this type of seagrass has on both hydrodynamics and morphodynamics in the coastal region after all of the collected experimental data has been analyzed. Projects of this kind are necessary to gain the detailed insight required to guarantee that the implementation approach is successful in the long term.

Posidonia oceanica beds are listed as priority habitats under the European Union's Habitat Directive (92/43/CEE) and have emerged as one of the key targets or the protection and management of the Mediterranean marine environment (Telesca et al., 2015). Within the framework of the Barcelona Convention, seagrass meadows also have a dedicated Action Plan under the "Protocol concerning Specially Protected Areas and Biological Diversity in the Mediterranean" (Telesca et al., 2015). These protection measures are warranted because the presence of this species has been declining at alarming rates due to climate change (warming and acidification) and human activities (anchoring, fish farming and coastal constructions). Unfortunately, it is a slow-growing species with a low recovery rate (Telesca et al., 2015) meaning

it more than likely requires some level of human intervention either through protection or restoration to ensure its future survival. Although *Posidonia oceanica* meadows are considered the most important and well-studied seagrass species of the Mediterranean Sea, there are still missing gaps in mapping the extent of their spatial distribution (Telesca et al., 2015), making it even more difficult to monitor them.

Aside from being the largest submerged aquatic vegetation ecosystem protected in Europe, seagrasses provide valuable ecosystem services such as maintaining biodiversity, oxygen production, water filtration and coastal protection (CRAM, 2020; Ondiviela et al., 2014). From a biodiversity standpoint, they aid in the growth of algae, fish and invertebrates and serve as important areas of breeding and refuge for various animal species (Figure 1.1) (Cavallaro et al., 2018; CRAM, 2020).

Figure 1.1 Photos of Posidonia oceanica meadows (CRAM, 2020)

From a coastal protection standpoint, they increase wave attenuation and modify sediment transport, but the details as to how and to what extent have not been clear because of their dynamic nature. The plant is composed of a root, called the rhizome, and its leaves. The root allows the plant to anchor itself into a sandy bottom and with the help of its the leaves facilitates in trapping sediment (Cavallaro et al., 2011). The purpose of many coastal protection studies involving *Posidonia oceanica*, such as this one, is to determine the driving factors behind this phenomenon and understand how to create an environment that enhances it. That way, meadow conditions could be improved accordingly to create the level of protection that is needed at a particular study site.

1.2 Motivation and objectives

Erosion, flooding and the overtopping of defense structures along the Mediterranean coast in Spain are ongoing issues that are only growing worse with time especially in the changing climate. There is less sediment being contributed by rivers and streams yet the demand to maintain the coastline remains high for economic and environmental reasons. Hardening the shoreline and beach nourishment are effective at meeting this demand but usually just locally and temporarily. This has motivated the coastal communities in Spain to explore alternative options for protecting the coast that could be more cost effective, require less maintenance and preserve the nature of the existing environment. The restoration of *Posidonia oceanica* meadows along the Mediterranean coast could be a possible nature-based solution that would take advantage of a resource that is already endemic to the region while providing an adequate amount of coastal protection.

The main objective of this work is to evaluate the influence of seagrass meadows on hydrodynamics from a modeling perspective. The idea is to create a reliable model that can capture how the hydrodynamic conditions are altered depending on whether or not a seagrass meadow is present. By using the results of this model, *Posidonia oceanica* meadows could be promoted as a viable coastal management strategy.

1.3 Structure of work

The introduction has already covered some background context of the problem and presented the motivation and objectives of this paper. The remainder of this work covers previous lab experiments using artificial seagrass, the COBALTO experiments that were completed at UPC in more detail, SWAN as the numerical model chosen to complete the objectives and the methodology used for modeling the flume experiments as well as a case study in Catalonia. Finally, there is a discussion of the results that includes identified limitations of this study followed by some concluding remarks.

Chapter 2 reviews lab experiments that studied the effects of seagrass on wave attenuation that have been completed in the relatively recent past. The goal of this section is to identify the seagrass parameters that were found to have significant impact on the results. Chapter 3 describes the

experiments run at UPC as part of the COBALTO project. The data from these tests are what is used for the numerical modeling portion of this analysis. Chapter 4 briefly explains the program capabilities of SWAN and how it models dissipation, specifically the dissipation associated with vegetation. Chapter 5 presents the model calibration methodology and results. Once the best fit between the model and measured data was attained, the calibrated parameters were applied to a location along the Catalan coast, described in Chapter 6. Chapter 7 is a discussion of the findings and limitations of this study. Chapter 8 summarizes the key takeaways and revisits how the main research objective of this work has been reached.

2 Seagrass meadows

The influence of seagrass meadows on hydrodynamics is in the coastal environment is not a straightforward topic. Many scientists have attempted to study their effects by means of a physical model, each with a different methodology and set of vegetation parameters. From the field study by Bradley and Houser (2009), wave energy dissipation by seagrass meadows was found to generally depend on the characteristics of the vegetated area (location, size, blade arrangement and density) and the morphology of the plant (geometry, relative height, buoyancy and rigidity). This chapter describes which of these seagrass parameters were further examined and found to be the more or less influential on wave attenuation based on past lab experiments. The factors that have been identified to have the most influence are submergence ratio, density of the meadow, flexibility of the plants and meadow length. At times, these parameters work together and it is difficult to separate out the influence of each individual variable or analyze it on its own due to the dynamic nature of seagrasses. It may be that a single parameter holds the most weight when analyzing wave attenuation under a specific wave condition, but it's important to consider that the opposite could also be true. The effect of that same parameter could become insignificant by the others under a different condition (Dijkstra and Uittenbogaard, 2010). Understanding the meaning of each parameter and its impact on wave attenuation played a significant role in setting up the physical experiment presented in the next chapter.

2.1 Submergence ratio

One of the most influential parameters on wave attenuation is the submergence ratio which relates vegetation height to water depth ($\alpha = h_s/h$). The general consensus is that as the submergence ratio increases there is a higher attenuation of incident wave height along the seagrass meadow (Cavallaro et al., 2011; John et al., 2018; Koftis et al., 2013; Luhar et al., 2017; Manca et al., 2012; Sánchez-González et al., 2011).

The papers by Koftis et al. (2013) and Manca et al. (2012) refer to an experimental study conducted in a large wave flume to evaluate the effects of *Posidonia oceanica* meadows on wave height

attenuation and wave induced velocities. The full range of this study has been explained in greater detail in Stratigaki et al. (2011). Tests were performed with regular and random waves in intermediate and shallow waters. Stem density and plant height were varied for every wave condition tested to create many different plant configurations. In this case, the submergence ratio was between 0.32 and 0.5 by setting the depth in the flume from 1.10 m to 1.70 m and keeping the plant height constant. One of the conclusions from these experiments was that the submergence ratio affects the fraction of the water column that is being occupied by the seagrass and therefore when it increases, wave attenuation become greater. Since energy dissipation over the meadow is due to the drag force induced by the seagrass, it was expected that a wave attenuation would be higher when a larger fraction of water was within the meadow (Koftis et al., 2013). Although it was found that dissipation rates were clearly affected by changes to the submergence ratio, they seemed to be more significantly impacted by changing wave period and orbital amplitude, at least for the submergence ratios tested in this particular case (Manca et al., 2012). In addition to producing greater differences in wave height reduction, it was observed that higher submergence ratios produced more flow reduction within the lower part of the canopy, closer to the sandy bottom of the flume (Manca et al., 2012).

Sánchez-González et al. (2011) set out with a similar objective in their experimental study after coming to the conclusion that there weren't many past studies carried out that dealt directly with *Posidonia oceanica*. Their set of test data explored wave height attenuation due to meadows at intermediate depths under an average wave climate of the Mediterranean Sea with a lot of effort put into maintaining similitude between the model and prototype (Sánchez-González et al., 2011). The submergence ratio was varied by changing the water depth in the flume from 0.30 m to 0.8 m and keeping plant height constant. One of their key results is that wave height attenuation is governed mainly by this ratio as attenuation is more pronounced for shallow waters compared to higher water depths. The reasoning provided was that at shallower depths, waves induce larger particle velocities acting along the blade length and so the energy flux being absorbed is higher (Sánchez-González et al., 2011).

Most recently, Luhar et al. (2017) carried out wave flume experiments using artificial plants that would be most similar to *Zostera marina* (eelgrass) and *Posidonia oceanica*. These experiments varied water depth and plant density for different sets of wave conditions, similarly to those previously presented, but they begin to examine the role of blade motion and posture on wave attenuation. The submergence ratio (l/h) ranged from 0.3 to 0.8 by varying the water depth from 0.16 m to 0.39 m and keeping all other parameters constant. Figure 2.1, modified from Luhar et al. (2017), shows the relationship found between modifying the submergence ratio and the decay per wavelength, expressed by the parameter $K_D a_0 \lambda$. Wave decay increased as the meadow occupied more of the water column, agreeing with the previously mentioned authors. For case H1, $l/h = 0.8$, resulting in a wave decay per wavelength value of 0.25. When l/h was decreased to 0.3 in case H4, the value decreased to 0.09. The predicted curve shown by the solid line in Figure 2.1 suggests that wave decay is likely to be negligible once the meadow is occupying 10% or less of the water column (Luhar et al., 2017). The variable l_e that is used in the prediction refers to the effective length of the blade as opposed to the total length of the blade. It's one of the parameters the authors use to describe the blade motion or behavior under hydrodynamic forcing and it is defined as the rigid blade length that leads to equivalent wave-energy dissipation (Luhar et al., 2017).

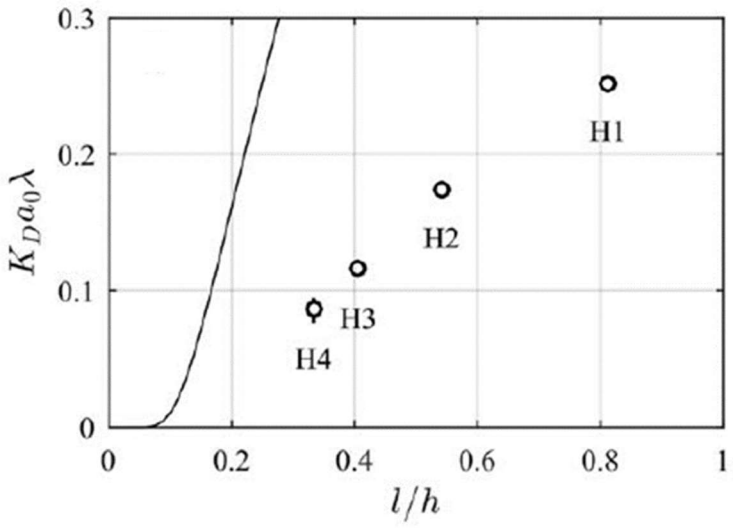

Figure 2.1 Measured wave decay per wavelength ($K_D a_0 \lambda$). Experiments H1-H4: varying water depth, plotted as l/h, the solid line shows predicted decay based on assuming $C_D = 1.95$ (corresponding to a flat plate normal to flow at high Reynolds number) and $l_e = l$. (Luhar et al., 2017)

2.2 Plant density and flexibility

As mentioned in the previous section, some authors investigated varying plant density in addition to the submergence ratio. Plant density of the vegetated region under consideration is defined as the number of plants per m^2. The previous studies that varied both submergence ratio and plant density have come to the conclusion that the latter has been found to have a higher effect on wave attenuation (Koftis et al., 2013; Luhar et al., 2017; Manca et al., 2012). Flexibility is not typically a parameter that is varied throughout an experiment but is instead considered at the onset, when the artificial plant material is selected and shaped. Trying to define plant motion and account for flexibility has been the focus of more recent studies in order to gain a better understanding of wave-meadow interactions (Cavallaro et al., 2018; Luhar et al., 2017) The link between plant flexibility and density is discussed later in this section.

The experiments that were referenced by Koftis et al. (2013) and Manca et al. (2012) used two different densities: 180 stems/m^2 and 360 stems/m^2. It was quite clear that the test with the densest canopy and the highest submergence ratio produced the greatest reduction in wave height (Koftis et al., 2013). Figure 2.2 illustrates that the tests with the higher density (solid symbols) resulted in having a higher height decay coefficient (K_i) signifying a greater level of wave attenuation. The average K_i being 0.016 m^{-1} for tests with 360 stems/m^2 and 0.007 m^{-1} for tests with 180 stems/m^2 (Manca et al., 2012). This difference in K_i tends to grow as the submergence ratio increases. Manca et al. (2012) also found that hydraulic roughness was larger for the denser canopy under both regular and irregular wave conditions while submergence ratio had little to no effect on roughness length.

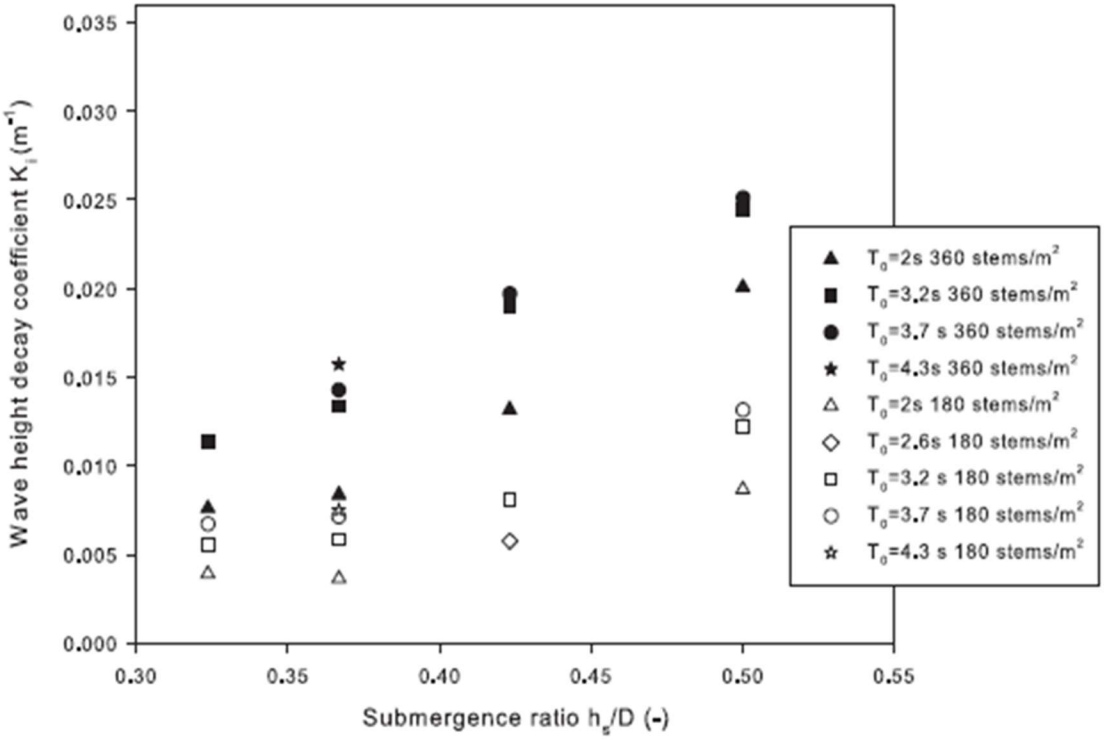

Figure 2.2 Effect of submergence ratio (h_s/D) and stem density on the wave height decay coefficient (K_i) for density = 360 stems/m^2 (solid symbols) and density = 180 stems/m^2 (open symbols) (Manca et al., 2012)

In the experiments carried out by Luhar et al. (2017), stem densities ranged from 300 to 1800 stems/m^2, which corresponded to blade densities from 1,800 to 10,800 blades/m^2. These authors agreed with the trend that wave decay increased with vegetation density but the results of their tests also found that wave decay increased linearly for lower vegetation densities but reached a plateau for the two highest densities tested. This was due to the fact that the number of drag-inducing elements increased and higher densities dampened wave-induced flow within the canopy, resulting in a lower amount of energy dissipation and wave decay (Luhar et al., 2017).

Further investigation of the blade motion was required to understand the processes occurring at these higher densities. Figure 2.3b below illustrates how the blade movement changes under higher energy conditions. Each blade individually, but also the plant as a whole, experiences an increase in orbital diameter and undergoes more movement in the horizontal and vertical directions under higher energy conditions.

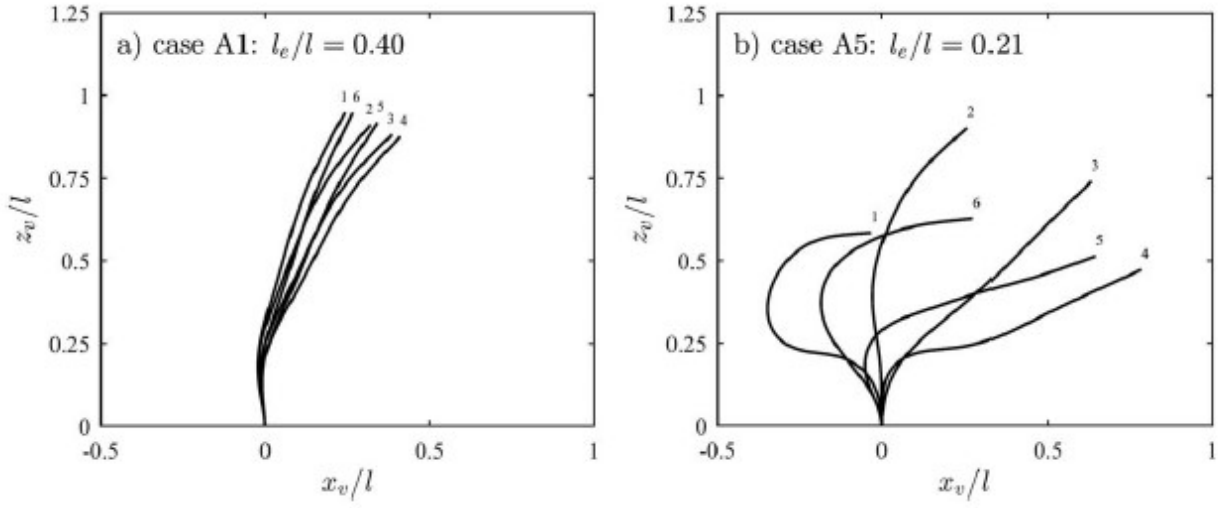

Figure 2.3 Posture at six different phases during a cycle for wave conditions corresponding to the lowest amplitude case A1 (a) and the highest amplitude case A5 (b) that were tested (Luhar et al., 2017)

Effective length (l_e) in Figure 2.3 was scaled using its varying relationship with the dimensionless parameters that govern and are used to describe blade motion: the Cauchy number (Ca) and the buoyancy parameter (B). For example, when the hydrodynamic forcing becomes much larger than the buoyancy of the blades and the restoring force due to the blade stiffness (as in Figure 2.3b), $l_e/l \sim Ca^{-1/3}$ (Luhar and Nepf, 2016), where Ca is calculated by

$$Ca = \frac{\rho b U_w^2 l^3}{EI} \qquad 2.1$$

and B is calculated by

$$B = \frac{(\rho - \rho_v) g b d l^3}{EI} \qquad 2.2$$

where g is gravity, b is blade width, d is blade thickness, l is blade length, E is the elastic modulus, ρ is the density of water, ρ_v is the blade density, I ($= bd^3/12$) is the second moment of area for the (rectangular) blade cross section and U_w is horizontal oscillatory velocity. EI is assumed to be constant along the entire length of the blade.

In the hydrodynamics study by Cavallaro et al. (2018), a dense Posidonia meadow at intermediate water depth was analyzed by means of physical model. Their main focus was wave attenuation which was evaluated by means of a drag coefficient. The drag coefficient C_D is used to quantify the resistance of the plant in the fluid environment (Cavallaro et al., 2018). They explain that the seagrass meadow introduces a variable hydraulic roughness as a consequence of the interaction between the plant and fluid. Blades will increasingly bend as the flow velocity increases until they are eventually lying on the bottom (Cavallaro et al., 2018) leading to a higher bed shear stress (Dijkstra and Uittenbogaard, 2010). They apply the relationship of C_D to the flexibility parameter Ca from equation 2.1 to compare how blade movement or posture affects wave height reduction. Figure 2.4 presents C_D as a function of Ca and compares several tests in which blade flexibility was a common factor.

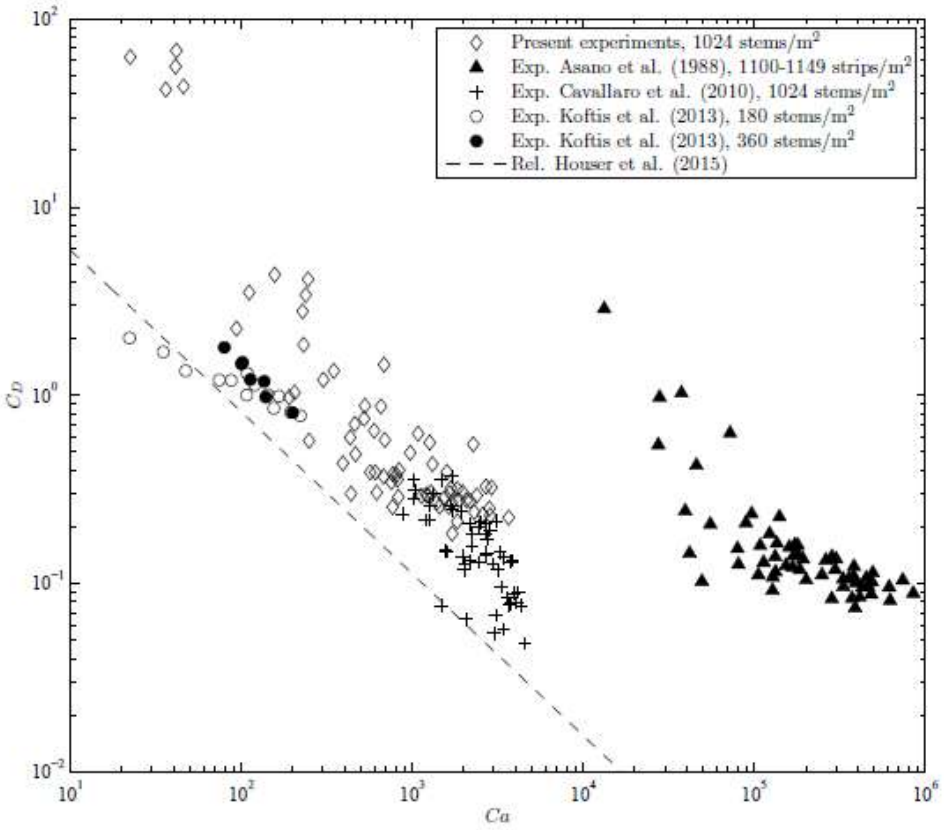

Figure 2.4 Drag coefficient C_D as a function of the Caucy number Ca, which takes into account blade flexibility (Cavallaro et al., 2018)

The main points are that when $Ca > 1000$, the leaves are bent so far that they are almost touching the bottom, and when $Ca < 500$, the leaves are more rigid against the flow and the drag force is greater (Cavallaro et al., 2018). Meadow height is smaller than the length of the design plant when $Ca > 1000$ which results in a smaller section of the water column experiencing the interaction (Cavallaro et al., 2018), similar to the effect of decreasing the submergence ratio. Due to the reduction of inside-meadow velocities in denser patches and greater bending of the leaves themselves, the interaction between the fluid and vegetation is lessened and the interference between neighboring blades is increased (Cavallaro et al., 2018; Luhar et al., 2017). It is also important to note that the results of the experiments carried out in Cavallaro et al. (2018) show that the present formulation dramatically underestimates C_D for small values of Ca, as is made clear by Figure 2.4. The overall trend is that C_D decreases as Ca increases which means that wave height reduction decreases as Ca increases as well.

As mentioned before, it is possible that in certain scenarios the impact of one parameter may be irrelevant because it is overshadowed by another or others. For example, in a numerical modeling study on flexible vegetation, Dijkstra and Uittenbogaard (2010) came to the conclusion that typically the structural rigidity of the sea grass *Zostera marina* was a more influential parameter than the meadow density. On the other hand, they point out that in a very dense field individual plant parameters like flexibility may not matter anymore (Dijkstra and Uittenbogaard, 2010). The plant position is unlikely to change simply because it has no space to.

2.3 Meadow length

The last main contributing factor with regards to the amount of wave height reduction achieved is the length of the seagrass meadow. As expected, longer vegetation fields result in a greater amount of wave reduction (Mendez and Losada, 2004). Wave height continually decreases from the location where it encounters the leading edge of the meadow until it passes through to the end of the patch. Manca et al. (2012) and John et al. (2018) observed that most of the wave energy had dissipated in the first few meters of the meadow although is does continue to dissipate over the

full length. This conclusion corresponds to the expression for the exponential wave height decay over submerged vegetation (Kobayashi et al., 1993) which is

$$\frac{H(x)}{H_0} = e^{-K_i \Delta x} \qquad 2.3$$

where $H(x)$ is the wave height measured along the vegetation field, H_0 is the wave height just in front of the leading edge of the field, Δx is the separating distance between the two measurements and K_i is the wave decay coefficient. The rate of decay decreases as the wave moves further past the leading edge of the meadow. One reason that this occurs is that as the wave propagates through the submerged vegetation, the more rigid vegetation intercepts the wave orbital velocities and the amount of turbulence is increased. The increase in turbulence causes greater energy dissipation which results in reduced wave heights (John et al., 2018). Another reason is that the higher bed shear stress that a more flexible meadow introduces is felt over a greater distance and period of time with longer meadow lengths. In this case where the canopy has collapsed, either from high flexibility or higher energy wave conditions, the leading edge of the meadow is not as effective and the canopy acts as a whole to equally distribute the wave force over the entire area (Fonseca et al., 2007).

3 Physical model

This chapter describes the physical flume tests that were carried out as a part of the COBALTO project (CTM2017-88036-R). It explains the experimental setup, the method for designing the artificial seagrass meadow and the different cases that were tested. A complete log of experiments completed can be found in Appendix A.

3.1 Experimental setup

A series of experiments was carried out in the Canal d'Investigació i Experimentació Marítima (CIEM) wave flume at the Universitat Politècnica de Catalunya, Barcelona. The facility description, the beach properties and the sensor information are presented in further detail in the following sections. Information regarding the seagrass meadow and the different test cases can be found in sections 3.2 and 3.3, respectively.

3.1.1 Facility description

The canal at the CIEM facility has glass walls, a concrete bottom and is 100 m long, 3 m wide and 4.5 m deep. Fresh water is used in the flume and the water is kept clear by its filtering and pumping system. It is equipped with a wedge paddle type that is suitable for intermediate depth waves. The paddle can generate regular or random waves based on either a specified spectrum or a measured time series. The system is hydraulically operated and controlled by a PC. It can generate wave heights up to 0.9 m with a still water level (SWL) of 2.65 m (Hydralab.eu, 2020). The geometric scale used was 1:2 for relating all model dimensions to the prototype. Froude similitude law was used for relating nearshore hydrodynamics and relevant sediment parameters of the model to full scale conditions.

3.1.2 Beach sediment and geometry

A sandy beach was built at the opposite end to the wave paddle to study the influence of seagrass on morphodynamics of a specific profile. The sediment consisted of d_{50} = 265 µm and the measured settling velocity (w_s) of the sediment was 0.034 m/s. An 11 m segment was kept at a

constant 0.1 m sediment depth as the base for the artificial meadow that would be installed 30 m from the wave paddle as shown in Figure 3.1. Beyond 41 m away from the paddle, the profile was constructed at a 1:15 gradient to the other end of the flume.

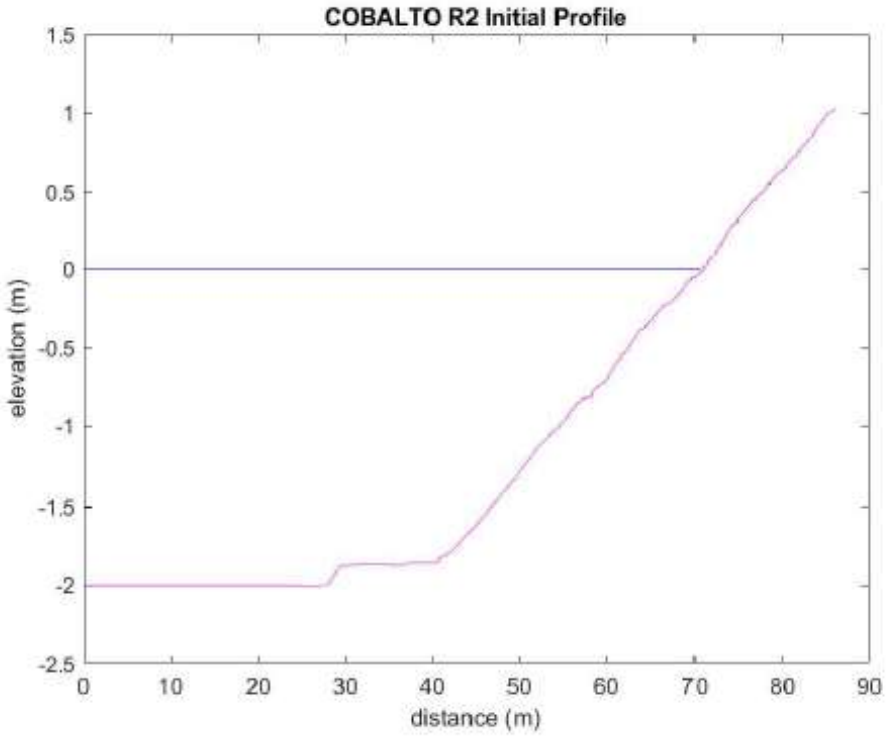

Figure 3.1 Initial bed elevation for test case R2 (typical for all cases)

3.1.3 Sensors: type and location

The main measurements performed include: total net sediment transport, wave height, velocities and suspended sediment concentrations. Net sediment transport was measured by a mechanical profiler while wave height, velocity and suspended sediment concentration measurements were collected by a variety of different sensors. Table 3.1 shows which pre-calibrated instruments were used to obtain each type of measurement.

Table 3.1 Parameters measured and instruments used for each

Measurement	Instrument
Total net sediment transport	Mechanical profiler
Wave height	Resistive Wave Gauges (RWG)
	Acoustic Wave Gauges (AWG)
	Pore Pressure Transducers (PPT)
Velocities and suspended sediment concentrations	Acoustic Doppler Velocimeters (ADV)
	Optical Backscatter Sensors (OBS)

The **mechanical profiler** consists of a mobile platform to which is attached an arm with a wheel at its end. As the platform moves with constant velocity through the flume, the arm adjusts as it adapts to the depth forms. A computer monitors and records its movement and depth changes to acquire the necessary information about the current profile being measured along the centerline of the flume.

Resistive Wave Gauges (RWG) measure the current flowing between a pair of parallel stainless-steel wires in an immersed probe. The measured current is proportional to the depth of immersion and is detected by capturing the voltage drop across two resistors. It is then converted into an output voltage that is proportional to the instantaneous depth of immersion to be recorded as the wave height.

Acoustic Wave Gauges (AWG) emit ultrasound pulses that reflect off of the measurement object and the signal is received back as an echo. Both long range and medium range sensors were used during these experiments. The long and medium range AWGs have application ranges from 0.18 m up to 3.5 m and 0.20 m up to 1.7 m, respectively.

Pore Pressure Transducers (PPT) output a signal intensity that can be related to a water height.

Acoustic Doppler Velocimeters (ADV) measure water speed using the Doppler effect. They transmit short pairs of sound pulses and then measure the change in frequency of the echoes. Sound reflects from particles suspended in water (zooplankton or sediment) rather than from the water itself.

Optical Backscatter Sensors (OBS) measure suspended solids and turbidity by detecting the intensity of infra-red light scattered by particles in the water.

Most of the measuring instruments were clamped onto the aluminum bars along the walls of the flume at fixed positions but some were installed on the mobile frame. The location of the mobile frame for each test can be found recorded as “xtape” in the experiment log in Appendix A.

The coordinate system was defined as X being in the direction along the flume, Y being the cross-shore distance of the flume, and Z being directed in the vertical direction. X is positive when going towards the shoreline with absolute 0 being at the wave paddle. Y is 0 at the wall on which the ADV and wave gauges were attached and is positive moving across the flume. Very few data use the Y-direction as reference. Z was measured as either Z_abs or Z_rel. Z_abs is 0 at the concrete bottom of the flume and is positive upwards through the water to the surface. Z_rel is measured as the relative distance between the sandy bottom and the elevation of the measuring equipment. The depth data was also captured in a post-processed file that contained the cleaned and corrected information collected by the mechanical profiler. This file uses the SWL to represent 0 so that positive values are assigned pointing out of the water and negative values are assigned with increasing water depth, such as in Figure 3.2.

Table 3.2 lists the exact locations at which the sensors were installed within the flume while Figure 3.2 provides a visual representation. There are no recorded values for z_abs for the RWGs and AWGs in the table as these sensors measure the water surface independently of their location. It can be seen in the figure that the RWGs were installed at or around the SWL and the AWGs were installed slightly higher than 0.5 m above the SWL. The RWGs are represented by vertical black lines, the AWGs by empty black squares, the PPTs by solid black squares, the ADVs by solid blue stars, and the OBSs by empty red circles.

Table 3.2 Sensor locations in wave flume all in units of m

RWG		AWG		PPT		ADV		OBS	
x	z_abs	x	z_abs	x	z_abs	x	z_abs	x	z_abs
10.86	-	18.18	-	20.51	0.255	27.6	0.225	31.91	0.235
10.86	-	24.84	-	22.26	0.245	27.6	0.465	31.93	0.485
26	-	29.31	-	24.03	0.366	41.43	0.335	39.05	0.455
27.53	-	37.01	-	30.8	0.245	41.43	0.465	41.32	0.465
31.93	-	48.53	-	33.67	1.22			41.32	0.335
35.03	-	53.65	-	36.9	1.415				
39.05	-	57.17	-	41.04	1.41				
43.11	-	59.83	-	45.11	1.37				
47.13	-	61.43	-	49.83	1.455				
51.08	-	62.75	-	55.54	1.355				
52.6	-	64.24	-	58.61	1.505				
54.11	-	65.74	-	59.55	1.86				
55.54	-	67.22	-	61.6	1.685				
		69.02	-	64.37	1.86				
		70.31	-						
		71.74	-						
		73.27	-						

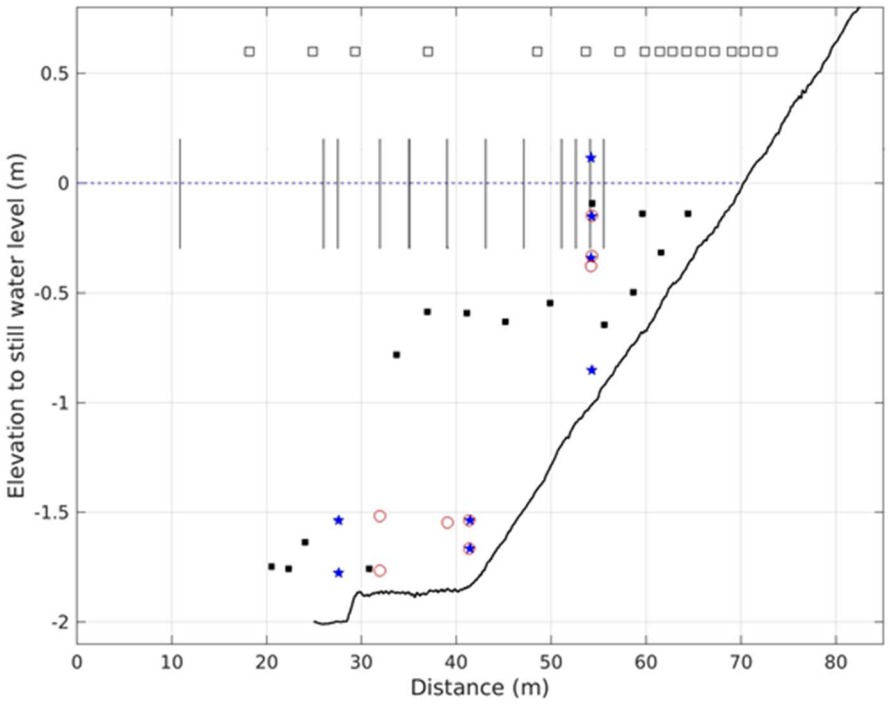

Figure 3.2 Locations of instruments for COBALTO experiments. RWGs are represented by vertical black lines, AWGs by empty black squares, PPTs by the solid black squares, ADVs by solid blue stars, and OBSs by empty red circles. The mobile trolley has 4 ADVS, 1 PPT and 3 OBSs attached to it and is located at x = 54.2 m on this figure.

There was a yellow trolley with a mobile frame that could be positioned along the flume with 1-cm accuracy and could move in the vertical direction with sub-mm accuracy. This frame was equipped with an additional PPT, three OBSs and four ADVs. In order to cover additional points that could be relevant for an extended analysis, the frame was relocated after every run.

3.2 Artificial seagrass meadow

Prior to running the COBALTO experiments, a series of testing was performed to determine the material and thickness that best resembled a real *Posidonia oceanica* plant. The materials and thicknesses tested are detailed in Table 3.3. These were evaluated based on orbital velocity and oscillatory movement under wave conditions. Orbital velocities were obtained using ADVs and movement behavior was obtained by calculating and measuring semi-orbital displacements from data collected by the ADVs and from video footage. More information regarding the ADVs is provided in section 3.1.3. The real plant samples (Figure 3.3) were collected on a beach in Catalonia after a storm that occurred on April 23, 2019. After comparing the results between the real plant and the artificial plants tested, the material selected was PVC with a thickness of 0.5 mm. The PVC plastic with a thickness of 0.3 mm thickness had an oscillatory movement that was closer to that of the real plant but was less rigid than the real plant. Preserving the rigidity with the thicker PVC was considered of higher priority. Modulus of elasticity ($E = 0.9 \times 10^9 N^{-2}$) and density ($\rho_s = 550\text{-}700\ kg\ m^{-3}$) of the material were similar to those given in Manca et al. (2012).

Table 3.3 List of materials and thicknesses tested against real Posidonia oceanica plant

Type of Plastic	Thickness (mm)
Polyvinyl Chloride (PVC)	0.15
	0.3
	0.5
	0.8
Polypropylene (PP)	0.3
	0.5
	0.8

Figure 3.3 Sample of real Posidonia plant; (a) length measurements and observed configuration (b) width measurement

The selected plant configuration consisted of four leaves, two longer leaves and two shorter leaves. Of the samples collected, the maximum length for the longer leaves was measured at 61 cm, while the shorter leaves were observed to be about 2/3 of that length at 40 cm (Figure 3.3). Typical leaf length for this plant has been found to vary between 10 and 150 cm depending on the time of year (CRAM, 2020). This information was used to simulate a mature *Posidonia* meadow at 1:2 scale with the long leaves being 60 cm and the short leaves being 40 cm (Figure 3.4). The reasoning was based on the fact that a longer leaf will have a greater hydrodynamic effect (de los Santos et al., 2013) and therefore the morphodynamic effects would be more quantifiable as a result than with a shorter leaf. If it's found that there is little to no effect with a meadow of this maturity, it can be assumed that shorter leaves would have an even smaller effect. The typical documented width for this type of plant is 1.0 cm (Figure 3.3b) which is in agreement with the findings of other authors (Ondiviela et al., 2014). Due to limitations in manufacturing this was modified to 1.6 cm or 0.8 cm at the model scale.

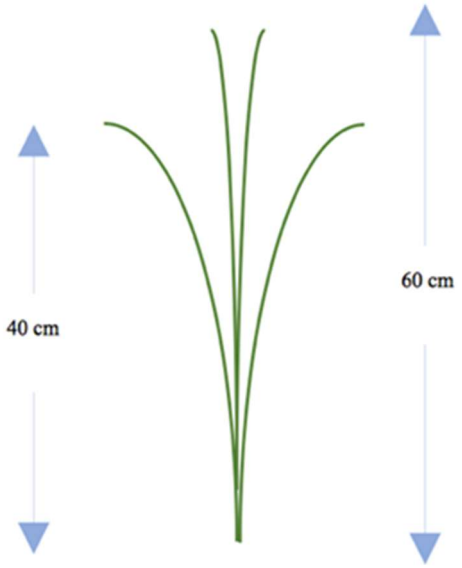

Figure 3.4 Posidonia oceanica plant model (scale 1:2)

A 6.8 cm thick strip of wood was used to simulate the characteristic rhizome of the plant. Each wooden strip was 2.9 m long, in order to use as much of the channel width as possible, and had 130 plants stapled and then taped to its sides. The plant density was chosen based on a low-density *Posidonia* meadow, 37-156 plants/m^2 (Mazzella et al., 1989), as a high-density meadow would be difficult to achieve within the manufacturing time and labor force available. A prototype density of 67 plants/m^2 was modeled at the 1:2 scale as 269 plants/m^2 over a 10 m long by 2.9 m wide area (7,800 plants total). Figure 3.5 shows the entire seagrass meadow on the left and a single wooden strip with the attached artificial plants on the right.

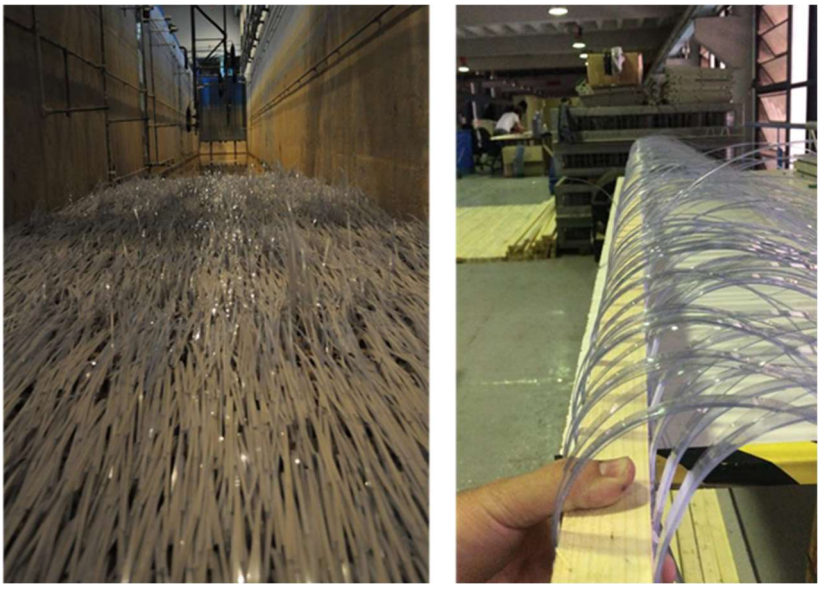

Figure 3.5 Photos of the artificial meadow; (left) full installation, (right) single wooden strip simulating plant rhizome

The wooden strips were spaced out about 4.2 cm from each other and fixed to a metal frame. Each metal frame fit 5 of these strips and the frames were fastened together for linearity and to increase the weight and rigidity of the structure. At each end, a strut was installed to fix the structure in place in order to prevent movement of the meadow in the flume due to wave action.

Lastly, the horizontal location in the flume and depth of the meadow were based on previous physical model experiments and field observations of other authors (Cavallaro et al., 2011; Koftis et al., 2013; Manca et al., 2012; Sánchez-González et al., 2011). These parameters are meant to simulate the natural location and conditions that *Posidonia* typically inhabit. The flat region was preferred as the sediment dynamics are lower at this section in comparison to the sloped region and the chance of the plant burying itself by trapping resuspended sediment is reduced. Regarding

the submersion depth, this type of seagrass has been observed to prefer water depths in closer proximity to the shoreline around 4 m, modeled as 2 m per the 1:2 geometric scale. Modeling seagrass at a shallower depth was important in order to observe a more significant influence on the shoreline.

3.3 Tests

Two different wave conditions were applied over a beach profile with and without *Posidonia*. The cases without vegetation are referred to as the benchmark conditions. Table 3.4 lists and describes the four cases that were tested as part of the COBALTO project.

Table 3.4 Test cases for COBALTO experiments

Case	Description	SWL (m)	H_s (m)	T_p (s)
BMR1	no vegetation; low energy	2.0	0.41	3.71
BMR2	no vegetation; high energy	2.0	0.6	3.71
R1	vegetation; low energy	2.0	0.41	3.71
R2	vegetation; high energy	2.0	0.6	3.71

High energy and low energy waves were the two conditions tested over the bottom profile specified in section 3.1.2. The wave heights were determined by the capacity of the wave paddle at the facility and they simulate mean wave conditions of the Mediterranean Sea along the Catalan coast. Each of the four cases was tested for 6 hours which were broken up into 12 25-minute runs. A total of 48 experiments were recorded. The bed profile was measured after each 25-minute run and was reconstructed after 12 runs to its original configuration, shown in Figure 3.1, before moving on to the next case.

The JONSWAP spectra with a peak enhancement factor (γ) of 3.3 was used to generate 500 irregular waves in each run. Significant wave height (H_s) and peak period (T_p) for each case are given in Table 3.4. Wave reflection was considered to be negligible in this experiment as it was assumed that the wave energy was dissipated upon breaking on the beach.

As described in section 3.2, the seagrass meadow was located at a fixed position and submergence ratio for the R1 and R2 cases. The plant density, the length of the meadow, the number of leaves per plant, and the plant leaf dimensions were all kept constant.

4 SWAN model

Simulating **WA**ves **N**earshore (SWAN) is the numerical model chosen to model the effect that seagrass meadows have on wave attenuation for both the physical experiments of COBALTO and the case study at Baix Camp on the Catalan coast. This chapter briefly explains how SWAN models waves and then how vegetation is introduced into the routine.

4.1 Description of SWAN

SWAN is a third-generation wave model that was developed at the Delft University of Technology (www.swan.tudelft.nl) and is used for obtaining realistic estimates of wave parameters in coastal areas (The SWAN Team, 2019). It is an extension of deep water third-generation wave models that don't include formulations for triad wave-wave interactions and depth-induced breaking for near-shore conditions (The SWAN Team, 2019). The model's numerical propagation scheme is more stable in shallow water because it is implicit, in contrast to other models of this type. For these reasons, SWAN is a more reliable model when considering coastal areas smaller than 20-30 km in the horizontal scale that have depths less than 20-30 m (Booij et al., 1999).

SWAN is an Eulerian model based on the wave action balance equation (Booij et al., 1999) expressed in Cartesian co-ordinates by:

$$\frac{\partial N}{\partial t} + \frac{\partial c_x N}{\partial x} + \frac{\partial c_y N}{\partial y} + \frac{\partial c_\sigma N}{\partial \sigma} + \frac{\partial c_\theta N}{\partial \theta} = \frac{S_{tot}}{\sigma} \qquad 4.1$$

Each of the terms on the left-hand side are either a source or a sink that add up to the S_{tot} on the right-hand side representing all physical processes that generate, dissipate, or redistribute wave energy at a point. N is the action density and is defined as energy density (E) divided by frequency (σ). The first term on the left-hand side represents the local rate of change of N in time and the second and third terms represent propagation in the x and y directions with velocities c_x and c_y, respectively. The fourth term represents shifting of the relative frequency due to variations in depths and currents and finally, the fifth term represents depth-induced and current-induced refraction (Booij et al., 1999).

Six processes contribute to S_{tot} in shallow water:

$$S_{tot} = S_{in} + S_{nl3} + S_{nl4} + S_{ds,w} + S_{ds,b} + S_{ds,br} \quad 4.2$$

S_{in} represents the wave-growth by wind, S_{nl3} and S_{nl4} represent the nonlinear wave-wave interactions of triads and quadruplets, respectively. The three S_{ds} terms capture the different sources of dissipation of wave energy. $S_{ds,w}$ represents dissipation due to white-capping, $S_{ds,b}$ represents dissipation due to bottom friction and $S_{ds,br}$ represents dissipation due to depth-induced wave breaking. In order to include wave damping due to vegetation, equation 4.2 has been extended in SWAN with $S_{ds,veg}$. This was the main term under consideration for modeling the influence of seagrass on coastal hydrodynamics and is expanded upon in the next section.

4.2 Vegetation module

SWAN has a designated VEGetation command that can be activated by the user if wave damping due to vegetation is to be considered. If this command isn't used, the model will not account for possible vegetation effects. It uses the cylinder approach suggested by Dalrymple et al., (1984) to express the wave dissipation due to vegetation assuming rigid plants. This formula was modified by Mendez and Losada (2004) for irregular waves and implemented into the model by Suzuki et al. (2012). Energy loss is calculated as work carried out by the vegetation. These plant-induced forces acting on the fluid are expressed in terms of a Morison-type equation (Dalrymple et al., 1984; Kobayashi et al., 1993). Neglecting swaying motion and inertial forces, the force per unit volume (F) is given by:

$$F = \frac{1}{2}\rho C_D b_v N_v u|u| \quad 4.3$$

where ρ is the water density, C_D is the drag coefficient, b_v is the plant stem (cylinder) diameter, N_v is the plant density and u is the horizontal velocity due to wave motion. Energy dissipation per unit

area over the entire height of vegetation is given by the Dalrymple et al. (1984) formula which is presented by Mendez and Losada (2004) as:

$$\varepsilon_v = \frac{2}{3\pi}\rho C_D b_v N_v \left(\frac{gk}{2\sigma}\right)^3 \frac{\sinh^3 k\alpha h \ + 3\sinh k\alpha h}{3k\cosh^3 kh} H^3 \qquad 4.4$$

where ε_v is the time-averaged dissipation rate, σ is wave frequency, k is wave number, αh is the vegetation height, h is the water depth and H is the wave height. Mendez and Losada (2004) modified equation 4.4 to allow estimation of the mean rate of wave dissipation per unit horizontal area, $\langle\varepsilon_v\rangle$, for irregular waves:

$$\langle\varepsilon_v\rangle = \frac{1}{2\sqrt{\pi}}\rho \tilde{C}_D b_v N_v \left(\frac{gk}{2\sigma}\right)^3 \frac{\sinh^3 k\alpha h \ + 3\sinh k\alpha h}{3k\cosh^3 kh} H_{rms}^3 \qquad 4.5$$

Where H is replaced with root mean square wave height H_{rms} and $\tilde{C}_D$ becomes a bulk drag coefficient that may be dependent on the applied Keulegan – Carpenter (KC) number. The bulk drag coefficient is the only parameter that requires calibration for the given plant type being evaluated. Suzuki et al. (2012) implemented the approach of Mendez and Losada (2004) into an additional dissipation term, $S_{ds,veg}$, that was added to equation 4.2 in SWAN. This term can be expanded to include frequencies and directions as follows:

$$S_{ds,veg}(\sigma,\theta) = \frac{D_{tot}}{E_{tot}} E(\sigma,\theta) \qquad 4.6$$

E_{tot} being the total wave energy and D_{tot} being the rate of dissipation of the total energy due to vegetation. A further breakdown of each term can be found in Suzuki et al. (2012). The final expression reads:

$$S_{ds,veg} = -\sqrt{\frac{2}{\pi}} g^2 \tilde{C}_D b_v N_v \left(\frac{\tilde{k}}{\tilde{\sigma}}\right)^3 \frac{\sinh^3 \tilde{k}\alpha h + 3\sinh \tilde{k}\alpha h}{3\tilde{k}\cosh^3 \tilde{k}h} \sqrt{E_{tot}} E(\sigma,\theta) \qquad 4.7$$

where $\tilde{\sigma}$ is the mean frequency and $\tilde{k}$ is the mean wave number. This dissipation term can be obtained by requesting SWAN to output the quantity DISVEG as a result.

Suzuki et al. (2012) also added the option to be able to vary the vegetation vertically. Each layer of vegetation is defined by a vegetation factor that takes into account its unique $\tilde{C}_D$, b_v and N_v parameters. Energy dissipation is calculated for each vertical segment up to the SWL individually and their individual contributions are added to determine the total amount of energy loss. This is not discussed in more detail in this paper as the *Posidonia oceanica* meadow being modeled was considered to be a single layer of vegetation. SWAN can also handle a horizontally varying vegetation density based on the NPLANTS input grid that the user provides, explained further in Chapter 5. Although vertical and horizontal variations of the vegetation characteristics can be accounted for by the model, the height of the vegetation cannot vary spatially.

5 Model calibration

This chapter describes the SWAN modeling strategy, the calibration methodology and results. The COBALTO benchmark cases were mainly used to verify that the SWAN model could produce accurate results for a flume scenario with the provided bottom profile. Data from cases R1 and R2 was then used to calibrate the plant geometry and drag coefficient inputs for implementation. The main challenge was determining how best to represent the seagrass meadow in the model as rigid cylinders. Once a geometry was selected, focus was placed on adjusting the parameters to reach a result that most closely replicated the COBALTO results. The last section in this chapter provides the results obtained along the calibration process, predominantly for the R2 case, and explains what conclusions were made at the end of this exercise.

5.1 Model strategy

The input parameters were selected to resemble those used in the COBALTO experiments as closely as possible. While most of the general model parameters were set to default, the water density was adjusted to 1000 kg/m^3 since the flume was filled with fresh water. It was also determined that running a stationary one-dimensional case in SWAN would be a simple way to accurately represent the physical tests in the flume. An example SWAN input file for the R2 case can be found in Appendix C. While all of the inputs can be seen in the example file, this section mainly elaborates only on the parameters that are more unique to simulating a flume scenario or a case that accounts for energy dissipation by vegetation.

5.1.1 Input grids

Each case had a minimum of at least a computational grid and a bottom profile input grid. There was a plant density input grid added to the model when investigating the cases with vegetation. A narrow 20-degree sector (10 degrees to each side) was applied to the computational grid in order to limit the spectral wave direction range. The SWAN “bottom” file, or bathymetry file, was modeled with a resolution of 2 cm and was created from the measurements taken by the mechanical

profiler. When in use, the plant density grid was used to define the presence of seagrass in the horizontal direction with the same resolution as that of the bottom input grid.

5.1.2 Boundary conditions

Boundary conditions for the model were set to be constant, coming solely from the direction of the wave paddle, and defined by the JONSWAP frequency spectrum with $\gamma = 3.3$. The significant wave height and peak period were taken from data collected by the second sensor in the flume at 18.18 m because it was assumed that the wave may not have sufficiently formed yet by the time it reached the location of the first sensor. It was also found key to apply an appropriate coefficient of directional spreading to see realistic results. The sensitivity for directional spreading in SWAN has previously been investigated to have an impact on the model output although it was seen to be fairly small (Suzuki et al., 2012). This parameter was set to 2.0 degrees to model mainly straight waves acting on the plants in the flume and minimize the incidence of angled waves.

5.1.3 Physical processes

SWAN also accounts for many physical processes by default in its computations. Since these didn't occur in the physical model, all were deactivated. This included whitecapping, quadruplet interactions, and wave breaking. Although wave breaking was present in the flume, the reason the process was turned off in the model was because the breaking zone began at around 50 m in the flume. The wave attenuation analysis focused around the vegetation section and was not studied into the breaker zone. As the vegetation was installed in the area between 30-40 m from the paddle, there were approximately 10 m beyond this section where wave breaking had minimal to no influence. The section beyond the 50 m will become critical when investigating the plants' effect on morphodynamics in future analysis.

5.1.4 Vegetation module

To account for energy dissipation by vegetation, the model requires an input for the height of the plant, its stem diameter, the number of plants per square meter and a drag coefficient. These are

not straightforward parameters when it came to trying to simulate *Posidonia oceanica*. The initial plant model that was used in the simulation was defined as having a height of 0.6 m, a stem diameter of 0.004 m, a density of 269 plants/m^2 and a drag coefficient of 0.2. The height and density values were taken directly from the geometry of the artificial seagrass in the experiments. In order to have a diameter, the plant had to be transformed into a representative cylinder. This was done by maintaining the volume of the four blades and the height of 0.6 m and solving for the diameter of a cylinder with an equivalent volume. The drag coefficient was selected to be 0.2 as it fit within the range determined by previous studies. Most commonly, the drag coefficient is estimated based on its relationship to one of two parameters: the Reynolds number (*Re*) or the Keulegan-Carpenter (*KC*) number. Formulas for the relationships between the *Re* and C_D have all been obtained on the basis of the experiment of Asano et al. (1988). Reynolds number was first adopted in the literature by Kobayashi et al. (1993) and is defined as:

$$Re = \frac{b_v u_c}{v} \qquad 5.1$$

where v is the kinematic viscosity and u_c is a characteristic fluid velocity acting on the meadow, taken to be the wave orbital velocity amplitude above the leaves. Later, the Keulegan-Carpenter number was found to potentially be an even more suitable link to C_D (Mendez and Losada, 2004):

$$KC = \frac{u_c T_p}{b_v} \qquad 5.2$$

where u_c is the maximum horizontal velocity and T_p is the peak wave period. There is no definite agreement in the scientific community regarding which of these relationships produces a stronger correlation. These parameters, like SWAN, don't take into account the flexibility of the vegetation so the initial drag coefficient chosen was based on the estimated ranges of earlier experiments. Sánchez-González et al. (2011) obtained C_D values between 0.1-1.0, Cavallaro et al. (2011) between 0.05-0.31, Cavallaro et al. (2018) between 0.2-4.0 and Koftis et al. (2013) between 0.75-2. All ranges are approximate and vary as a consequence of applying different methodologies. Other values that have been published for *Posidonia oceanica* were either for lab studies using

different types of vegetation or field studies. A C_D value closer to the low end of the overall range was selected because the artificial plants utilized in COBALTO were more flexible than those in past studies to more accurately represent the properties of a real plant.

Being aware that this initial model wasn't the only way to represent the true plant, a sensitivity analysis was carried out to analyze whether slight changes to each individual parameter would have a significant impact on the results. The different plant geometry options are presented in Table 5.1 below and the results can be found in Appendix D.

Table 5.1 Plant geometries for SWAN sensitivity analysis

		Cases tested for parameter sensitivity														
		control	h1	h2	h3	d1	d2	d3	d4	n1	n2	n3	c1	c2	c3	c4
Parameters	plant height (m)	0.6	0.5	0.4	0.3	0.6	0.6	0.6	0.6	0.6	0.6	0.6	0.6	0.6	0.6	0.6
	stem diameter (m)	0.004	0.004	0.004	0.004	0.0048	0.0044	0.0036	0.0032	0.004	0.004	0.004	0.004	0.004	0.004	0.004
	density (plants/m^2)	269	269	269	269	269	269	269	269	336	404	538	269	269	269	269
	drag coefficient C_d	0.2	0.2	0.2	0.2	0.2	0.2	0.2	0.2	0.2	0.2	0.2	0.1	0.15	0.25	0.3

The conclusion was that even the more drastic changes, such as doubling the plant density, resulted in only about a 1% difference in significant wave height. Since the model was not too sensitive to the vegetation parameter changes, further model calibration continued with the original control case geometry. The following section describes the methodology for obtaining a better fit of the significant wave height between the experiment data and numerical model using the drag coefficient as the main calibration parameter.

5.2 Methodology

Significant wave height was calculated through two different methods: by using the spectrum and by using zero-crossing analysis. Both methods were applied to the data gathered by the WGs, AWGs and PPTs to compile the final value tables that are found in Appendix B. These are the values that were used for the purpose of any data-to-model comparisons. Any outliers were considered to be caused by instrument error and were removed from the data. All four cases were analyzed but the main focus in this chapter is the higher energy case (R2), although additional results for the benchmark and R1 cases can be found in Appendix E. Based on the results in

Appendix D, it looked as if SWAN may not be a sensitive enough model for the scale of the experiments and it would be more beneficial to focus on the higher energy case where the magnitude of the changes would be greater.

The first step was plotting the SWAN results for significant wave height against the available data as in Figure 5.1. This plot compares the obtained H_s values along the length of the flume up to 50 m where the wave breaking zone first begins. The model values were already within 5-10 cm of the measured ones but more attention was needed in the vegetated range between 30 and 40 m where overprediction by the model was greater.

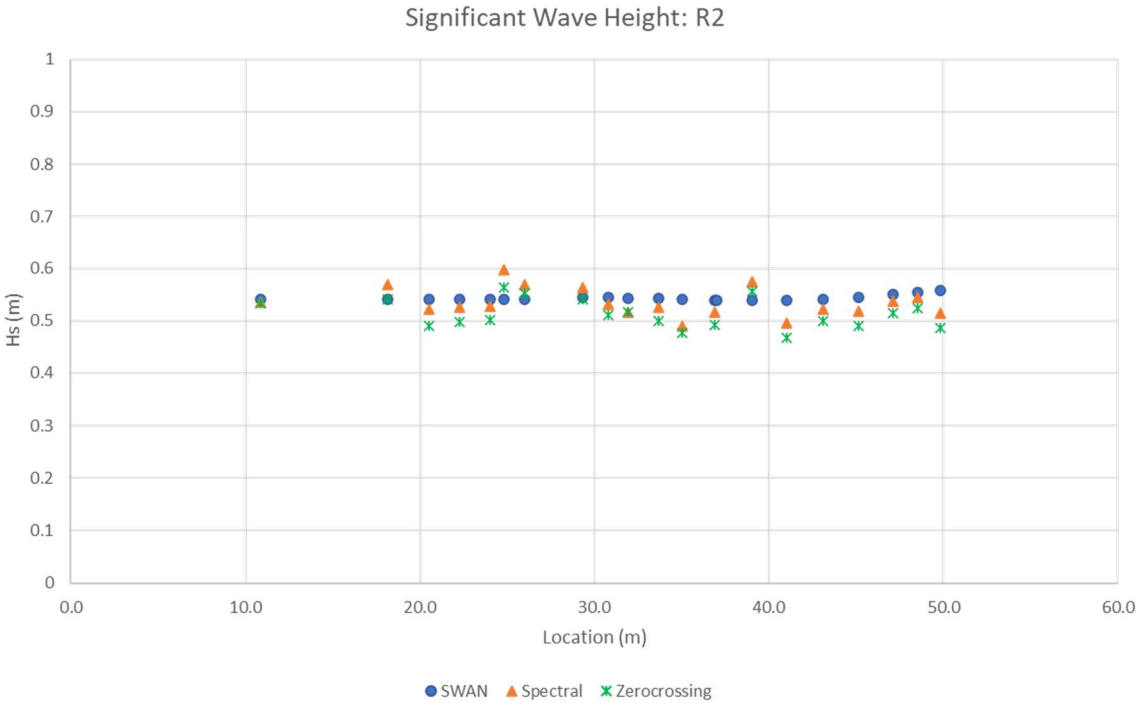

Figure 5.1 Comparison of modeled to measured H_s values

The individual data points in the model data were then compared to both the spectral and zero-crossing data sets, as shown in Figure 5.2. The goal of this was to establish some consistency and narrow down the amount of collected data to only the most representative values for comparison. A ratio value of one, shown by the red line on the plot, signifies an exact correlation between the model and measured result at the sensor locations.

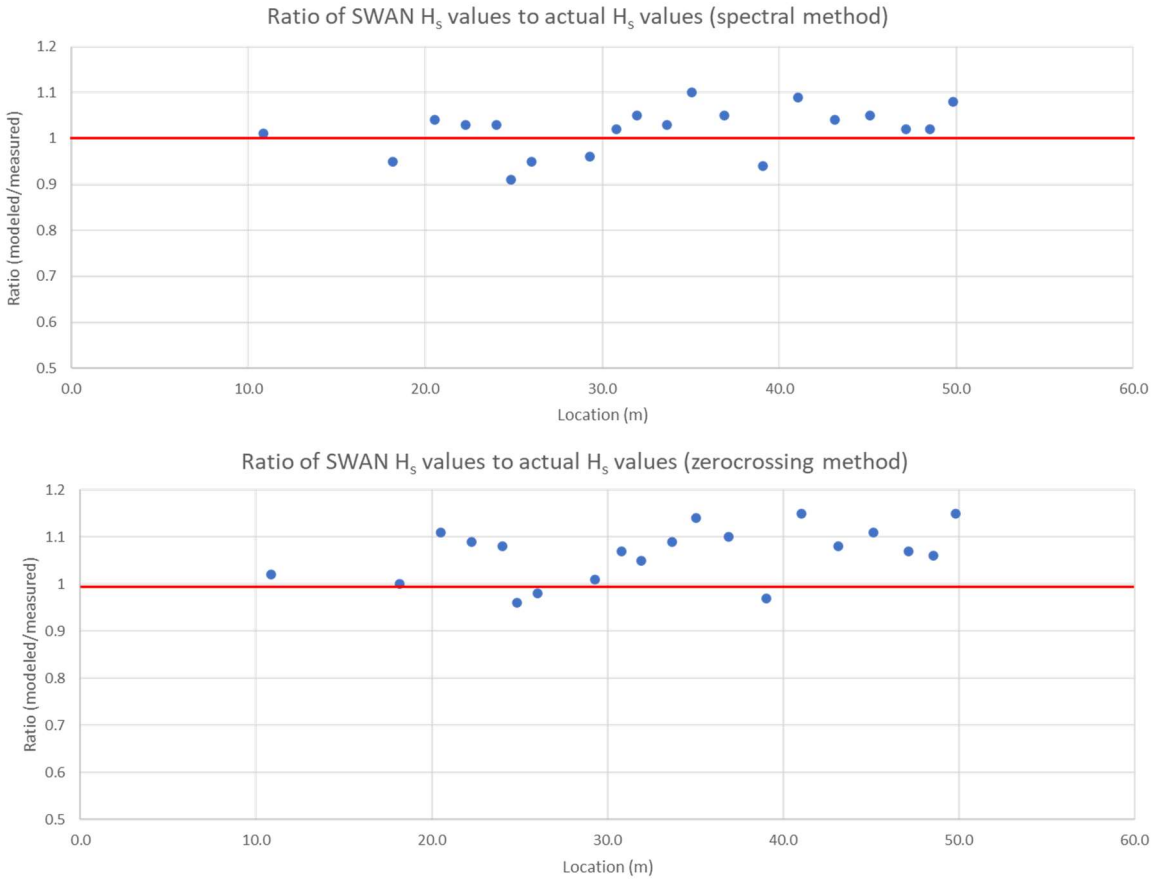

Figure 5.2 Ratios between modeled and measured results for R2; spectral (above), zerocrossing(below)

From this point on, only the H_s values taken from the spectrum were considered as the correlation between them and the model was found to be stronger. This was most likely due to the fact that SWAN also calculates significant wave height from the energy spectrum.

A series of additional plots were produced to explore the sensitivity of the model to changes in the drag coefficient parameter. A larger range of values was tested than was initially used for the sensitivity analysis since the effect of the original estimate turned out to be minimal. Model calibration results in section 5.3 use drag coefficient values of 0.3, 0.7, 1.0 and 1.5 in order to obtain a better fit for significant wave height.

Besides looking at wave height, the variance density spectrum was created for both the modeled and measured case. The purpose of analyzing the spectrums was to see if the presence of the vegetation possibly shifted the occurrence of certain frequencies or changed the shape of the

spectrum beyond the seagrass range in any kind of way. Some calibration with the drag coefficient was performed to determine how it might affect the peak of the spectrum and to what extent.

As it was clear that the numerical model was slightly overpredicting, the initial H_s input was then given more attention. Instead of using the value of merely the second sensor, all the data points up to 30 meters were averaged under the assumption that they should ideally be equal. Up to this location the waves have not yet reached the vegetated section nor have they felt the sloping sandy bottom. The small 0.5 cm discrepancy in one direction or the other is due to the fact that these data points were all collected using different instruments. Each of these is calibrated in a slightly different manner and the way each collects and treats the data varies as well.

Another approach that was used in interpreting the results was through computation of the transmission coefficient or damping coefficient (Mendez and Losada, 2004). Under the assumption that the wave height at the seaward limit of the vegetation is $H(x=0) = H_0$, the transmission coefficient is calculated by

$$K_v = \frac{H_t}{H_o} \qquad 5.3$$

where K_v is the damping coefficient and H_t is the transmitted wave height. This parameter could be calculated directly, but in this situation, it was calibrated primarily by visual inspection between H_s plots.

The last step taken in the calibration process was an error metrics calculation. Performance of the numerical model was defined by the mean ratio calculated for significant wave height, similar to the approach of Lynett, et al. (2017):

$$Mean\ Ratio_{Hs} = \frac{1}{n}\sum_{i=1}^{N} \frac{Hs_{mod}^{i}}{Hs_{obs}^{i}} \qquad 5.4$$

where the subscripts *mod* and *obs* are in reference to the model predictions and observations made from the physical experiment, respectively, and *N* represents the number of sensor locations. The numerical and physical models are considered to be in perfect agreement with one another when the mean ratio is equal to 1.

5.3 Results

This section presents the results achieved from following the outlined calibration methodology. Figure 5.3 presents the variance density spectrums for the BMR2 and R2 cases at PPT sensors located at 24.03 m and 45.11 m. The graphics were generated using a MATLAB script from the Maritime Engineering Laboratory (LIM) at UPC. On each graph the blue bars symbolize the spectrum calculated from the collected data and the solid red line symbolizes the spectrum created by SWAN. The model was run with a C_D of 1.5 in the R2 case presented with the thought being it would produce the most extreme result and any changes would be visually recognizable.

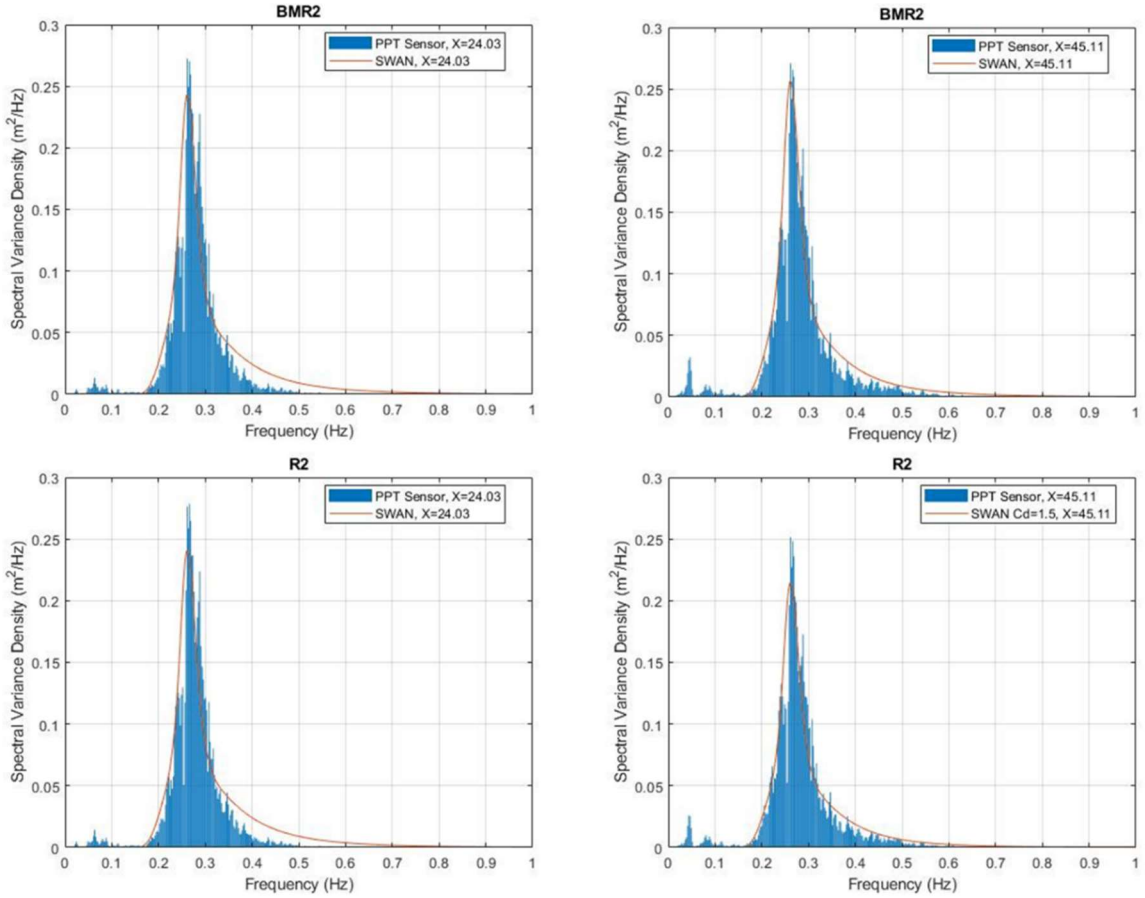

Figure 5.3 Energy spectrum comparison between measured and modeled results for BMR2 and R2 (C_d=1.5)

The top two plots show how the waves are starting to slightly increase in height as they approach the shore from x = 24.03 m to x = 45.11 m. The two plots on the left should be identical as there is no influence from the seagrass yet. The plot in the bottom right corner shows what happens to the spectrum just 5 m beyond the seagrass patch. As expected, the peak is smaller and energy is decreased when comparing to the location at 24.03 m in the R2 case. It is also smaller than the peak at the same location for case BMR2 in the top right corner. Furthermore, it was observed that the presence of vegetation had no influence on the actual shape of the spectrum. It had been expected that the plots would confirm that in addition to attenuating wave energy, the meadow would serve as a low-pass filter where higher frequencies in the spectra would experience higher levels of attenuation (Bradley and Houser, 2009). Beyond a few additional runs to test out different drag coefficients, the focus shifted back to analyzing wave height for continued calibration. It was found that applying lower drag coefficients (1.0, 0.7 and 0.3) resulted in an increase in the spectrum peak beyond the vegetation. These plots are attached in Appendix E.

Figure 5.4 illustrates yet another approach at exploring different plant geometries in parallel with varying the drag coefficient. The surface area of the blade that the wave is acting upon was kept constant but the dimensions were altered from the control case. The height of the plant was changed to 0.3 m and the width to 0.008 m. The reasoning being that 0.008 m was the true dimension of the plant perpendicular to the waves and 0.3 m was justified by the fact that these plants are quite flexible and tend to bend over with the wave as seen on the recorded videos from the COBALTO experiments. This phenomenon of asymmetry in posture of the plants is referred to as “streaming”, where the blades lay horizontally in the direction of wave propagation under the wave crest but remain more upright under the wave trough (Luhar et al., 2010). Not only were the blades not standing up at 0.6 m throughout the test, as rigid cylinders would have, but not all of the blades in the plant configuration were 0.6 m long to begin with. For these reasons, it seemed more logical to use a smaller plant height that was actually more regularly acting on the waves. By doubling the plant width and halving the plant height, the resulting H_s remained nearly identical.

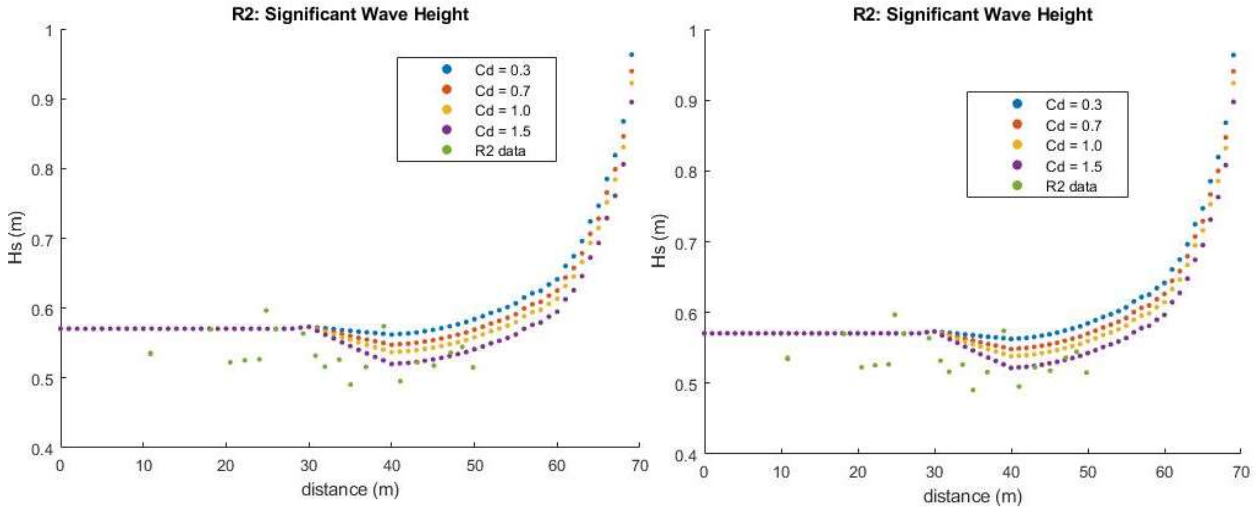

Figure 5.4 Results of varying C_d for h=0.6m and d=0.004m (left) and h=0.3m and d=0.008m (right)

The revelation that a similar result could be reproduced while applying a more representative geometry motivated additional tests applying this new geometry. These tests, shown in Figure 5.5, took a closer look at examining how a difference in 0.1 m of height paired with different drag coefficients affected the hydrodynamic result.

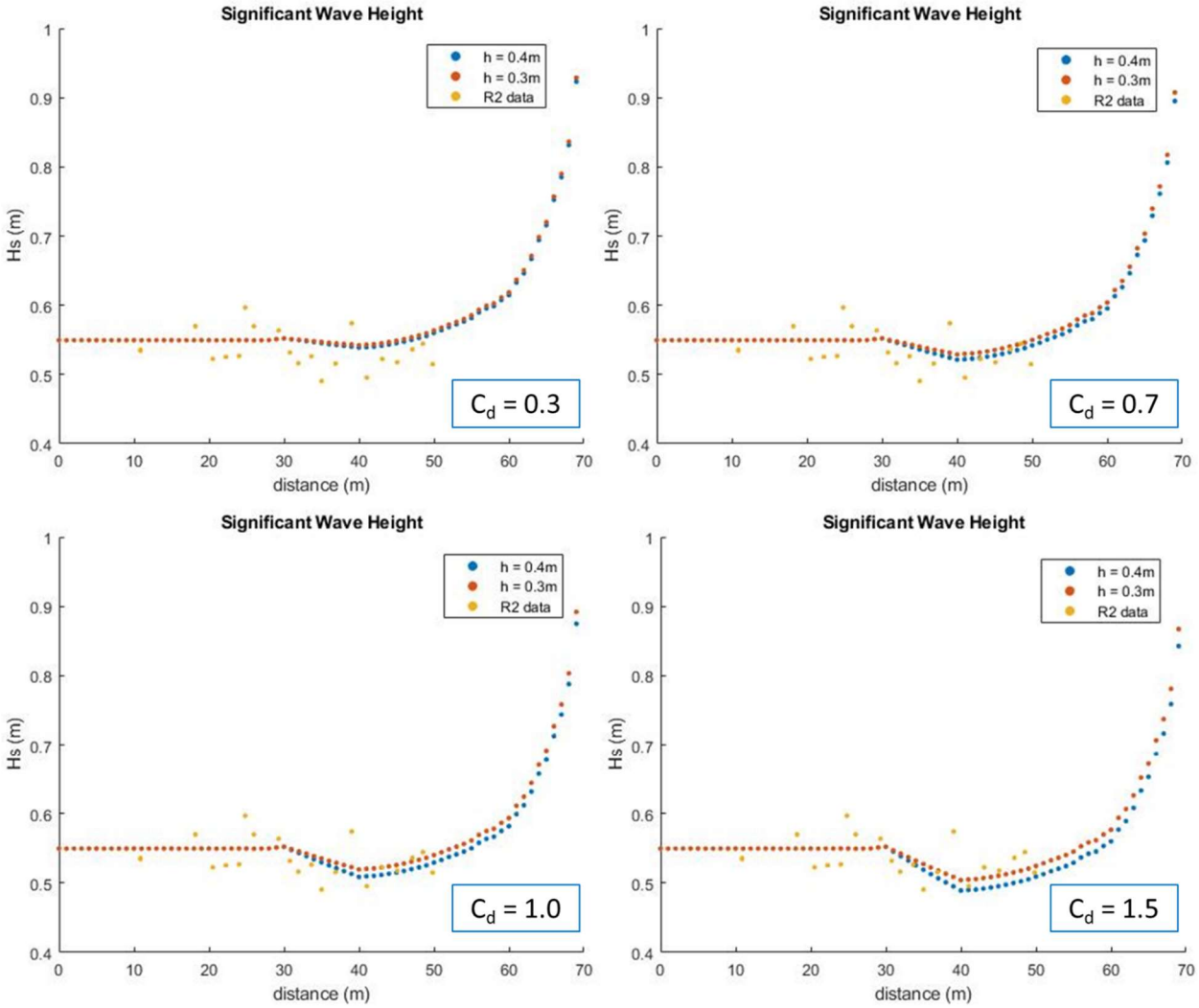

Figure 5.5 Plots comparing plant height variation on Hs results with different C_d values

The results in Figure 5.5 demonstrate that the difference in the plant height had a much smaller impact than the value of the drag coefficient. Considering all the factors, the plant dimensions that were assumed to most realistically represent the artificial plant were a plant width of 0.008 m and a plant height of 0.4 m. Final calibration would only include making adjustments to the drag coefficient. This bulk drag C_d would account for the inability to implement the flexibility of the vegetation along with other physical processes that may exist in the flume setting but aren't yet fully understood and were not accounted for (Christie et al., 2018; Suzuki et al., 2012). Wave energy dissipation by vegetation could be caused by processes besides the work done by the drag force such as turbulence as well as surface friction of the artificial vegetation and flume walls, as

suggested by Chen et al. (2018). Once the averaged H_s was introduced into the model, it became easier to fine-tune the bulk drag coefficient to get a better fit between the data and the model. The overprediction in the model still existed but was decreased. In the lower graphs of Figure 5.6, the orange dots resemble the new data points after averaging a group of measurements before and after the meadow range. The upper two graphs show the same calibrated SWAN result just plotted with the original measured data for comparison. At this point, many approaches were investigated and it became clear that the process could continue on with still different plant geometries or flow conditions. A value of 0.7, which was used for creating the plots in Figure 5.6, was settled on for the drag coefficient for at least the R2 case.

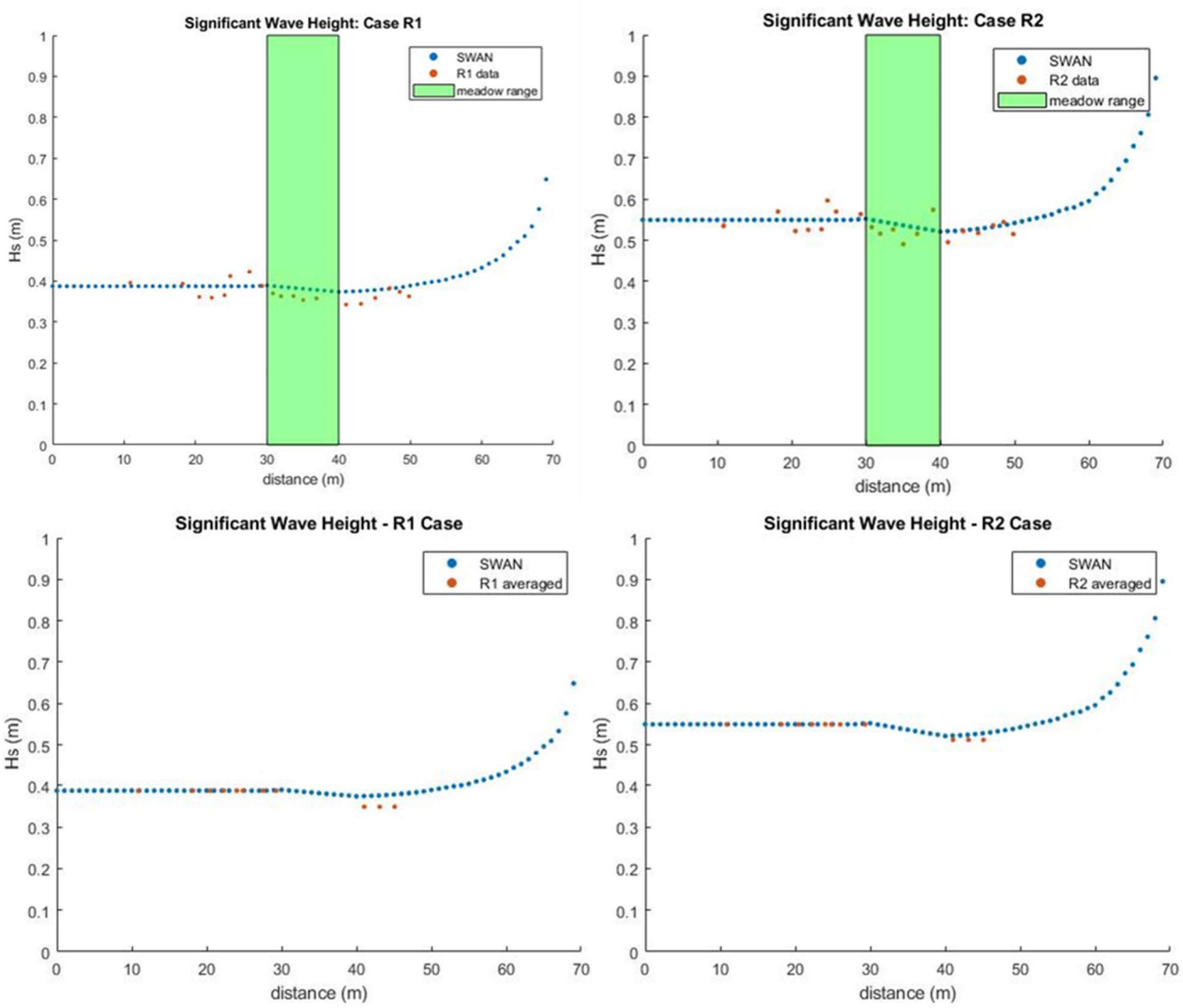

Figure 5.6 Calibrated SWAN model compared to original data (above) and averaged data (below)

The transmission coefficients were calculated based on the initial and transmitted H_s data of the lower two graphs in Figure 5.6. For the R2 case, K_v values were found to be 0.95 and 0.93 for SWAN and the data, respectively. These values correspond to approximately a 4-7% reduction in wave height before and after the seagrass. For the R1 case, K_v values were found to be 0.97 and 0.90 for SWAN and the data, respectively. These values correspond to approximately a 3-10% reduction in wave height.

Lastly, the R1 and R2 mean ratio computations for H_s are laid out in Table 5.2. It can be understood from the result of this type of error metric calculation that in both scenarios the model slightly overpredicts (mean ratio is greater than 1). Still, in both cases, the fit between the model and the data is considered to be very good since the mean ratio is within 5% of 1.0. The R2 case has a better fit as its mean ratio is closer to 1.0 than the mean ratio of R1. Measurement errors were removed from the data set and shown as no data (-) in the table.

Table 5.2 Data used for error metric calculation of numerical model

Sensor location (m)	R1			R2		
	H_s measured (m)	H_s modeled (m)	Ratio	H_s measured (m)	H_s modeled (m)	Ratio
10.86	0.396	0.387	0.98	0.5345	0.550	1.03
10.86	-	-	-	0.5358	0.550	1.03
18.18	0.393	0.387	0.98	0.5698	0.550	0.96
20.51	0.361	0.387	1.07	0.5225	0.550	1.05
22.26	0.359	0.387	1.08	0.5254	0.550	1.05
24.03	0.365	0.387	1.06	0.5268	0.550	1.04
24.84	0.412	0.387	0.94	0.5967	0.550	0.92
26	-	-	-	0.5697	0.549	0.96
27.53	0.423	0.387	0.92	-	-	-
29.31	0.388	0.389	1.00	0.5637	0.552	0.98
30.8	0.370	0.388	1.05	0.5319	0.550	1.03
31.93	0.363	0.386	1.06	0.5162	0.546	1.06
33.67	0.363	0.383	1.06	0.5263	0.540	1.03
35.03	0.354	0.381	1.08	0.4906	0.536	1.09
36.9	0.358	0.378	1.06	0.5158	0.530	1.03
39.05	-	-	-	0.5741	0.524	0.91
41.04	0.343	0.374	1.09	0.4954	0.522	1.05
43.11	0.344	0.376	1.09	0.5224	0.524	1.00
45.11	0.359	0.378	1.05	0.5177	0.528	1.02
47.13	0.383	0.381	1.00	0.5362	0.533	0.99
48.53	0.374	0.384	1.03	0.5445	0.537	0.99
49.83	0.363	0.388	1.07	0.5151	0.541	1.05
		Ratio Sum	19.67		Ratio Sum	21.28
		Mean Ratio	1.04		Mean Ratio	1.01

6 Application to the Baix Camp seagrass meadow

Baix Camp is a comarca of Catalonia that is located on the coast of the Mediterranean Sea. Since the bathymetry, seagrass cartography, and wave climate data were available in this area, it was chosen as the site at which to apply the information learned in Chapter 5 regarding the wave attenuating properties of *Posidonia oceanica*. The first task was to correlate the existing hydrodynamic condition with the existing seagrass layout in this region. The second task was to compare the cases of seagrass being present against a case without seagrass. After accomplishing these two tasks, the end goal was to determine how much energy could be dissipated over the course of a year with the presence of the seagrass by means of a transmission coefficient.

6.1 Seagrass cartography and bathymetry

A seagrass map layer was created from a polygon shapefile identifying all of the different seagrasses that are located along the coast of Catalonia (agricultura.gencat.cat). This file was last updated in 2019 and uses the ETRS 1989 UTM Zone 31N coordinate system. Additional species that can be found in this file include *Cymodocea nodosa*, *Zostera noltii*, *Caulerpa prolifera*, and *Ruppia cirrhosa*. Figure 6.1 is an enlarged view of the area of interest to show the existing patches of the *Posidonia oceanica* meadows in this region.

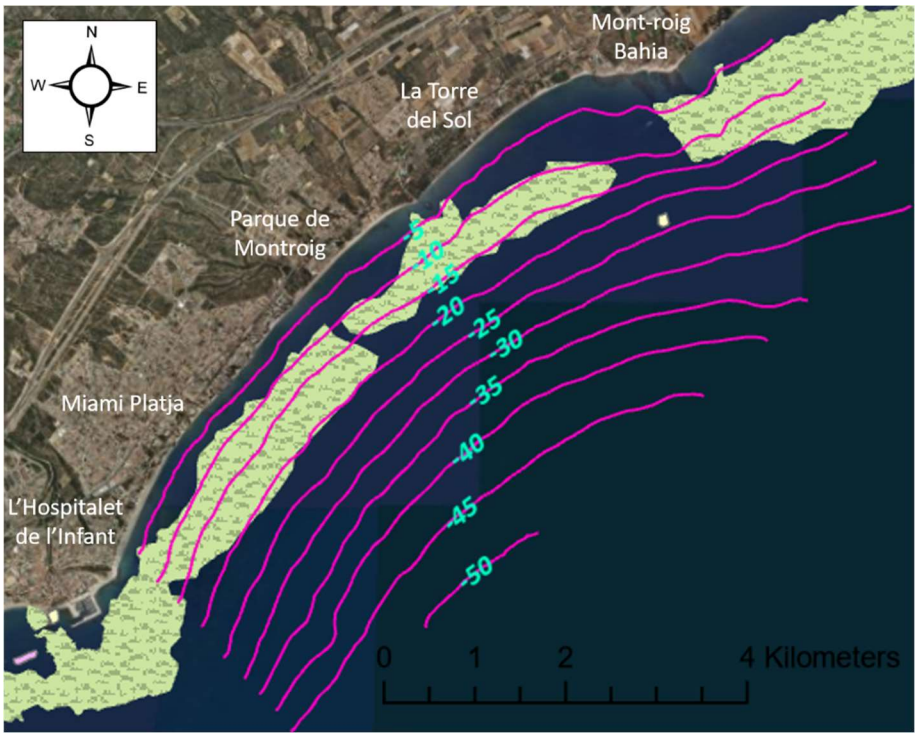

Figure 6.1 Map of existing bathymetry and Posidonia oceanica in study area

Besides the vegetation patches, the existing bottom contours in this area are shown in Figure 6.1. The bathymetric data was first imported as points (www.navionics.com), from which a raster surface was created. Once the data was in this format, bottom contours were extracted from the raster surface. The end result, reveals that the contours in this area are relatively constant. There are no unique or dramatic features, like canyons, along the bottom here. There does seem to be a wider platform in the shallow region of the northeast corner just off of the cape. It appears that the seagrass has a wider coverage in that flatter zone before the contours continue to descend beyond 20 m in depth. This is likely due to the fact that this particular seagrass prefers and thrives at depth conditions between 10-20 m although it has also been known to exist in deeper water. Another observation of interest are the gaps or breaks in the seagrass. According to Telesca et al. (2015), the presence of seagrass depends on three main factors: physical variables (e.g. temperature, salinity, depth, turbidity) which regulate its physiological activity, climate change and anthropogenic pressures. As the contours are regularly spaced, it would be assumed that the seagrass meadows would stretch evenly along this part of the coast (assuming homogeneity in the remaining physical factors). For example, when looking further south in this stretch toward the Ebro Delta, it is logical that the seagrass meadow doesn't extend through it because of the

freshwater input affecting the salinity and temperature (Telesca et al., 2015). Since these holes can't be associated with the factors mentioned, it is likely that they are a result of human activity.

6.2 Wave climate

A wave climate was defined from a data set collected by an offshore buoy near Tarragona (Puertos del Estado, 2019). The data set contained measurements that were collected hourly for the years 2004 to 2018. Although many parameters were generated, the only ones utilized in this analysis were significant wave height (Hm0), mean wave period (Tm02) and wave direction (Dmd). In the approach presented in this work, the available data was used to represent a year's worth of data. The first step was filtering out the wave directions that would have minimal effect on this location and this was completed using a MATLAB script found in Appendix F. The full range of wave directions that were considered is illustrated in Figure 6.2. Taking the north direction as 0°, the range begins at 70° and ends at 190°. Any waves approaching from offshore outside of these limits were omitted from the data set under the assumption that Baix Camp is geographically sheltered by Cap Salou to the north and the Ebro Delta to the south. The remaining wave data was sorted into eight 15° sectors to condense the number of wave conditions under evaluation.

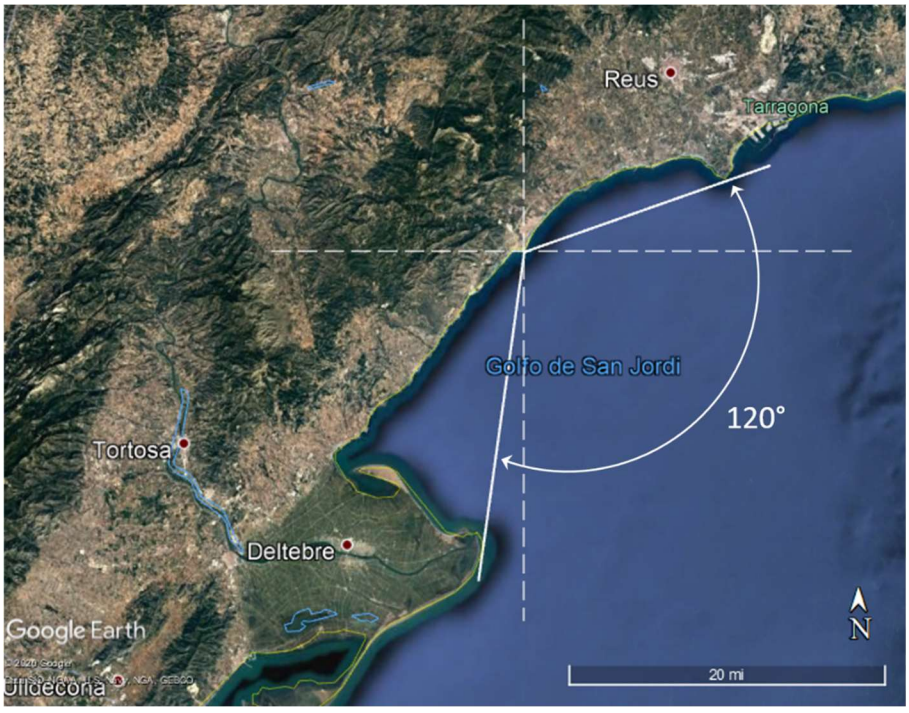

Figure 6.2 Wave directions considered in analysis (70°-190° where North = 0°)

Contingency tables, found in Appendix G, were generated for each sector of significant wave height and mean wave period. The mean periods were sorted into bins of 2 s increments and the significant wave heights into bins of 0.5 m increments. H_{morf} values could then be calculated for each respective period of a given direction. The H_{morf} parameter is defined as the representative wave height that represents the mean energy content of a time span, in this case of a year.

$$H_{morf} = \sqrt{\frac{\sum_{i=1}^{N} {H_i}^2 f_i}{\sum_{i=1}^{N} f_i}} \qquad 6.1$$

In equation 6.1, H_i is the significant wave height for an event, f_i is the corresponding frequency at which it occurs over the year and N is the total number of events. After this process was completed, there were 4-5 wave conditions established for each direction, each with a unique H_{morf} and $Tm02$, for a total of 33 conditions. A benefit of calculating the wave height in this manner is that it is an effective way of filtering out non representative wave conditions that may possibly occur but at very low frequencies.

6.3 Modeling strategy

Three nested grids were set up to run the SWAN simulation (Figure 6.3). Domain 1 was the coarsest grid with limits from 2.809×10^5E m to 3.877×10^5E m and 4.475×10^6N m to 4.569×10^6N m. Domain 3 was the finest grid with limits from 3.254×10^5E m to 3.349×10^5E m and 4.538×10^6N m to 4.547×10^6N m. All coordinates are in reference to ETRS 1989 UTM Zone 31N. The advantage of using nested grids is that the waves can first be computed on the coarse grid covering a larger region and then the results could be refined on a finer grid covering a smaller region. The fine grid uses the boundary conditions that are computed on the coarse grid (The SWAN Team, 2019).

Figure 6.3 Visual of nested grid boundaries applied in SWAN

Once the computational grids were set up, SWAN was run with the 33 different wave conditions that were computed in MATLAB and explained in section 6.2. These initial simulations accounted for wave breaking, bottom friction (Madsen formulation) and triad interactions but did not account for the presence of vegetation. A new input grid then had to be created for implementation of the vegetation layer into the model. Based on the current cartography of the seagrass, the proposed seagrass meadow would exist at a constant density at all locations where depths were between 10 and 20 m. The height and density of the seagrass were scaled up from the physical experiments to 0.8 m and 67 plants/m^2, respectively. The stem diameter was input as being 1 cm, not quite the scaled experimental value, which is the actual reported width for *Posidonia oceanica.* This parameter was modeled as 0.8 cm in the flume because of manufacturing limitations. The drag coefficient of 0.7 was maintained since it had been calibrated in Chapter 5 for similar wave conditions in the flume at a smaller scale. The SWAN model was then run another 33 times to compute the outputs for the case including this proposed seagrass meadow. Although the output DISSip was of main concern for the analysis in this thesis, other outputs were computed for potential future examination. This list of outputs included but was not limited to: DISBot (energy

dissipation due to bottom friction), UBOT (rms value of the maxima of the orbital velocity near the bottom), TMBOT (bottom wave period) and URMS (rms value of the orbital velocity near the bottom).

The final task was to create a 1-year snapshot of the accumulated amount of energy dissipation at this location. An initial graphical representation was generated by using a MATLAB script (see Appendix F) to sum the dissipation contribution from each condition. This needed to be carried out twice again, once for the case without vegetation and once for the case with vegetation. It is important to explain that the total amount of dissipation from each direction was multiplied by the occurrence frequency (Appendix H) of that given direction. In this way, the dissipation from one direction was not treated as occurring 100 percent of the time over the course of a year. Each of the eight dissipation grids represented the total amount of annual energy reduction that could be attributed to a given directional sector. At this point, all eight grids were summed together to compute the total dissipation grid for all directions under consideration. This final grid was converted into a text file and imported into ArcGIS Pro where it could be transformed into a raster dataset. Lastly, contours were extracted from the raster surface and overlaid onto a topographic base map, the existing seagrass cartography and the existing bathymetry data to create the graphics that are presented in section 6.4.

6.4 Results

This section presents and interprets the results that were gathered by applying the described modeling methodology to the Baix Camp case on the Catalan coast. The figures have been designed to present only the most relevant information to the parameter being considered and have been simplified to an extent for clarity.

6.4.1 Present wave climate and seagrass distribution

Before introducing a seagrass meadow into the model, it was important to review the existing conditions in the region in order to set this condition as a base or control case to be used for comparisons in the future. At first, only the existing seagrass meadow locations were overlaid with

the current wave climate to investigate what levels of energy dissipation the vegetation is able to tolerate (Figure 6.4).

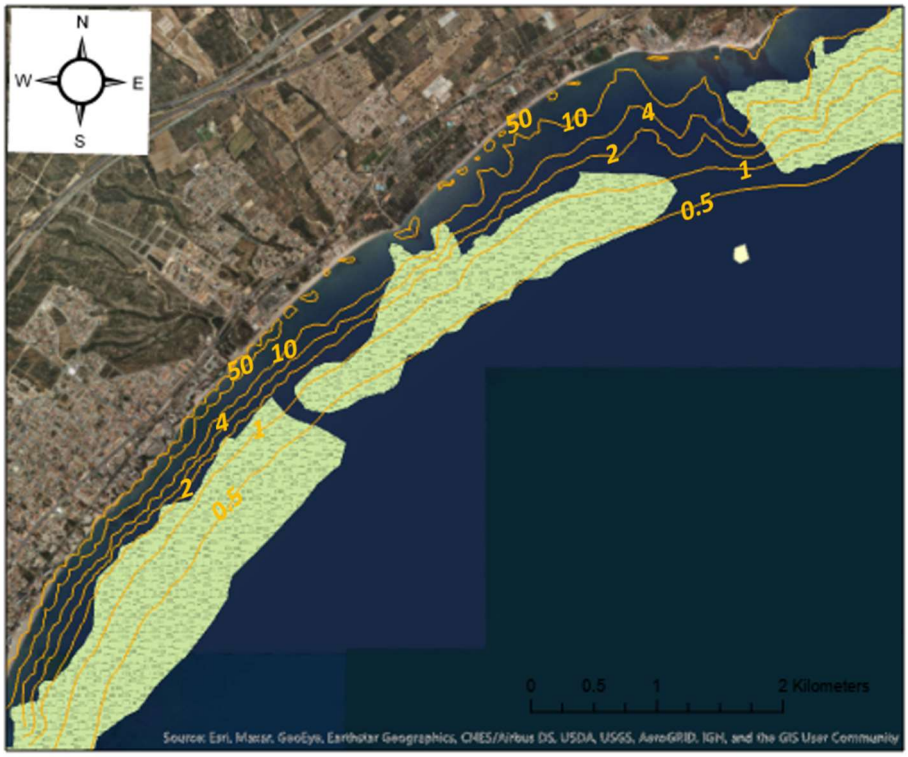

Figure 6.4 Dissipation (W/m^2) contours of current wave climate overlaid onto existing seagrass meadow locations

It appears as though on average the *Posidonia oceanica* prefers to lie along the 1 W/m^2 dissipation line. As the amount of energy being released increases closer to shore and dissipation is in the order of 2 W/m^2 or greater, this preferred condition is lost, which is why there is currently little to no seagrass in these areas. It is interesting that the seagrass patch in the northeast corner extends beyond even the 10 W/m^2 dissipation line. This could be because the bathymetry is most likely much shallower around the cape, increasing the submergence ratio significantly. From this result, it seems as though there is no exact energy threshold that *Posidonia oceanica* can thrive at since there are many other factors at play.

6.4.2 Without seagrass

Next, the impact of the existing bathymetry was investigated. Figure 6.5 shows the how the current energy dissipation is distributed as the depth decreases still with the assumption that there is no vegetation. In areas where the bathymetry is relatively homogeneous, it appears that dissipation is

occurring as expected, where it is concentrating up against the shoreline due to wave breaking. At the northern part of this segment of coastline, there is a wider shelf or plateau that exists around the cape. It makes sense that the dissipation increases where this plateau happens since the waves begin to feel the bottom in this area sooner than along the rest of the coast in this area. From this result, it can be concluded that the dissipation rate grows from 1-10 W/m^2 between the bottom contours of -10 m to -5 m.

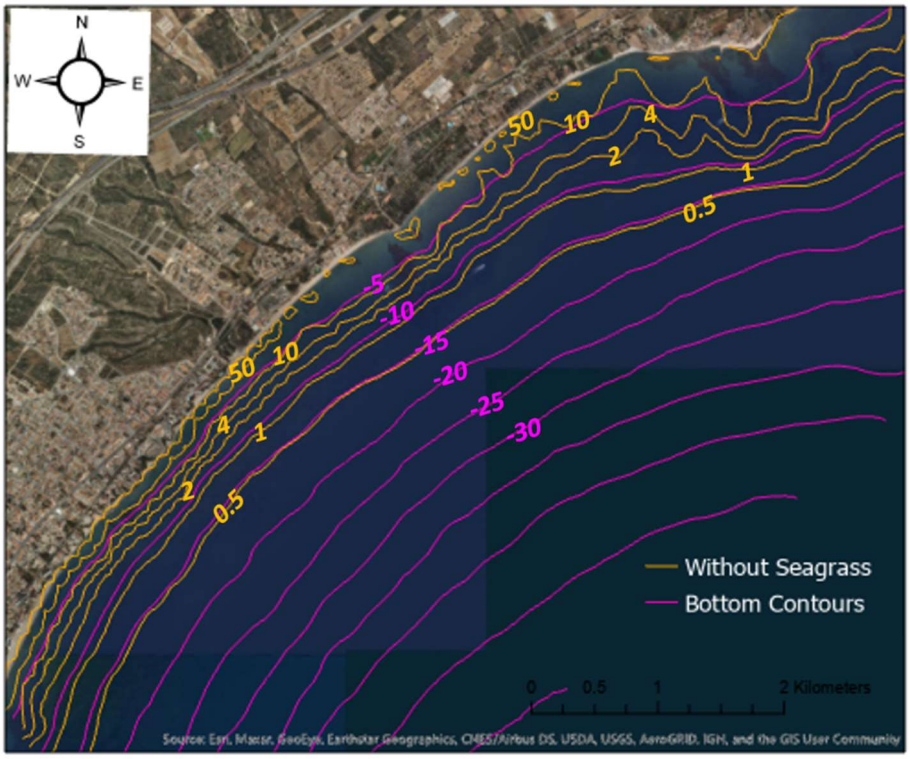

Figure 6.5 Dissipation (W/m^2) contours of current wave climate overlaid onto existing bathymetry

6.4.3 With seagrass

Now that the existing conditions had been analyzed, it was time to introduce a seagrass meadow layer into the SWAN model. The seagrass band was defined to be present at depths from -20 m to -10 m, which is why these are the main contours labeled in Figure 6.6. It can be seen that the dissipation lines have shifted further offshore, signifying that the waves are experiencing some attenuation before they reach the breaking zone closer to the shore. Interestingly, the dissipation lines look as if they have formed something similar to a plateau band over the vegetation range.

The cape in the northeast region again produced more unique results as the dissipation values are easily reaching high points above 10 W/m^2.

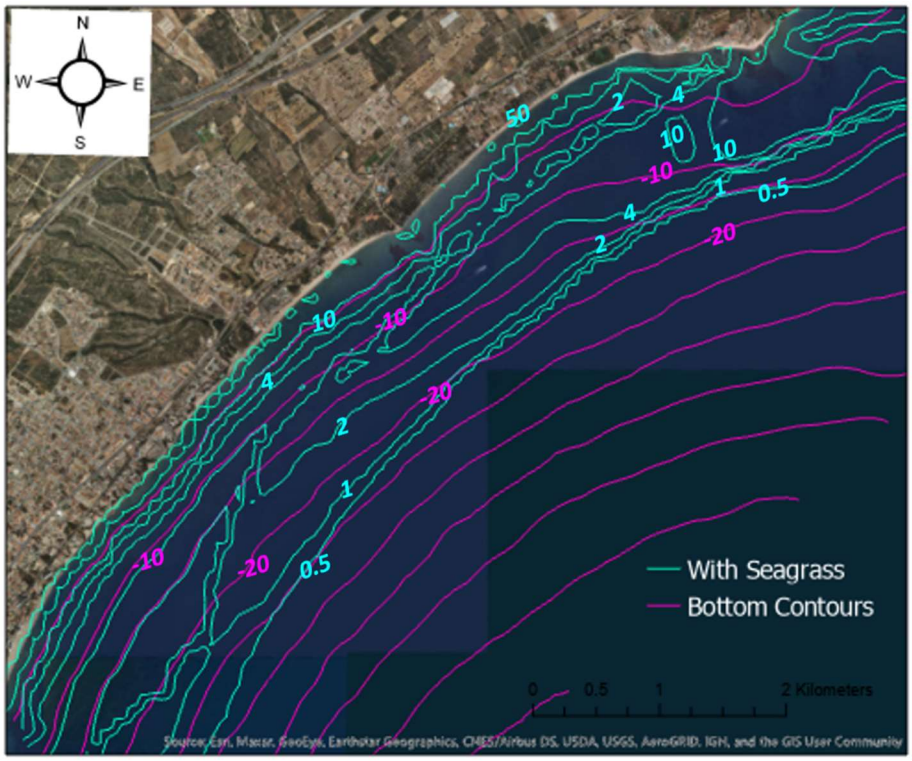

Figure 6.6 Dissipation (W/m^2) contours of attenuated wave climate overlaid onto existing bathymetry

6.4.4 Comparison

The remaining results use different techniques to compare the case without seagrass to the case with seagrass against each other. One way to compare these two scenarios is to lay them out side by side as is shown in Figure 6.7. The image on the left, dissipation rate without seagrass, portrays that there is little to no dissipation until the waves reach very shallow depths meaning that most of the wave energy is reaching shore. Contrary to that, the image on the right which accounts for seagrass, shows a band where energy is being dissipated at a higher rate further offshore so that a reduced amount is making it to the shore. The band seems to taper away closer to the southern part of the study area. The cause could be that this part of the coastline is experiencing higher wave heights that are occurring more frequently leading to a smaller influence of the seagrass meadow in this zone. It is difficult to say with higher certainty what is happening at both ends at this grid resolution.

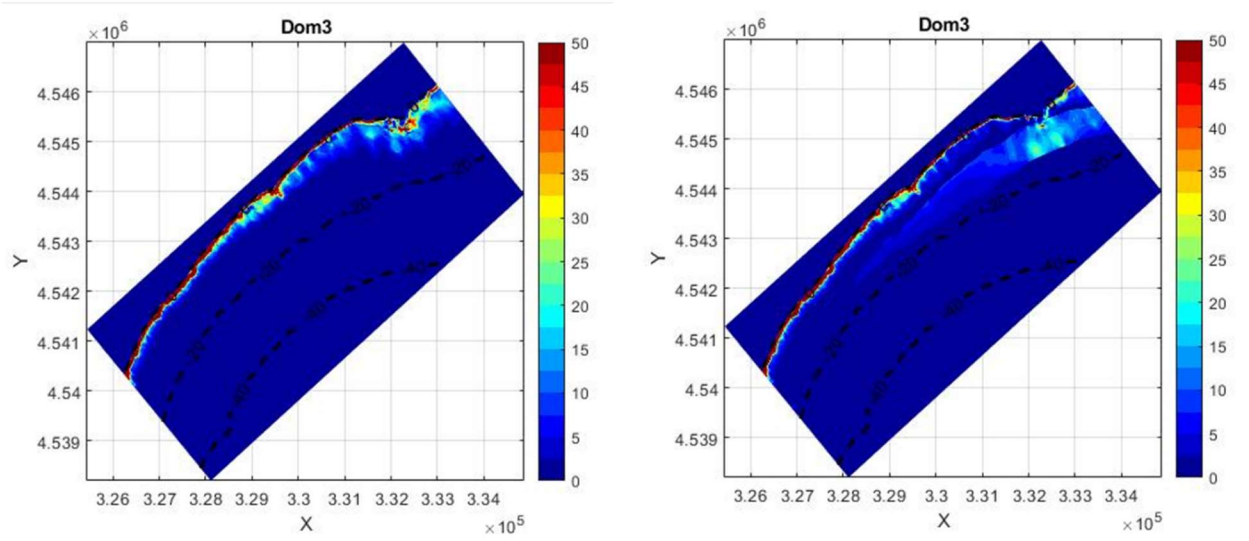

Figure 6.7 Total dissipation (W/m^2) over a year along the Baix Camp coast; without seagrass (left), with seagrass (right)

Figure 6.8 is the result of exporting the grids from Figure 6.7 and extracting the boundary lines of more distinct dissipation rate values. This figure helps visualize how much further out offshore each dissipation line moves when vegetation is added into the environment. It appears as though the 0.5, 1 and 2 W/m^2 lines have moved approximately twice as far offshore when a seagrass meadow with the specified set of parameters is present. That stronger band of dissipation is still seen parallel to the coastline in the north with a high concentration adjacent to the cape. The section lines A, B and C are explained and used later on in this section.

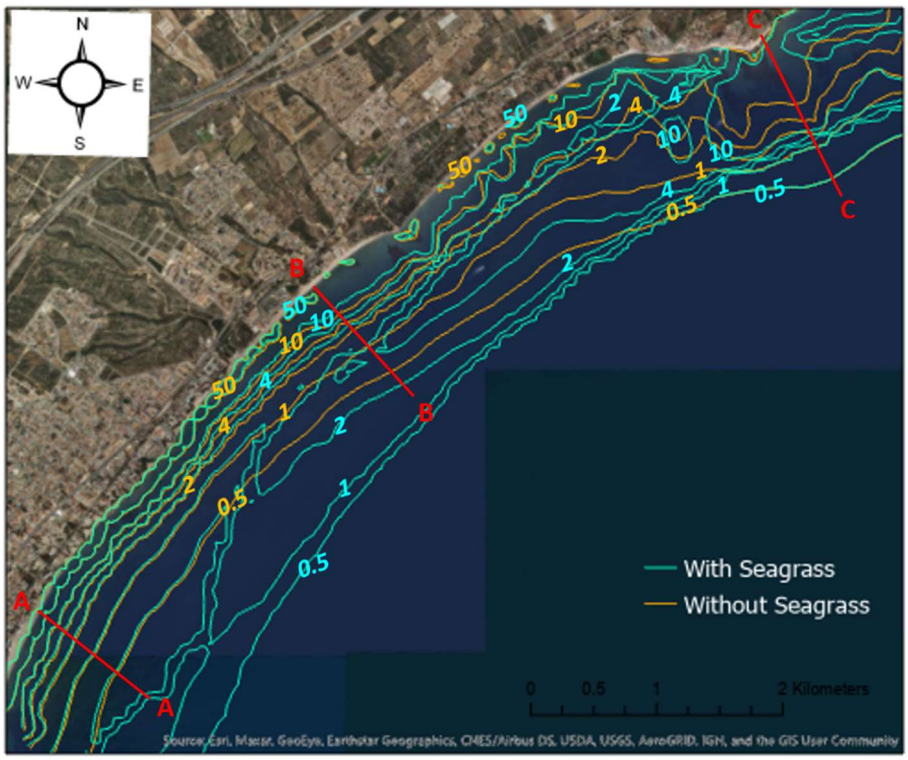

Figure 6.8 Dissipation (W/m^2) contours of current wave climate and attenuated wave climate

In addition to visual comparison of the dissipation contours, the transmission coefficient (K) was calculated for certain wave conditions to attain a more quantitative result for this application. Four out of the eight directional sectors were compared to determine whether direction, wave height or wave period had more influence on wave attenuation than the others. This was accomplished through dividing the significant wave height matrix of the scenario with seagrass by the significant wave height matrix of the scenario without seagrass to get a ratio. Here is where the sections A, B and C were used to make sure each region along the Baix Camp coast was being represented and to be able to catch any differences in the results. Since the proposed seagrass meadow was located at depths of 10-20 m, the K value was measured at approximately 8 m, so just shoreward of the meadow to determine the amount of attenuation that could be attributed to it as opposed to other sources. Table 6.1 is a summary of all these measurements for every wave condition considered. Waves coming from 123° and 138° were evaluated because they were assumed to show the most amount of wave height reduction since at these directions the waves would be coming in just about perpendicular to the coast. Waves coming from 93° and 168° were evaluated to explore if different

wave directions had an impact on the levels of dissipation. The wave heights and wave periods associated with these directions were taken from the contingency tables found in Appendix G.

Table 6.1 Transmission coefficients (K) measured at 8m deep contour (past vegetation band of 20-10m depth) on transects A, B and C for wave conditions with varying wave direction, height and period

Direction (°)	H_{morf} (m)	Tm02 (s)	K (A)	K (B)	K (C)
93	0.50	2	1	1	1
93	0.93	4	1	1	1
93	1.40	6	1	0.97	0.97
93	2.05	8	0.98	0.93	0.94
123	0.50	2	1	1	1
123	0.72	4	1	1	1
123	1.11	6	1	0.97	0.97
123	2.10	8	0.98	0.92	0.93
138	0.50	2	1	1	1
138	0.69	4	1	1	1
138	1.18	6	1	0.97	0.97
138	2.05	8	0.98	0.92	0.93
168	0.50	2	1	1	1
168	0.70	4	1	1	1
168	1.26	6	1	0.98	0.97
168	2.35	8	0.98	0.92	0.93

By looking at the values in this table, the wave direction does not appear to have much impact as the *K* values are nearly identically when comparing all four directions. As expected, the small wave heights and small wave periods are still being fully transmitted beyond the meadow ($K = 1$) since they most likely don't reach deep enough in the water column to feel any drag being generated by the vegetation below. Only at the higher wave heights and wave periods does the wave height reduction become apparent. It is noticeable that the wave attenuation trend is similar at sections B and C but at section A the seagrass has almost negligible influence. Using the proposed methodology, the percentage of wave height reduction will be in the 0-8% range per this table. In addition to finding a *K* at a single depth, *K* was measured at multiple locations along each of the three sections, starting at a depth of 20 m all the way to a depth of 0 m. The bottom profile along each transect is illustrated in Figure 6.9 and the coefficient *K* is plotted at the locations at which it was calculated.

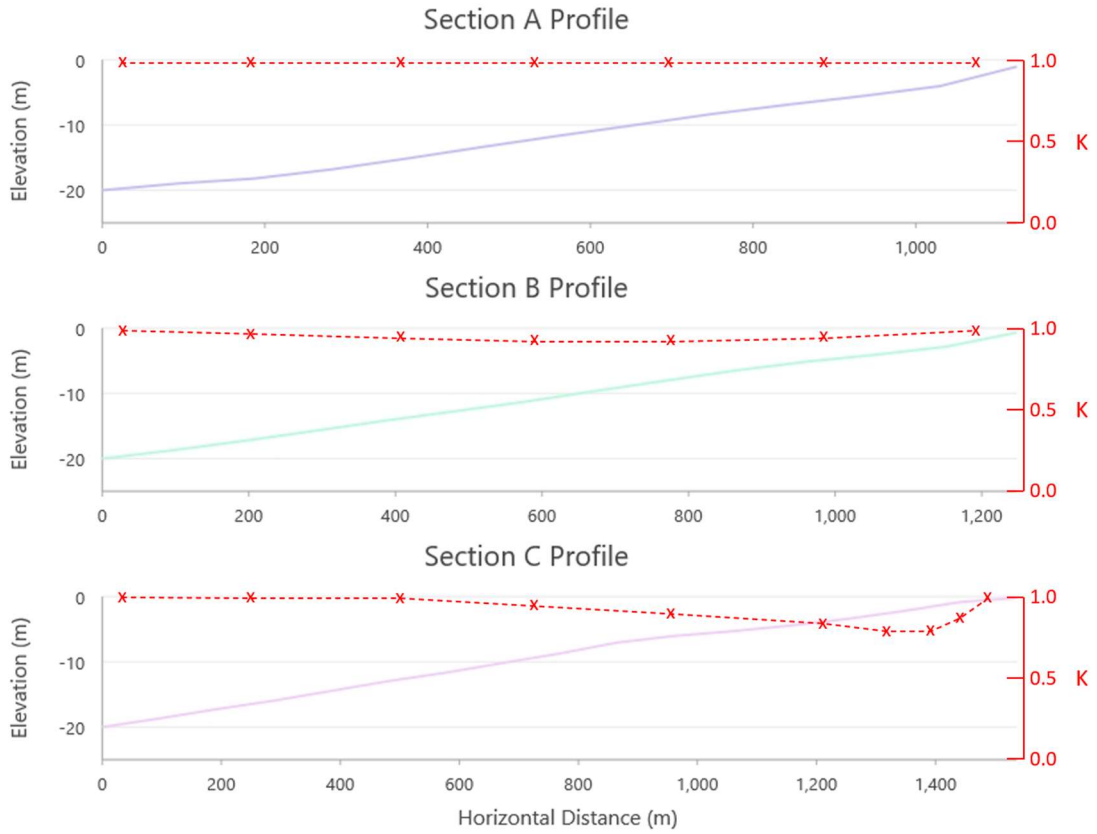

Figure 6.9 Transmission coefficient (K) along transects A, B and C (defined in Figure 6.8); bottom profiles shown from offshore (left) to onshore (right)

The A and B profiles demonstrate the trend that could be expected of the *K* profile after the waves pass the meadow. After around -10 m of elevation, the level of attenuation typically remains the same and eventually the wave height increases again due to shoaling. This trend doesn't seem to exist at section C. Instead, *K* continues to decrease at an increasing rate until the waves just about reach the shoreline. One explanation for this could be that there is a high concentration of wave rays near this location from refraction at the cape, which is something that doesn't happen where there is a more homogeneous bathymetry. This concentration of wave rays results in a high energy situation so the potential amount of energy that could be dissipated is much greater. When the seagrass meadow is introduced to the environment, more dissipation is induced because the densely concentrated energy scatters and the level diminishes from high to low.

7 Discussion

This section will emphasize and interpret the significant points identified in the results sections of Chapters 5 and 6. It will also discuss the limitations of the methods used and the uncertainties of these results with comparison to the findings of other relatable studies.

The results of the parameter sensitivity analysis indicated that none of the vegetation parameters had a significant impact on wave height for the range of values explored. The maximum difference was calculated to be 1.2% and that was reached by doubling the density of the meadow. This suggests that either the SWAN model is not sensitive enough to pick up on the small variations of these inputs or that the actual geometry of the individual plants and meadow is negligible compared to weight of the drag coefficient parameter. The geometry is limited to extreme minimum or maximum values while the drag coefficient can be adjusted to any number in theory. It could be useful to run the same kind of sensitivity analysis with a longer meadow (> 10 m) to see if the impact of any of the other variables becomes more apparent.

A C_d of 0.7 was calibrated to provide the best fit for the wave condition of the R2 case. When comparing the modeled and measured results using this value, the mean ratio for the R2 case is 1.01 and for the R1 case is 1.04. Although 1.04 is less than 5% from a perfect fit, it could still be improved by implementing a larger C_d value for the wave condition of the R1 case. This result builds on the existing evidence that as wave height is increased and the condition becomes more turbulent, the ability of the seagrass to attenuate energy tends to decrease because the vegetation either moves with the flow or becomes streamlined (Bradley and Houser, 2009; Zeller et al., 2014). It is probable that more of the blades are bent over or moving passively with the flow so less drag is being generated (Luhar et al., 2017) and the meadow can be characterized by a lower C_d. In higher energy cases it would be more accurate to include a bottom friction component to the physical processes the model should account for because although the drag is reduced, the canopy shear layer is now lower in the water column and the bed experiences a higher stress (Beudin et al., 2017). This part of the analysis could continue on indefinitely as there is potentially an endless number of parameter combinations that could improve the calibration depending on the conditions under consideration.

The reliability of the result is impacted by the limitations in SWAN to model this type of vegetation. As other authors have pointed out, it lacks the capacity to deal with complicated plant shapes, the swaying motion of the plant or mechanical interactions between plants (Beudin et al., 2017; Dijkstra and Uittenbogaard, 2010). Another limitation in SWAN is being able to input a variable drag coefficient. Currently, each run is defined by a fixed drag coefficient while in reality this value is sensitive to many different factors and can change over the length of the meadow. It experiences a decrease in areas of the meadow where the blades are in a collapsed position and the exposed frontal blade area is reduced (Bradley and Houser, 2009). Christie et al. (2018) applied this method for a salt marsh wave attenuation study by temporarily modifying the SWAN-Veg module to account for a varying C_d based on Re. They found that this strategy produced a better fit for high energy (storm) wave conditions than for initial wave heights less than 0.3 m in their flume study. This improvement would require further investigation to apply such an approach appropriately to seagrass but it is something to consider.

The results of the application of the model to the Baix Camp case carry a lot more uncertainty since it is no longer a controlled environment that is contained within a flume. Unlike the flume simulation, neither the bathymetry data file nor the computational grid was homogeneous. For example, the computational grid was set up with a mesh that had 10 m spacing in the horizontal direction but a 100 m spacing in the vertical direction. This led to a poor resolution of the raster layers created from this data which were used to generate the contours displayed in the figures. Creating an even finer grid would have smoothed out some of the results, especially between the water and land boundary, by reducing the exaggeration of high and low points. This is why the dissipation lines in the figures are mere approximations and only a select set of contours were chosen to be shown.

Since there haven't been prior studies that translate an experimental drag coefficient to a real case along the Spanish coast, a lot of the methodology for doing so was open to experimentation. The vegetation parameters were scaled as closely as possible from the lab tests and the dimensionless drag coefficient was taken to be the same assuming similar wave conditions were being compared.

The seagrass was modeled to exist between depths of 10-20 m based on the location of the existing seagrass in the region from the available seagrass cartography. This led to having a submergence ratio of 0.08 or smaller. In order to better relate to the submergence ratio of the flume experiments, the meadow could have been modeled to extend to shallower depths (approximately 5 m). Modeling from 5 m deep and deeper would also be in better agreement with Infantes et al. (2012) who state that *Posidonia oceanica* canopies often occupy less than 20% of the water column height. Additional model runs with a modified vegetation input layer could verify if this would have a significant impact on the results, but again, a refinement of the grid at shallower depths would be required.

From the dissipation analysis, the main observed result is that the dissipation rate is greater further seaward with a modeled seagrass meadow when compared to the condition that doesn't account for dissipation by vegetation. The results demonstrate that there is a jump in dissipation rate where the leading edge of the meadow lies. When comparing the transmission coefficients between the flume experiments and the Baix Camp case, the results indicate that they match up quite well. Wave height reduction rates were in the range of 4-7% for the R2 case and in the range of 0-8% for Baix Camp scenario. Both ranges are significantly lower than the maximum reduction of 35% and 40% measured in prior studies (Koftis et al., 2013; Luhar et al., 2017; Manca et al., 2012). This could suggest that these ranges are relatively robust, understanding that there are a lot of additional factors overlook in the Baix Camp case, and altering the parameters would have minimal impact on the outcome. The amount of wave reduction calculated still seems relatively low and supports the statement of Houser et al. (2014) that flexible vegetation provides little to no shoreline protection except with a very wide meadow with a high density. Looking back at the lab experimental setup, a meadow with low plant density was modeled, which could explain the high rates of wave transmission.

It is beyond the scope of this study but to make the model as realistic as possible there are several other factors that should be considered. First, the sediment dynamics at the Baix Camp coast need to be analyzed with and without the presence of seagrass. A different numerical model would need to be used since SWAN does not deal with the sediment aspect of the coastal environment. Only

then can the dynamic interactions between plant, water and sediment be better understood. The ability of seagrass to anchor into sand and prevent resuspension may be more effective as an erosion protection measure than the blades are at attenuating the waves before they reach shore. Second, with a changing climate it is important to account for sea level rise by introducing a changing water level into the model. Seagrass is a living plant and can adapt to rising sea levels but a threshold probably exists that needs to be identified. Finally, the analysis should take into account more biological factors of *Posidonia ocean* if it is to be used since seagrass is always changing with time. This model is an example of what the meadow could appear like but only at a single point in time. For example, the time of year could have a very strong influence on the coastal protection capabilities of the seagrass as they go through an annual cycle of growth and loss of leaves. In spring and summer, wave attenuation is highest correlating to the time period when the seagrass biomass is highest, while the opposite is true for fall and winter as water temperatures drop and storms become more frequent (CRAM, 2020; Reidenbach and Thomas, 2018). It would be beneficial if variable plant heights could be input into the model as it doesn't exist in a homogeneous state in the field. Currently, patches can be accounted for in the NPLANTS grid but it is not possible to input varying heights. Incorporating the effects of other organisms on the blades either living in or moving through the meadow would be another biological improvement to the simulation (Dijkstra and Uittenbogaard, 2010).

8 Conclusions

The model confirms that seagrass meadows do have an influence on hydrodynamics. For the average wave climate condition tested, a maximum wave height reduction of 8% can be expected with negligible change in wave period. A higher rate of wave reduction and energy dissipation can be achieved at very high densities and shallow depths where higher submergence ratios are present. The meadow behaves differently under varying wave conditions and therefore it is important to consider the most common or representative wave conditions for the given area of study. These results suggest that seagrass meadows could be more beneficial when applied in combination with harder structures especially in the fall and winter months when *Posidonia oceanica* is not as prevalent. Overall, the application of seagrass meadows for coastal protection needs to be evaluated on a case by case basis as this is a very site-specific solution. These results should be taken into account when considering promoting it for coastal management strategies and policies along the Spanish coastline.

References

Asano, T., Tsutsui, S., and Sakai, T. (1988). Wave damping characteristics due to seaweed. *Proceedings of 35th Coastal Engineering Conference in Japan,* (JSCE), pp.138-142.

Beudin, A., Kalra, T.S., Ganju, N.K. and Warner, J.C. (2017). Development of a coupled wave-flow-vegetation interaction model. *Computers & Geosciences*, 100, pp.76–86.

Booij, N., Ris, R. and Holthuijsen, L. (1999). A third-generation wave model for coastal regions: 1. Model description and validation. *Journal of Geophysical Research: Oceans*, 104(C4), pp.7649-7666.

Bradley, K. and Houser, C. (2009). Relative velocity of seagrass blades: Implications for wave attenuation in low-energy environments. *Journal of Geophysical Research*, 114(F1).

Cavallaro, L., Lo Re, C., Paratore, G., Viviano, A. and Foti, E. (2011). RESPONSE OF POSIDONIA OCEANICA TO WAVE MOTION IN SHALLOW-WATERS - PRELIMINARY EXPERIMENTAL RESULTS. *Coastal Engineering Proceedings*, 1(32), p.49.

Cavallaro, L., Viviano, A., Paratore, G. and Foti, E. (2018). Experiments on Surface Waves Interacting with Flexible Aquatic Vegetation. *Ocean Science Journal*, 53(3), pp.461–474.

Chen, H., Ni, Y., Li, Y., Liu, F., Ou, S., Su, M., Peng, Y., Hu, Z., Uijttewaal, W. and Suzuki, T. (2018). Deriving vegetation drag coefficients in combined wave-current flows by calibration and direct measurement methods. *Advances in Water Resources*, 122, pp.217–227.

Christie, E., Möller, I., Spencer, T. and Yates, M. (2018). MODELING WAVE ATTENUATION DUE TO SALTMARSH VEGETATION USING A MODIFIED SWAN MODEL. *Coastal Engineering Proceedings*, (36), p.73.

CRAM. (2020). *Praderas De Posidonia (Posidonia Oceanica)*. [online] Available at: https://cram.org/catalogo-de-especies/fondos-marinos/fanerogamas-marinas/praderas-de-posidonia/ [Accessed 30 March 2020].

Dalrymple, R.A., Kirby, J.T. and Hwang, P.A. (1984). Wave Diffraction Due to Areas of Energy Dissipation. *Journal of Waterway, Port, Coastal, and Ocean Engineering*, 110(1), pp.67–79.

de los Santos, C.B., Brun, F.G., Vergara, J.J. and Pérez-Lloréns, J.L. (2013). New aspect in seagrass acclimation: leaf mechanical properties vary spatially and seasonally in the temperate species Cymodocea nodosa Ucria (Ascherson). *Marine Biology*, 160(5), pp.1083–1093.

Dijkstra, J. and Uittenbogaard, R. (2010). Modeling the interaction between flow and highly flexible aquatic vegetation. *Water Resources Research*, 46(12).

Fonseca, M.S., Koehl, M.A.R. and Kopp, B.S. (2007). Biomechanical factors contributing to self-organization in seagrass landscapes. *Journal of Experimental Marine Biology and Ecology*, 340(2), pp.227–246.

Houser, C., Trimble, S. and Morales, B. (2014). Influence of Blade Flexibility on the Drag Coefficient of Aquatic Vegetation. *Estuaries and Coasts*, 38(2), pp.569–577.

Hydralab.eu. (2020). *HYDRALAB+*. [online] Available at: https://hydralab.eu/facilities--instruments/facilities-in-hydralab/Large-wave-flumes/CIEM/ [Accessed 30 March 2020].

Infantes, E., Orfila, A., Simarro, G., Terrados, J., Luhar, M. and Nepf, H. (2012). Effect of a seagrass (Posidonia oceanica) meadow on wave propagation. *Marine Ecology Progress Series*, 456, pp.63–72.

John, B.M., Mohit Babu, I., Shirlal, K.G. and Rao, S. (2018). Experimental Investigations of Wave Height Attenuation by Submerged Artificial Vegetation. *Hydrologic Modeling*, pp.499–509.

Kobayashi, N., Raichle, A.W. and Asano, T. (1993). Wave Attenuation by Vegetation. *Journal of Waterway, Port, Coastal, and Ocean Engineering*, 119(1), pp.30–48.

Koftis, T., Prinos, P. and Stratigaki, V. (2013). Wave damping over artificial Posidonia oceanica meadow: A large-scale experimental study. *Coastal Engineering*, 73, pp.71-83.

Luhar, M., Coutu, S., Infantes, E., Fox, S. and Nepf, H. (2010). Wave-induced velocities inside a model seagrass bed. *Journal of Geophysical Research*, 115(C12).

Luhar, M., Infantes, E., Orfila, A., Terrados, J. and Nepf, H.M. (2013). Field observations of wave-induced streaming through a submerged seagrass (Posidonia oceanica) meadow. *Journal of Geophysical Research: Oceans*, 118(4), pp.1955–1968.

Luhar, M. and Nepf, H.M. (2016). Wave-induced dynamics of flexible blades. *Journal of Fluids and Structures*, 61, pp.20–41.

Luhar, M., Infantes, E. and Nepf, H. (2017). Seagrass blade motion under waves and its impact on wave decay. *Journal of Geophysical Research: Oceans*, 122(5), pp.3736–3752.

Lynett, P.J., Gately, K., Wilson, R., Montoya, L., Arcas, D., Aytore, B., Bai, Y., Bricker, J.D., Castro, M.J., Cheung, K.F., David, C.G., Dogan, G.G., Escalante, C., González-Vida, J.M., Grilli, S.T., Heitmann, T.W., Horrillo, J., Kânoğlu, U., Kian, R., Kirby, J.T., Li, W., Macías, J., Nicolsky, D.J., Ortega, S., Pampell-Manis, A., Park, Y.S., Roeber, V., Sharghivand, N., Shelby, M., Shi, F., Tehranirad, B., Tolkova, E., Thio, H.K., Velioğlu, D., Yalçıner, A.C., Yamazaki, Y., Zaytsev, A. and Zhang, Y.J. (2017). Inter-model analysis of tsunami-induced coastal currents. *Ocean Modelling*, 114, pp.14–32.

Manca, E., Cáceres, I., Alsina, J.M., Stratigaki, V., Townend, I. and Amos, C.L. (2012). Wave energy and wave-induced flow reduction by full-scale model Posidonia oceanica seagrass. *Continental Shelf Research*, 50–51, pp.100–116.

Mazzella, L., Scipione, M.B. and Buia, M.C. (1989). Spatio-Temporal Distribution of Algal and Animal Communities in a Posidonia oceanica Meadow. *Marine Ecology*, 10(2), pp.107–129.

Mendez, F.J. and Losada, I.J. (2004). An empirical model to estimate the propagation of random breaking and nonbreaking waves over vegetation fields. *Coastal Engineering*, 51(2), pp.103–118.

Ondiviela, B., Losada, I., Lara, J., Maza, M., Galván, C., Bouma, T. and van Belzen, J. (2014). The role of seagrasses in coastal protection in a changing climate. *Coastal Engineering*, 87, pp.158-168.

Puertos del Estado (2019). *Clima medio de oleaje, Boya de Tarragona*. [online] Ministerio de Fomento. Available at: www.puertos.es [Accessed May 2020].

Reidenbach, M.A. and Thomas, E.L. (2018). Influence of the Seagrass, Zostera marina, on Wave Attenuation and Bed Shear Stress Within a Shallow Coastal Bay. *Frontiers in Marine Science*, 5.

Sánchez-González, J.F., Sánchez-Rojas, V. and Memos, C.D. (2011). Wave attenuation due to Posidonia oceanica meadows. *Journal of Hydraulic Research*, 49(4), pp.503–514.

Stratigaki, V., Manca, E., Prinos, P., Losada, I.J., Lara, J.L., Sclavo, M., Amos, C.L., Cáceres, I. and Sánchez-Arcilla, A. (2011). Large-scale experiments on wave propagation over Posidonia oceanica. *Journal of Hydraulic Research*, 49(sup1), pp.31–43.

Suzuki, T., Zijlema, M., Burger, B., Meijer, M. and Narayan, S. (2012). Wave dissipation by vegetation with layer schematization in SWAN. *Coastal Engineering*, 59(1), pp.64-71.

The SWAN team (2019). *SWAN Scientific and Technical Documentation*. SWAN Cycle III version 41.31 ed. Delft: Delft University of Technology.

The SWAN team (2019). *SWAN User Manual*. SWAN Cycle III version 41.31 ed. Delft: Delft University of Technology.

Telesca, L., Belluscio, A., Criscoli, A., Ardizzone, G., Apostolaki, E.T., Fraschetti, S., Gristina, M., Knittweis, L., Martin, C.S., Pergent, G., Alagna, A., Badalamenti, F., Garofalo, G., Gerakaris, V., Louise Pace, M., Pergent-Martini, C. and Salomidi, M. (2015). Seagrass meadows (Posidonia oceanica) distribution and trajectories of change. *Scientific Reports*, 5(1).

Zeller, R.B., Weitzman, J.S., Abbett, M.E., Zarama, F.J., Fringer, O.B. and Koseff, J.R. (2014). Improved parameterization of seagrass blade dynamics and wave attenuation based on numerical and laboratory experiments. *Limnology and Oceanography*, 59(1), pp.251–266.

Appendices

A Log of COBALTO Flume Experiments

Test	Waves		SWL	Filename	Profiles init. // meas.	time (min)	Remarks
1	0.1 m // 4.24 s	reg	2.0	260419_1	P0	1'	Tests to verify the real plant and surrogates movement.
2	0.4 m // 4 s	reg	2.0	260419_2		1'	
3	0.8 m // 4 s	reg	2.0	260419_3		1'	
4	0.2 m // 2.83 s	reg	2.0	260419_4		1'	
5	0.4 m // 2.83 s	reg	2.0	260419_5		1'	
6	0.4 m // 2.47 s	reg	2.0	260419_6		1'	
7	0.2 m // 2.47 s	reg	2.0	260419_7		1'	
8	0.5 m // 2.12 s	reg	2.0	260419_8		1'	
9	0.25 m // 2.12 s	reg	2.0	260419_9		1'	
10	0.35 m // 3.54 s	reg	2.0	260419_10		1'	
11	0.18 m // 3.54 s	reg	2.0	260419_11		1'	
12	0.2 m // 4.24 s	reg	2.0	260419_12		1'	
13	1 m // 3 s	reg	2.0	260419_13		1'	
14	0.1 m // 4.24 s	reg	2.0	260419_14		1'	
15	0.5 m // 3 s	reg	2.0	260419_15		1'	
16	0.8 m // 3.5 s	reg	2.0	260419_16		1'	
17	0.4 m // 3.5 s	reg	2.0	260419_17		1'	
18	0.6 m // 5 s	reg	2.0	260419_18		1'	
19	0.36 m // 5 s	reg	2.0	260419_19		1'	
20	0.4 m // 6 s	reg	2.0	260419_20		1'	
21	0.2 m // 6 s	reg	2.0	260419_21		1'	
							Install AWG, ADV and change connections. Redo the profile. Fill the flume and calibration
22	0.41 m // 3.71 s	rand	2.0	080519_0	P0 // P1	25 '	Jonswap, gamma 3.3, seeding number 1 (xtape = 44.46 m)
23	0.41 m // 3.71 s	rand	2.0	080519_1	P0 // P2		Upper ADV emerged. (xtape = 48.5 m)
24	0.41 m // 3.71 s	rand	2.0	080519_2	P0 // P3		(xtape = 40 m)
25	0.41 m // 3.71 s	rand	2.0	080519_3	P0 // P4		(xtape = 33.32 m)
26	0.41 m // 3.71 s	rand	2.0	080519_4	P0 // P5		(xtape = 26.192 m)
27	0.41 m // 3.71 s	rand	2.0	080519_5	P0 // P6		(xtape = 44.46 m)
28	0.41 m // 3.71 s	rand	2.0	080519_6	P0 // P7		Upper ADV is most of time emerged. (xtape = 48.53 m)

							At the end of this day the ADV sampling volume were changed to 2.4/9.1 for all ADVs
29	0.41 m // 3.71 s	rand	2.0	090519_0	P0 // P8		(xtape = 44.46 m)
30	0.41 m // 3.71 s	rand	2.0	090519_1	P0 // P9		Pc2 for Adv did not trigger properly and the recording started around 3 s later than usual. (xtape = 48.53 m)
31	0.41 m // 3.71 s	rand	2.0	090519_2	P0 // P10		(xtape = 40 m)
32	0.41 m // 3.71 s	rand	2.0	090519_3	P0 // P11		(xtape = 33.32 m)
33	0.41 m // 3.71 s	rand	2.0	090519_4	P0 // P12		At the beginning of this test x00 = 63.43. (xtape = 26.291 m)
							Empty the flume and redo the profile.
34	0.6 m // 3.71 s	rand	2.0	150519_0	P13 // P14		(xtape = 44.46 m)
35	0.6 m // 3.71 s	rand	2.0	150519_1	P13 // P15		(xtape = 48.5 m)
36	0.6 m // 3.71 s	rand	2.0	150519_2	P13 // P16		(xtape = 40 m)
37	0.6 m // 3.71 s	rand	2.0	160519_0	P13 // P17		(xtape = 33.32 m)
38	0.6 m // 3.71 s	rand	2.0	160519_1	P13 // P18		(xtape = 26.196 m)
39	0.6 m // 3.71 s	rand	2.0	160519_2	P13 // P19		(xtape = 44.46 m)
40	0.6 m // 3.71 s	rand	2.0	160519_3	P13 // P20		(xtape = 48.53 m). Different Freq for adv pc_1 and pc_2
41	0.6 m // 3.71 s	rand	2.0	160519_4	P13 // P21		(xtape = 44.46 m). Different Freq for adv pc_1 and pc_2
42	0.6 m // 3.71 s	rand	2.0	160519_5	P13 // P22		(xtape = 48.53 m). Different Freq for adv pc_1 and pc_2
43	0.6 m // 3.71 s	rand	2.0	170519_0	P13 // P23		(xtape = 40 m).
44	0.6 m // 3.71 s	rand	2.0	170519_1	P13 // P24		(xtape = 33.32 m)
45	0.6 m // 3.71 s	rand	2.0	170519_2	P13 // P25		(xtape = 26.196 m)
							Empty the flume and redo the profile. We place the meadow on the flume
46	0.41 m // 3.71 s	rand	2.0	220719_0	P26 // P27		(xtape = 44.46 m)
47	0.41 m // 3.71 s	rand	2.0	220719_1	P26 // P28		(xtape = 48.5 m)
48	0.41 m // 3.71 s	rand	2.0	220719_2	P26 // P29		(xtape = 40 m)
49	0.41 m // 3.71 s	rand	2.0	220719_3	P26 // P30		(xtape = 33.32 m)
50	0.41 m // 3.71 s	rand	2.0	230719_0	P26 // P31		(xtape = 26.12 m)
51	0.41 m // 3.71 s	rand	2.0	230719_1	P26 // P32		(xtape = 44.46 m)
52	0.41 m // 3.71 s	rand	2.0	230719_2	P26 // P33		(xtape = 48.53 m)
53	0.41 m // 3.71 s	rand	2.0	230719_3	P26 // P34		(xtape = 44.46 m)
54	0.41 m // 3.71 s	rand	2.0	230719_4	P26 // P35		(xtape = 48.53 m)
55	0.41 m // 3.71 s	rand	2.0	240719_0	P26 // P36		(xtape = 39.94 m)
56	0.41 m // 3.71 s	rand	2.0	240719_1	P26 // P37		(xtape = 33.32 m)
57	0.41 m // 3.71 s	rand	2.0	240719_2	P26 // P38		(xtape = 26.146 m)

58	0.6 m // 3.71 s	rand	2.0	240719_3	P26 // NaN		Run to test if the meadow holds this energetic case.
							Empty the flume and redo the profile.
59	0.6 m // 3.71 s	rand	2.0	040919_0	P39 // P40		(xtape = 44.46 m)
60	0.6 m // 3.71 s	rand	2.0	040919_1	P39 // P41		(xtape = 48.5 m). ADV 3 from pc1 has been removed from acquisition system
61	0.6 m // 3.71 s	rand	2.0	040919_2	P39 // P42		(xtape = 40 m). ADV 3 from pc1 has been removed from acquisition system
62	0.6 m // 3.71 s	rand	2.0	040919_3	P39 // P43		(xtape = 33.32 m). ADV 3 from pc1 has been removed from acquisition system
63	0.6 m // 3.71 s	rand	2.0	040919_4	P39 // P44		(xtape = 26.19 m). ADV 3 from pc1 has been removed from acquisition system
64	0.6 m // 3.71 s	rand	2.0	040919_5	P39 // P45		(xtape = 44.46 m). ADV 3 from pc1 has been removed from acquisition system
65	0.6 m // 3.71 s	rand	2.0	050919_0	P39 // P46		(xtape = 48.5 m). ADV 3 from pc1 has been removed from acquisition system
66	0.6 m // 3.71 s	rand	2.0	050919_1	P39 // P47		(xtape = 44.46 m). ADV 3 from pc1 has been removed from acquisition system
67	0.6 m // 3.71 s	rand	2.0	050919_2	P39 // P48		(xtape = 48.5 m). ADV 3 from pc1 has been removed from acquisition system
68	0.6 m // 3.71 s	rand	2.0	050919_3	P39 // P49		(xtape = 40 m). ADV 3 from pc1 has been removed from acquisition system
69	0.6 m // 3.71 s	rand	2.0	050919_4	P39 // P50		(xtape = 33.32 m). ADV 3 from pc1 has been removed from acquisition system
70	0.6 m // 3.71 s	rand	2.0	050919_5	P39 // P51		(xtape = 26.192 m). ADV 3 from pc1 has been removed from acquisition system

B Significant Wave Heights from WGs, AWGs and PPTs

BMR1 H_s (m) at Sensor Locations								
x (m)	WG (spectral)	WG (zerocrossing)	x (m)	AWG (spectral)	AWG (zerocrossing)	x (m)	PPT (spectral)	PPT (zerocrossing)
10.86	0.370	0.364	24.84	0.398	0.369	22.26	0.368	0.353
31.93	0.361	0.353	18.18	0.380	0.354	20.51	0.369	0.352
26	0.389	0.377	61.43	0.454	0.544	24.03	0.369	0.354
27.53	0.391	0.379	48.53	0.386	0.364	30.8	0.371	0.359
39.05	0.377	0.366	53.65	0.371	0.378	33.67	0.371	0.357
47.13	0.390	0.378	59.83	0.410	0.482	55.54	0.379	0.367
51.08	0.355	0.356	57.17	0.392	0.431	36.9	0.372	0.360
35.03	0.350	0.341	29.31	0.379	0.350	41.04	0.366	0.352
52.6	0.405	0.411	73.27	0.022	0.016	45.11	0.382	0.371
54.11	0.376	0.399	62.75	0.320	0.343	49.83	0.384	0.370
55.54	0.379	0.416	64.24	0.299	0.307	58.61	0.333	0.326
43.11	0.419	0.407	65.74	0.243	0.226	61.6	0.311	0.295
10.86	0.369	0.363	67.22	0.197	0.167	59.55	0.339	0.353
			69.02	0.146	0.114	64.37	0.273	0.263
			70.31	0.079	0.063	31.945	NaN	NaN
			71.74	0.034	0.019			
			37.01	0.144	0.121			

BMR2 H_s (m) at Sensor Locations								
x (m)	WG (spectral)	WG (zerocrossing)	x (m)	AWG (spectral)	AWG (zerocrossing)	x (m)	PPT (spectral)	PPT (zerocrossing)
10.86	0.554	0.546	24.84	0.601	0.566	22.26	0.531	0.504
31.93	0.525	0.519	18.18	0.573	0.544	20.51	0.536	0.504
26	0.561	0.542	61.43	0.704	0.732	24.03	0.529	0.503
27.53	0.567	0.548	48.53	0.592	0.569	30.8	0.534	0.512
39.05	0.506	0.491	53.65	0.520	0.544	33.67	0.539	0.510
47.13	0.564	0.548	59.83	0.571	0.605	55.54	0.519	0.486
51.08	1.531	1.530	57.17	0.539	0.577	36.9	0.532	0.507
35.03	0.501	0.484	29.31	0.559	0.533	41.04	0.526	0.499
52.6	0.568	0.584	73.27	0.039	0.024	45.11	0.549	0.522
54.11	0.527	0.594	62.75	0.392	0.391	49.83	0.548	0.517
55.54	0.521	0.597	64.24	0.344	0.325	58.61	0.436	0.394
43.11	0.680	0.665	65.74	0.292	0.266	61.6	0.367	0.322
10.86	0.548	0.542	67.22	0.257	0.206	59.55	0.423	0.402
			69.02	0.214	0.170	64.37	0.322	0.296
			70.31	0.156	0.139	31.945	NaN	NaN
			71.74	0.090	0.069			
			37.01	0.831	0.607			

R1 H_s (m) at Sensor Locations								
x (m)	WG (spectral)	WG (zerocrossing)	x (m)	AWG (spectral)	AWG (zerocrossing)	x (m)	PPT (spectral)	PPT (zerocrossing)
10.86	0.396	0.389	24.84	0.412	0.389	22.26	0.359	0.344
31.93	0.363	0.357	18.18	0.393	0.374	20.51	0.361	0.343
26	3.014	2.914	61.43	0.506	0.633	24.03	0.365	0.351
27.53	0.423	0.407	48.53	0.374	0.354	30.8	0.370	0.359
39.05	2.543	2.448	53.65	0.349	0.348	33.67	0.363	0.350
47.13	0.383	0.366	59.83	0.396	0.466	55.54	0.361	0.346
51.08	0.954	0.941	57.17	0.368	0.399	36.9	0.358	0.345
35.03	0.354	0.342	29.31	0.388	0.366	41.04	0.343	0.328
52.6	0.398	0.398	73.27	0.023	0.017	45.11	0.359	0.344
54.11	0.367	0.382	62.75	0.304	0.335	49.83	0.363	0.348
55.54	0.371	0.400	64.24	5.738	6.540	58.61	0.316	0.306
43.11	0.344	0.331	65.74	0.231	0.217	61.6	0.299	0.286
10.86	88.933	85.016	67.22	0.185	0.159	59.55	0.328	0.335
			69.02	0.135	0.106	64.37	0.271	0.264
			70.31	0.071	0.051	31.941	NaN	NaN
			71.74	0.032	0.020			
			37.01	0.541	0.433			

R2 H_s (m) at Sensor Locations								
x (m)	WG (spectral)	WG (zerocrossing)	x (m)	AWG (spectral)	AWG (zerocrossing)	x (m)	PPT (spectral)	PPT (zerocrossing)
10.86	0.535	0.533	24.84	0.597	0.564	22.26	0.525	0.498
31.93	0.516	0.517	18.18	0.570	0.541	20.51	0.522	0.489
26	0.570	0.551	61.43	0.658	0.693	24.03	0.527	0.502
27.53	4.695	4.551	48.53	0.545	0.524	30.8	0.532	0.510
39.05	0.574	0.555	53.65	0.501	0.518	33.67	0.526	0.499
47.13	0.536	0.515	59.83	0.552	0.621	55.54	0.499	0.470
51.08	0.502	0.501	57.17	0.528	0.581	36.9	0.516	0.491
35.03	0.491	0.476	29.31	0.564	0.541	41.04	0.495	0.467
52.6	0.546	0.556	73.27	0.044	0.026	45.11	0.518	0.489
54.11	0.508	0.558	62.75	0.386	0.379	49.83	0.515	0.486
55.54	0.506	0.569	64.24	0.346	0.333	58.61	0.417	0.385
43.11	0.522	0.500	65.74	0.290	0.270	61.6	0.375	0.329
10.86	0.536	0.536	67.22	0.252	0.210	59.55	0.422	0.403
			69.02	0.210	0.159	64.37	0.325	0.301
			70.31	0.159	0.135	31.941	NaN	NaN
			71.74	0.095	0.078			
			37.01	0.794	0.589			

C SWAN input file example

```
!************** HEADING ************************************
! R2 with Hs 0.570m, Tp 3.828s from second sensor
! R2 calibrated to Hs 0.549m, Tp 3.828s
!
PROJect  'COBALTO'  'R2'
!
!*************** MODEL INPUT *********************************
!
SET 0 90 0.05 200 1 9.81 1000
!
MODE STATionary ONEDimensional
!
COORDinates CARTesian
!
CGRID REGular 0 0 0 86 0 4300 0 SECtor -10 10 201 0.1 1.0 200
!
INPgrid BOTtom REGular 0 0 0 4300 0 0.02
READinp BOTtom 1 'R2.bot' 1 0 FREe
!
INPgrid NPLAnts REGular 0 0 0 4300 0 0.02
READinp NPLAnts 1 'posidonia.den' 1 0 FREe
!
BOUnd SHAPespec JONswap 3.3 PEAK DSPR POWer
!BOUndspec SIDE West CCW CONstant PAR 0.570 3.828 0 800
BOUndspec SIDE West CCW CONstant PAR 0.549 3.828 0 800
!
OFF WCAP
OFF QUADrupl
OFF BREaking
!
!          height   stem diameter  nr of stems   Cd
VEGEtation  0.4        0.008          269        0.7
!
!************** OUTPUT REQUESTS ****************************************
!
CURVE 'LINE1' 0 0 100 100 0
POINTS 'SensR2' 10.9 0 18.2 0 20.5 0 22.3 0 24 0 24.8 0 26 0 27.5 0 29.3 0 30.8 0 31.9 0
33.7 0 35 0 36.9 0 37 0 39.1 0 41 0 43.1 0 45.1 0 47.1 0 48.5 0 49.8 0
!POINTs 'SPEC24' 24 0
!POINTs 'SPEC34' 33.7 0
!POINTs 'SPEC45' 45.1 0
!
TABLE   'LINE1'  HEADer 'R2.tab' DIST DEP HSign RTP TM01 TM02 FSPR DIR DSPR WLENgth DISVeg
!TABLE   'SensR2'  HEADer 'SensR2.tab' XP DEP HSign RTP TM01
!SPECout 'SPEC24' SPEC1D ABSolute 'R224.txt'
!SPECout 'SPEC34' SPEC1D ABSolute 'R234.txt'
!SPECout 'SPEC45' SPEC1D ABSolute 'R245.txt'
!
TEST 1 0
COMPute
STOP
```

D SWAN Vegetation Parameter Sensitivity Analysis

	Values in table represent the % change in significant wave height compared to control case													
Location (m)	**h1 0.5 m**	**h2 0.4 m**	**h3 0.3 m**	**d1 0.0048 m**	**d2 0.0044 m**	**d3 0.0036 m**	**d4 0.0032 m**	**n1 336**	**n2 404**	**n3 538**	**c1 0.1**	**c2 0.15**	**c3 0.25**	**c4 0.3**
30	0	0	0	0	0	0	0	0	0	0	0	0	0	0
30.5	0	0	0	0	0	0	0	0	0	0	0	0	0	0
31	0	0	0	0	0	0	0	0	0	0.1	0	0	0	0
31.5	0	-0.1	-0.1	0	0	0	0	0	0.1	0.2	-0.1	0	0	0.1
32	0	-0.1	-0.1	0	0	0	0	0.1	0.1	0.2	-0.1	-0.1	0.1	0.1
32.5	0	-0.1	-0.1	0.1	0	0	-0.1	0.1	0.1	0.3	-0.1	-0.1	0.1	0.1
33	-0.1	-0.1	-0.2	0.1	0	0	-0.1	0.1	0.2	0.3	-0.2	-0.1	0.1	0.2
33.5	-0.1	-0.1	-0.2	0.1	0	0	-0.1	0.1	0.2	0.4	-0.2	-0.1	0.1	0.2
34	-0.1	-0.2	-0.2	0.1	0	0	-0.1	0.1	0.2	0.5	-0.2	-0.1	0.1	0.2
34.5	-0.1	-0.2	-0.3	0.1	0.1	-0.1	-0.1	0.1	0.3	0.5	-0.3	-0.1	0.1	0.3
35	-0.1	-0.2	-0.3	0.1	0.1	-0.1	-0.1	0.1	0.3	0.6	-0.3	-0.2	0.1	0.3
35.5	-0.1	-0.2	-0.3	0.1	0.1	-0.1	-0.1	0.2	0.3	0.7	-0.3	-0.2	0.2	0.3
36	-0.1	-0.3	-0.4	0.1	0.1	-0.1	-0.1	0.2	0.4	0.7	-0.4	-0.2	0.2	0.4
36.5	-0.1	-0.3	-0.4	0.2	0.1	-0.1	-0.2	0.2	0.4	0.8	-0.4	-0.2	0.2	0.4
37	-0.2	-0.3	-0.4	0.2	0.1	-0.1	-0.2	0.2	0.4	0.8	-0.4	-0.2	0.2	0.4
37.5	-0.2	-0.3	-0.5	0.2	0.1	-0.1	-0.2	0.2	0.5	0.9	-0.5	-0.2	0.2	0.5
38	-0.2	-0.3	-0.5	0.2	0.1	-0.1	-0.2	0.2	0.5	1	-0.5	-0.2	0.2	0.5
38.5	-0.2	-0.4	-0.5	0.2	0.1	-0.1	-0.2	0.3	0.5	1	-0.5	-0.3	0.3	0.5
39	-0.2	-0.4	-0.6	0.2	0.1	-0.1	-0.2	0.3	0.6	1.1	-0.6	-0.3	0.3	0.6
39.5	-0.2	-0.4	-0.6	0.2	0.1	-0.1	-0.2	0.3	0.6	1.2	-0.6	-0.3	0.3	0.6
40	-0.2	-0.4	-0.6	0.2	0.1	-0.1	-0.2	0.3	0.6	1.2	-0.6	-0.3	0.3	0.6
40.5	-0.2	-0.4	-0.7	0.3	0.1	-0.1	-0.3	0.3	0.6	1.2	-0.6	-0.3	0.3	0.6
41	-0.2	-0.4	-0.7	0.3	0.1	-0.1	-0.3	0.3	0.6	1.2	-0.6	-0.3	0.3	0.6
41.5	-0.2	-0.4	-0.7	0.3	0.1	-0.1	-0.3	0.3	0.6	1.2	-0.6	-0.3	0.3	0.6
42	-0.2	-0.4	-0.7	0.3	0.1	-0.1	-0.3	0.3	0.6	1.2	-0.6	-0.3	0.3	0.6
42.5	-0.2	-0.4	-0.7	0.3	0.1	-0.1	-0.3	0.3	0.6	1.2	-0.6	-0.3	0.3	0.6
43	-0.2	-0.4	-0.7	0.2	0.1	-0.1	-0.3	0.3	0.6	1.2	-0.6	-0.3	0.3	0.6
43.5	-0.2	-0.4	-0.7	0.3	0.1	-0.1	-0.3	0.3	0.6	1.2	-0.6	-0.3	0.3	0.6
44	-0.2	-0.4	-0.7	0.3	0.1	-0.1	-0.3	0.3	0.6	1.2	-0.6	-0.3	0.3	0.6
44.5	-0.2	-0.4	-0.7	0.3	0.1	-0.1	-0.3	0.3	0.6	1.2	-0.6	-0.3	0.3	0.6
45	-0.2	-0.4	-0.7	0.3	0.1	-0.1	-0.3	0.3	0.6	1.2	-0.6	-0.3	0.3	0.6
45.5	-0.2	-0.4	-0.7	0.2	0.1	-0.1	-0.3	0.3	0.6	1.2	-0.6	-0.3	0.3	0.6
46	-0.2	-0.4	-0.7	0.3	0.1	-0.1	-0.3	0.3	0.6	1.2	-0.6	-0.3	0.3	0.6
46.5	-0.2	-0.4	-0.7	0.2	0.1	-0.1	-0.3	0.3	0.6	1.2	-0.6	-0.3	0.3	0.6
47	-0.2	-0.4	-0.6	0.2	0.1	-0.1	-0.3	0.3	0.6	1.2	-0.6	-0.3	0.3	0.6
47.5	-0.2	-0.4	-0.6	0.3	0.1	-0.1	-0.2	0.3	0.6	1.2	-0.6	-0.3	0.3	0.6
48	-0.2	-0.4	-0.6	0.2	0.1	-0.1	-0.3	0.3	0.6	1.2	-0.6	-0.3	0.3	0.6
48.5	-0.2	-0.4	-0.6	0.2	0.1	-0.1	-0.2	0.3	0.6	1.2	-0.6	-0.3	0.3	0.6
49	-0.2	-0.4	-0.6	0.2	0.1	-0.1	-0.2	0.3	0.6	1.2	-0.6	-0.3	0.3	0.6
49.5	-0.2	-0.4	-0.6	0.3	0.1	-0.1	-0.2	0.3	0.6	1.2	-0.6	-0.3	0.3	0.6
50	-0.2	-0.4	-0.6	0.2	0.1	-0.1	-0.2	0.3	0.6	1.2	-0.6	-0.3	0.3	0.6

E Supplemental SWAN results

Comparison of modeled to measured H_s values for BMR1, BMR2 and R1

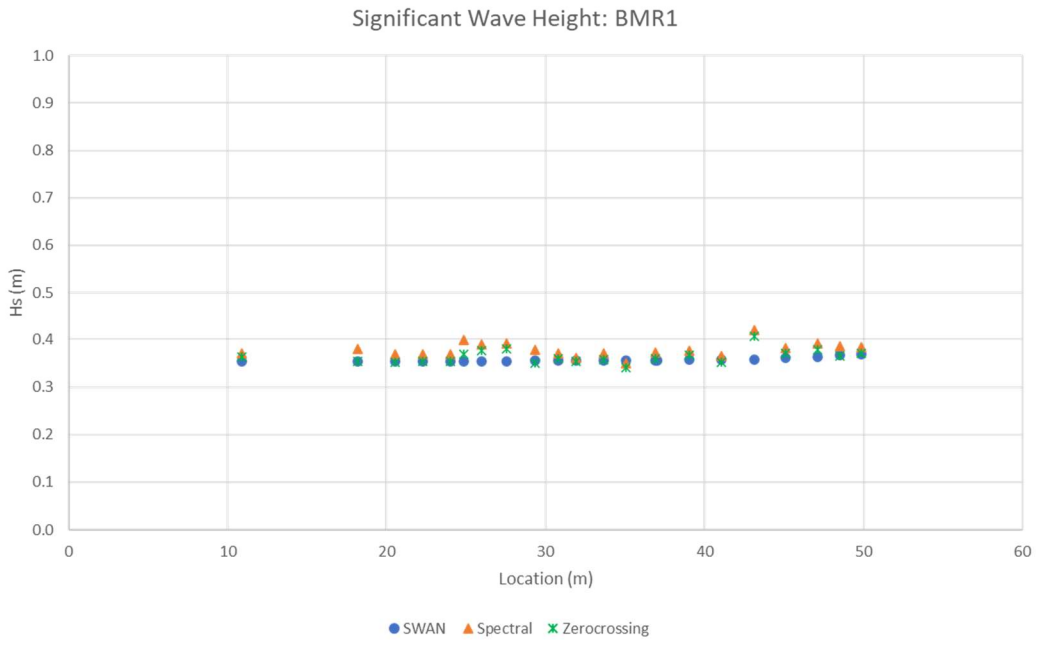

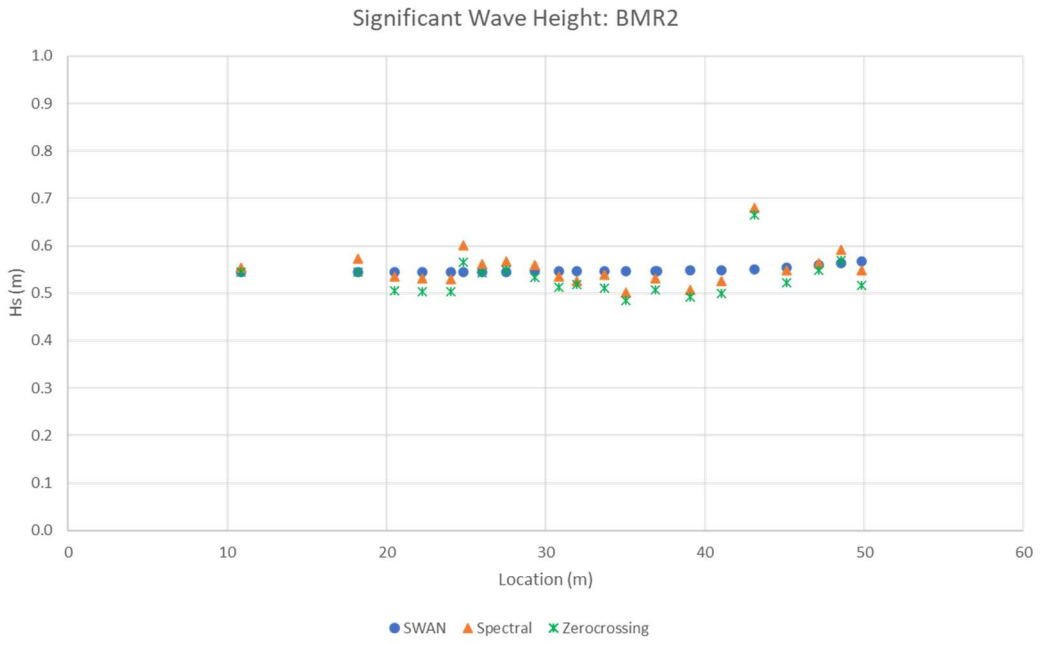

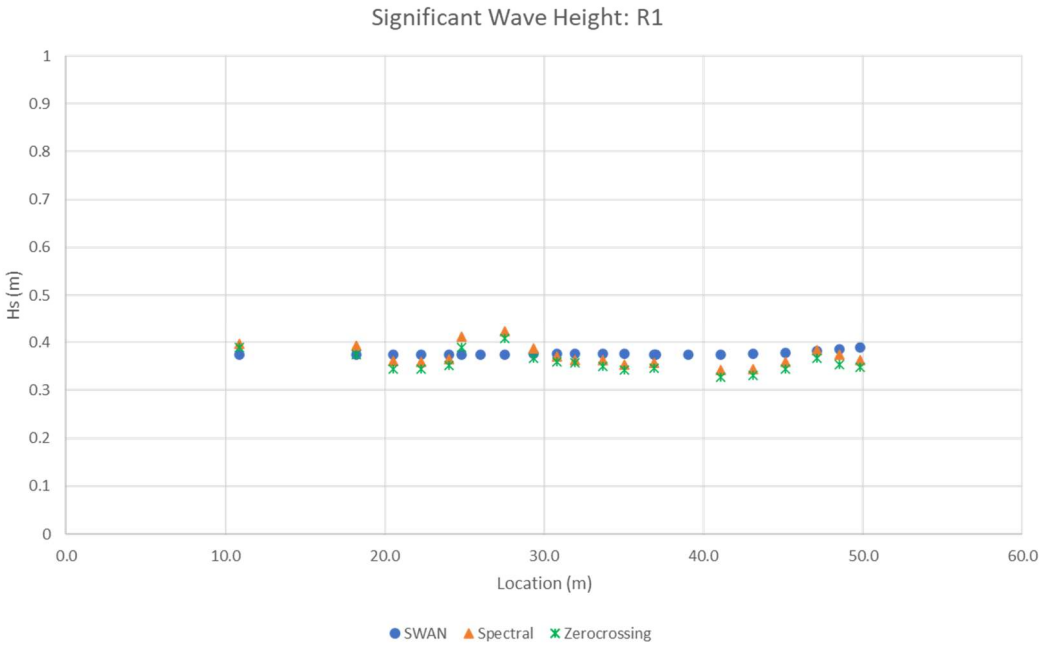

Energy spectrum comparison between measured and modeled results

BMR1:

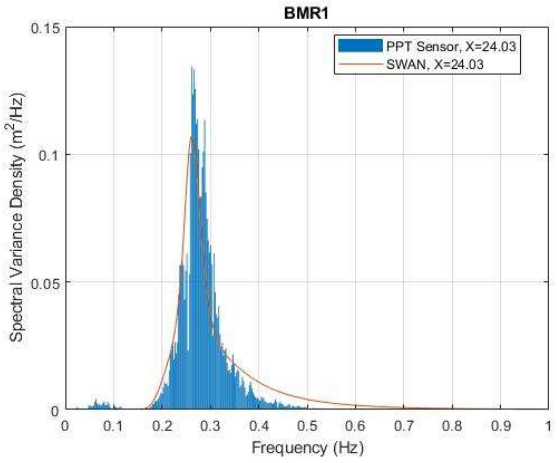

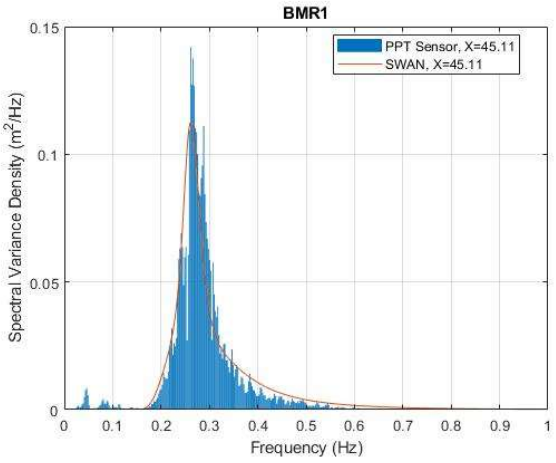

BMR2:

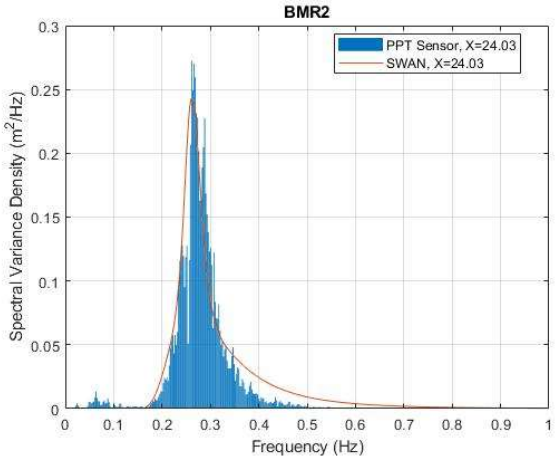
BMR2
PPT Sensor, X=24.03
SWAN, X=24.03
Spectral Variance Density (m²/Hz)
Frequency (Hz)

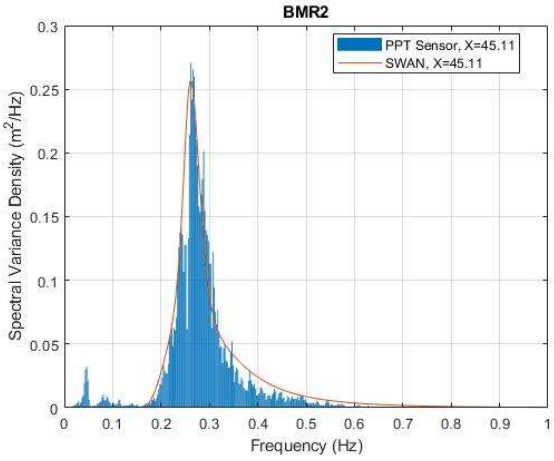
BMR2
PPT Sensor, X=45.11
SWAN, X=45.11
Spectral Variance Density (m²/Hz)
Frequency (Hz)

R1:

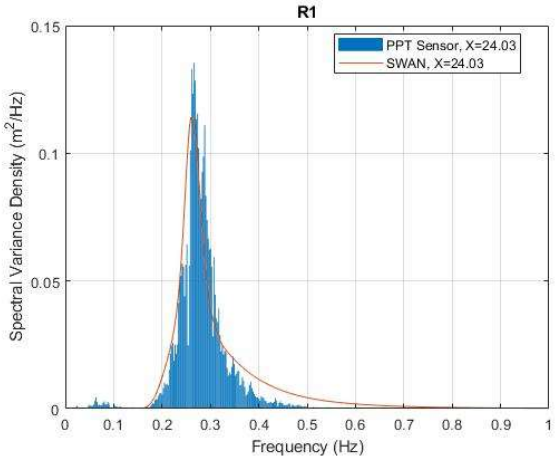
R1
PPT Sensor, X=24.03
SWAN, X=24.03
Spectral Variance Density (m²/Hz)
Frequency (Hz)

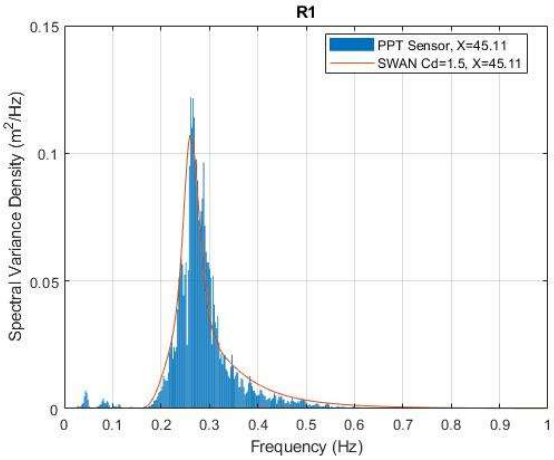
R1
PPT Sensor, X=45.11
SWAN Cd=1.5, X=45.11
Spectral Variance Density (m²/Hz)
Frequency (Hz)

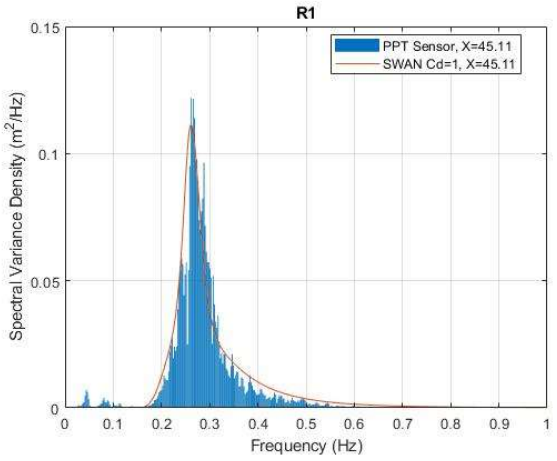
R1
PPT Sensor, X=45.11
SWAN Cd=1, X=45.11
Spectral Variance Density (m²/Hz)
Frequency (Hz)

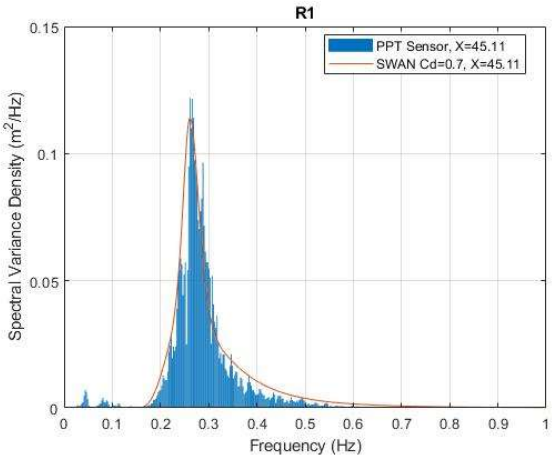
R1
PPT Sensor, X=45.11
SWAN Cd=0.7, X=45.11
Spectral Variance Density (m²/Hz)
Frequency (Hz)

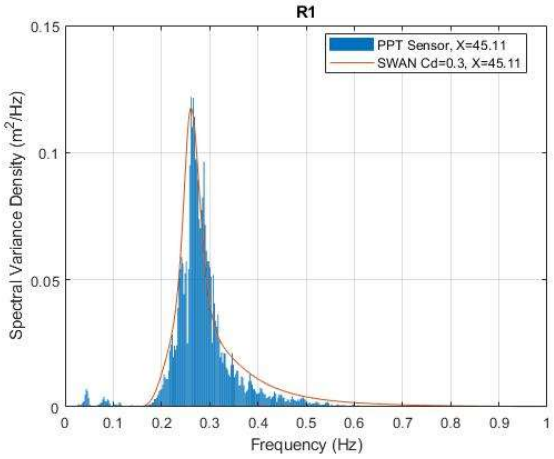
R1
PPT Sensor, X=45.11
SWAN Cd=0.3, X=45.11
Spectral Variance Density (m²/Hz)
Frequency (Hz)

R2:

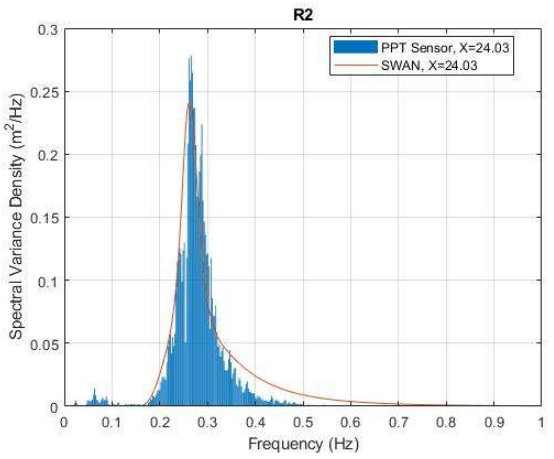
R2
PPT Sensor, X=24.03
SWAN, X=24.03
Spectral Variance Density (m²/Hz)
Frequency (Hz)

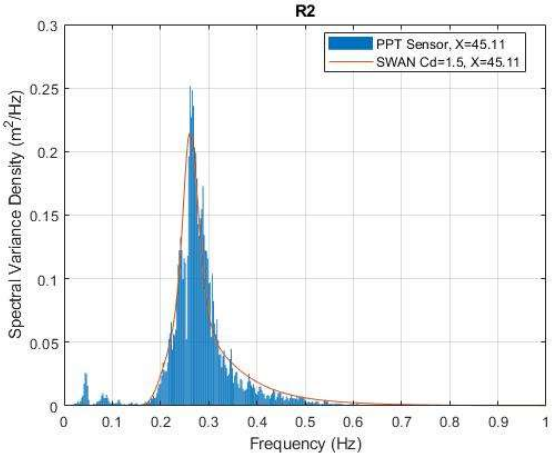
R2
PPT Sensor, X=45.11
SWAN Cd=1.5, X=45.11
Spectral Variance Density (m²/Hz)
Frequency (Hz)

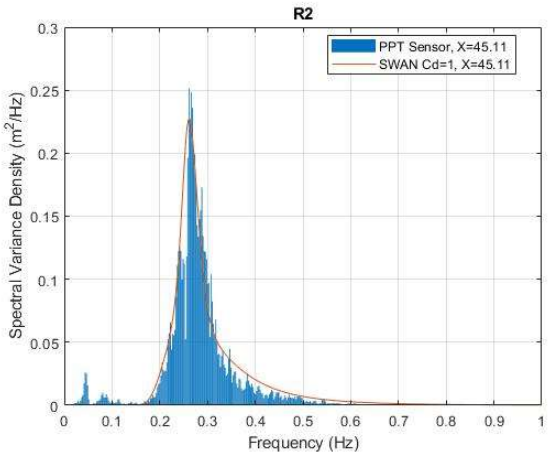
R2
PPT Sensor, X=45.11
SWAN Cd=1, X=45.11
Spectral Variance Density (m²/Hz)
Frequency (Hz)

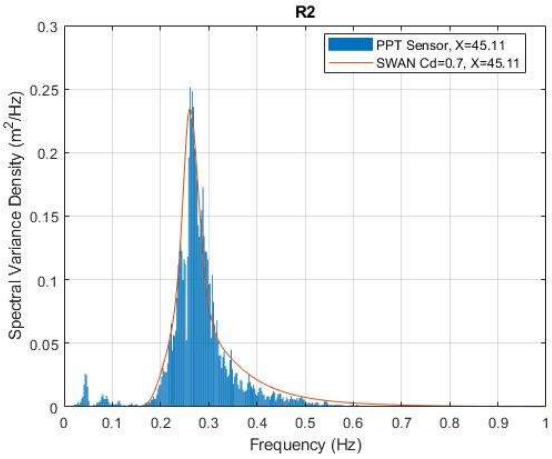
R2
PPT Sensor, X=45.11
SWAN Cd=0.7, X=45.11
Spectral Variance Density (m²/Hz)
Frequency (Hz)

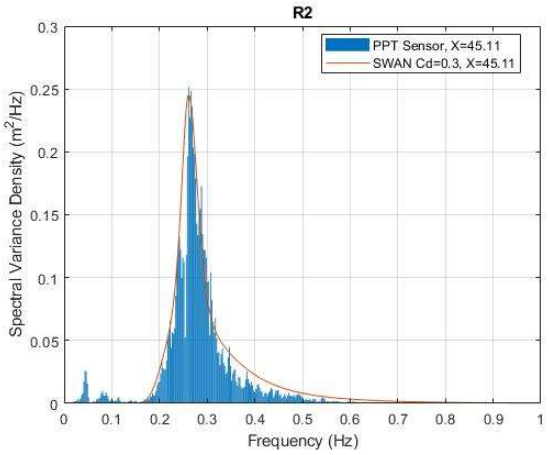
R2
PPT Sensor, X=45.11
SWAN Cd=0.3, X=45.11
Spectral Variance Density (m²/Hz)
Frequency (Hz)

Results of varying C_d for h=0.6m and d=0.004m (left) and h=0.3m and d=0.008m (right)

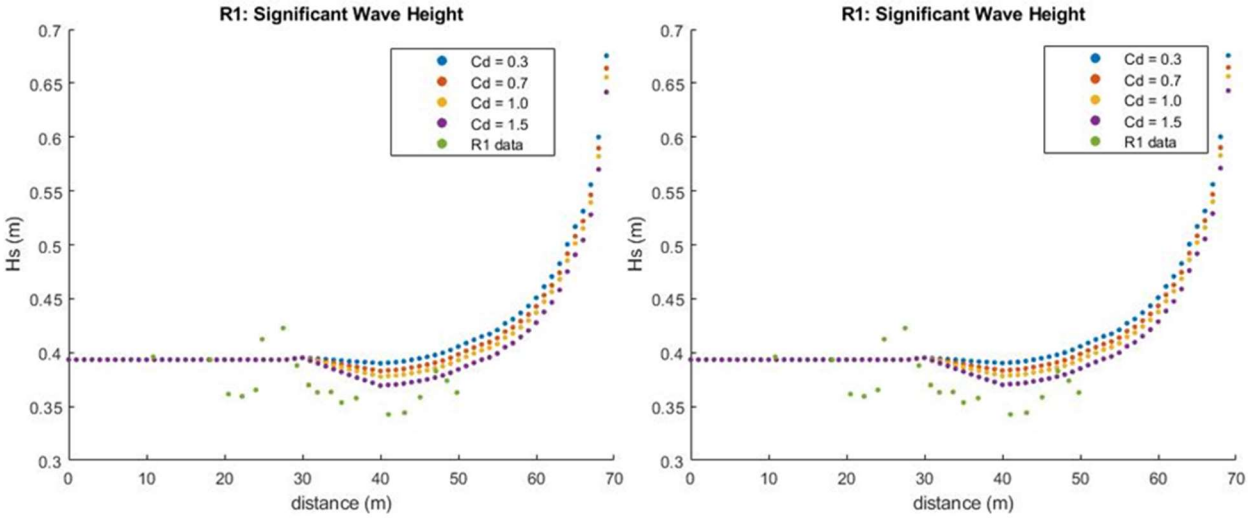

Plots comparing plant height variation on Hs results with different C_d values

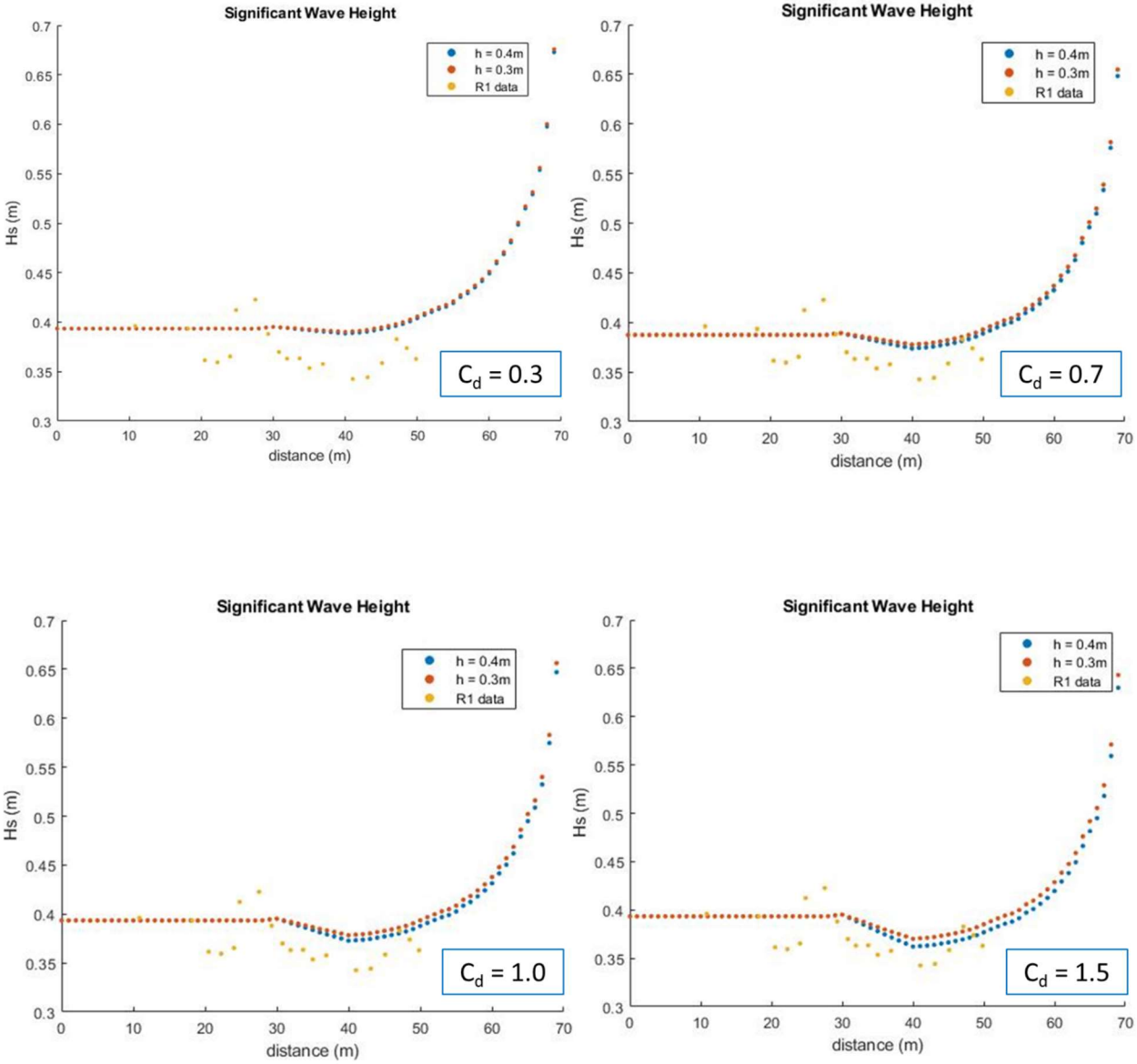

Figures to clarify averaged measured results (green dots) before and after meadow

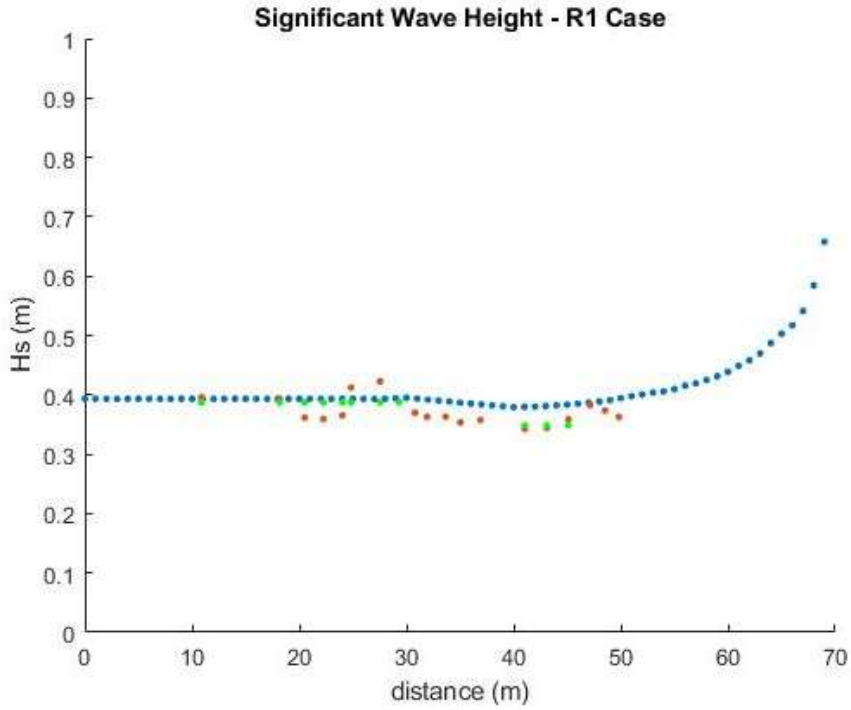

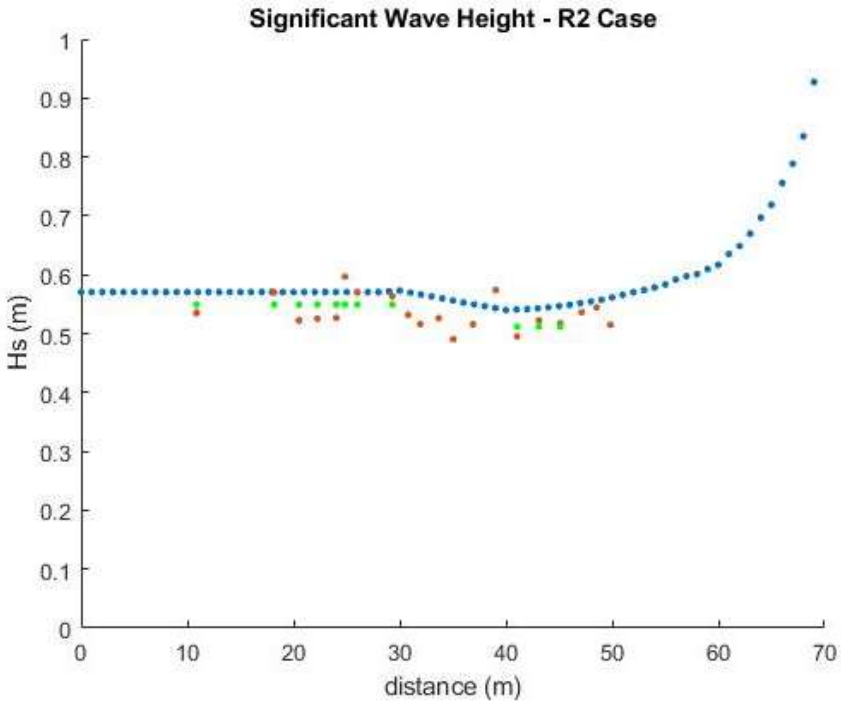

F MATLAB code

Script for analyzing Tarragona wave buoy data

```
%script for reading in direcitonal data and calculating Hmorf
clc
clearvars -except Tarragona

%read data
load('Tarragona.mat');
direction = Tarragona(:,8);

%grouping into bins between 70 and 120 degrees in 15 degree increments
S1 = Tarragona(direction > 70 & direction <= 85, :);    % Sector 1
S2 = Tarragona(direction > 85 & direction <= 100, :);   % Sector 2...etc
S3 = Tarragona(direction > 100 & direction <= 115, :);
S4 = Tarragona(direction > 115 & direction <= 130, :);
S5 = Tarragona(direction > 130 & direction <= 145, :);
S6 = Tarragona(direction > 145 & direction <= 160, :);
S7 = Tarragona(direction > 160 & direction <= 175, :);
S8 = Tarragona(direction > 175 & direction < 190, :);

%H morf
[H_S1] = H_morf(S1);
[H_S2] = H_morf(S2);
[H_S3] = H_morf(S3);
[H_S4] = H_morf(S4);
[H_S5] = H_morf(S5);
[H_S6] = H_morf(S6);
[H_S7] = H_morf(S7);
[H_S8] = H_morf(S8);
```

Function for calculating H_{morf} values for each directional sector

```
function [H_morf_A] = H_morf(A)

dTm = 2;            %increment of peak period in s
dHmo = 0.5;         %increment of Hmo in m

M = max(A);
Max_Hmo = M(5);
Max_Tm = M(6);      %use Tm instead of Tp

n = ceil(Max_Hmo / dHmo);
m = ceil(Max_Tm / dTm);


%Contingency Table
A_X = zeros(n,m);
for i = 1:length(A)
   if A(i,5) > 0 && A(i,6) > 0
   A_X(ceil(A(i,5) / dHmo) , ceil(A(i,6) / dTm)) = A_X(ceil(A(i,5) / dHmo) , ceil(A(i,↙
6) / dTm)) + 1;
   end
end

%H morphology

for j = 1:m
    sum1 = 0;
    sum2 = 0;
    for i = 1:n
    sum1 = A_X(i,j)*(i*dHmo)^2 + sum1;
    sum2 = A_X(i,j) + sum2;
    end
    H_morf_A(1,j) = sqrt(sum1 / sum2);
    H_morf_A(isnan(H_morf_A)) = 0;
end


end
```

Script for summing dissipation rate of all wave conditions over a year

```
clc

%Initialize Data File Size
valRows = 487;
valCols = 362;
%Initialize File Name Characters
Alphabet = 'abcdefgh';
%Initialize Number of Tests in Each Character Test
numTestA = 5;
numTestElse = 4;
%Select which variable to plot, this can be changed to be user input
varName = 'Dissip';
%Initialize Multi Dimensional Matrix for Data
plotDataA = zeros(valRows,valCols,1,numTestA);
plotDataElse = zeros(valRows,valCols,length(Alphabet)-1,numTestElse);
plotDataASum = zeros(valRows,valCols);
plotDataElseSum = zeros(valRows,valCols,length(Alphabet)-1);

DepthA = zeros(valRows,valCols,1,numTestA);
DepthElse = zeros(valRows,valCols,length(Alphabet)-1,numTestElse);

XpA = zeros(valRows,valCols,1,numTestA);
XpElse = zeros(valRows,valCols,length(Alphabet)-1,numTestElse);

YpA = zeros(valRows,valCols,1,numTestA);
YpElse = zeros(valRows,valCols,length(Alphabet)-1,numTestElse);

%Loop through data files and assign values to Data Matrices by accessing data stored↙
in structure array. Value to be called is a string variable called varName.
%Variable called output is temporary
for letter = 1:length(Alphabet)
    if letter == 1
        for index = 1:numTestA
            output = load(sprintf('dom3%s%d.mat',Alphabet(letter),index));
            plotDataA(:,:,letter,index) = double(output.(varName));
            plotDataA(isnan(plotDataA))=0;
            [plotDataASum] = plotDataA(:,:,letter,index)+plotDataASum;
            XpA(:,:,letter,index) = double(output.Xp);
            YpA(:,:,letter,index) = double(output.Yp);
            DepthA(:,:,letter,index) = double(output.Depth);
        end
    else
        for index = 1:numTestElse
            output = load(sprintf('dom3%s%d.mat',Alphabet(letter),index));
            plotDataElse(:,:,letter-1,index) = double(output.(varName));
            plotDataElse(isnan(plotDataElse))=0;
            [plotDataElseSum(:,:,letter-1)]=plotDataElse(:,:,letter-1,index)↙
+plotDataElseSum(:,:,letter-1);
            XpElse(:,:,letter-1,index) = double(output.Xp);
            YpElse(:,:,letter-1,index) = double(output.Yp);
            DepthElse(:,:,letter-1,index) = double(output.Depth);
        end
    end
end

%Sum all variable values
```

```
 55 %Multiply Sum by Frequency Read in by Load Function not Hard Coded
 56 freqData = load('freq.mat');
 57 freq = double(freqData.freq);
 58 plotDataASum = plotDataASum * freq(1,1);
 59 plotDataBSum = plotDataElseSum(:,:,1)*freq(1,2);
 60 plotDataCSum = plotDataElseSum(:,:,2)*freq(1,3);
 61 plotDataDSum = plotDataElseSum(:,:,3)*freq(1,4);
 62 plotDataESum = plotDataElseSum(:,:,4)*freq(1,5);
 63 plotDataFSum = plotDataElseSum(:,:,5)*freq(1,6);
 64 plotDataGSum = plotDataElseSum(:,:,6)*freq(1,7);
 65 plotDataHSum = plotDataElseSum(:,:,7)*freq(1,8);
 66 plotDataSum =  plotDataASum + plotDataBSum + plotDataCSum + plotDataDSum +↙
plotDataESum + plotDataFSum + plotDataGSum + plotDataHSum;
 67
 68 %Depth, X, and Y only require values from one file as they are constants.
 69 %Depth values need to be inverted for proper plotting.
 70 DepthA(isnan(DepthA))=0;
 71 [Depth] = DepthA(:,:,1,1);
 72 Depth=-Depth;
 73 XpA(isnan(XpA))=0;
 74 [XpASum] = XpA(:,:,1,1);
 75 YpA(isnan(YpA))=0;
 76 [YpASum] = YpA(:,:,1,1);
 77
 78 figure
 79 field=pcolor(XpASum,YpASum,plotDataSum);shading interp;colorbar;
 80 %Caxis ranges vary too much to dynamically range
 81 %minC = min(plotDataSum(:));
 82 %maxC = max(plotDataSum(:));
 83 caxis([0 100]);
 84 hold on;
 85 [cs,h]=contour(XpASum,YpASum,Depth,[-200:20:0],'k','linewidth',2,'linestyle','--');
 86 clabel(cs,h,'LabelSpacing',72,'fontsize',10);
 87
 88 %labels and minor details
 89 xlabel('X');
 90 ylabel('Y');
 91 grid on
 92 axis equal
 93 axis square
 94 title(['Dom3']);
 95 hold off;
 96 drawnow;
 97
 98 %Format timestamp in ISO8601
 99 formatIso = 'yyyymmddTHHMMSS';
100 time = datestr(now,formatIso);
101 fname=strcat(sprintf('Dom3_%s.png',time));
102 print('-dpng',fname);
103 savefig(sprintf('Dom3_%s',time));
```

G Contingency tables of significant wave height and mean wave period

Sector 1 (70° - 85°)		Tm02 (s)					
		0 - 2	2 - 4	4 - 6	6 - 8	8 - 10	10 - 12
Hm0 (m)	0.0 - 0.5	2	1116	140	0	0	
	0.5 - 1.0	0	2396	1188	13	0	
	1.0 - 1.5	0	642	1376	64	0	
	1.5 - 2.0	0	32	1143	103	0	
	2.0 - 2.5	0	0	505	102	2	
	2.5 - 3.0	0	0	183	94	5	
	3.0 - 3.5	0	0	54	39	1	
	3.5 - 4.0	0	0	14	28	0	
	4.0 - 4.5	0	0	0	25	0	
	4.5 - 5.0	0	0	0	7	0	
	5.0 - 5.5	0	0	0	10	0	
	5.5 - 6.0	0	0	0	5	0	
	6.0 - 6.5	0	0	0	5	0	
	6.5 - 7.0						
	7.0 - 7.5						
	7.5 - 8.0						
Hmorf		0.50	1.01	1.78	2.97	2.95	

Sector 2 (85° - 100°)		Tm02 (s)					
		0 - 2	2 - 4	4 - 6	6 - 8	8 - 10	10 - 12
Hm0 (m)	0.0 - 0.5	3	2128	344	0		
	0.5 - 1.0	0	2759	1791	13		
	1.0 - 1.5	0	615	1009	45		
	1.5 - 2.0	0	19	502	39		
	2.0 - 2.5	0	0	104	19		
	2.5 - 3.0	0	0	61	14		
	3.0 - 3.5	0	0	8	2		
	3.5 - 4.0	0	0	3	0		
	4.0 - 4.5	0	0	0	1		
	4.5 - 5.0						
	5.0 - 5.5						
	5.5 - 6.0						
	6.0 - 6.5						
	6.5 - 7.0						
	7.0 - 7.5						
	7.5 - 8.0						
Hmorf		0.50	0.93	1.40	2.05		

Sector 3 (100° - 115°)		Tm02 (s)					
		0 - 2	2 - 4	4 - 6	6 - 8	8 - 10	10 - 12
Hm0 (m)	0.0 - 0.5	3	3155	469	0		
	0.5 - 1.0	0	2339	1244	1		
	1.0 - 1.5	0	234	502	11		
	1.5 - 2.0	0	2	139	27		
	2.0 - 2.5	0	0	31	7		
	2.5 - 3.0	0	0	18	6		
	3.0 - 3.5	0	0	1	0		
	3.5 - 4.0						
	4.0 - 4.5						
	4.5 - 5.0						
	5.0 - 5.5						
	5.5 - 6.0						
	6.0 - 6.5						
	6.5 - 7.0						
	7.0 - 7.5						
	7.5 - 8.0						
Hmorf		0.50	0.80	1.19	2.11		

Sector 4 (115° - 130°)		Tm02 (s)					
		0 - 2	2 - 4	4 - 6	6 - 8	8 - 10	10 - 12
Hm0 (m)	0.0 - 0.5	1	3294	367	0		
	0.5 - 1.0	0	1498	616	0		
	1.0 - 1.5	0	93	216	2		
	1.5 - 2.0	0	1	56	11		
	2.0 - 2.5	0	0	14	5		
	2.5 - 3.0	0	0	6	0		
	3.0 - 3.5						
	3.5 - 4.0						
	4.0 - 4.5						
	4.5 - 5.0						
	5.0 - 5.5						
	5.5 - 6.0						
	6.0 - 6.5						
	6.5 - 7.0						
	7.0 - 7.5						
	7.5 - 8.0						
Hmorf		0.50	0.72	1.11	2.10		

Sector 5 (130° - 145°)		Tm02 (s)					
		0 - 2	2 - 4	4 - 6	6 - 8	8 - 10	10 - 12
Hm0 (m)	0.0 - 0.5	3	3216	203	0		
	0.5 - 1.0	0	1188	351	1		
	1.0 - 1.5	0	43	136	0		
	1.5 - 2.0	0	1	53	4		
	2.0 - 2.5	0	0	16	2		
	2.5 - 3.0	0	0	5	0		
	3.0 - 3.5						
	3.5 - 4.0						
	4.0 - 4.5						
	4.5 - 5.0						
	5.0 - 5.5						
	5.5 - 6.0						
	6.0 - 6.5						
	6.5 - 7.0						
	7.0 - 7.5						
	7.5 - 8.0						
Hmorf		0.50	0.69	1.18	2.05		

Sector 6 (145° - 160°)		Tm02 (s)					
		0 - 2	2 - 4	4 - 6	6 - 8	8 - 10	10 - 12
Hm0 (m)	0.0 - 0.5	2	3507	135	0		
	0.5 - 1.0	0	1257	369	0		
	1.0 - 1.5	0	36	145	0		
	1.5 - 2.0	0	3	48	1		
	2.0 - 2.5	0	0	7	1		
	2.5 - 3.0	0	0	3	0		
	3.0 - 3.5	0	0	2	0		
	3.5 - 4.0						
	4.0 - 4.5						
	4.5 - 5.0						
	5.0 - 5.5						
	5.5 - 6.0						
	6.0 - 6.5						
	6.5 - 7.0						
	7.0 - 7.5						
	7.5 - 8.0						
Hmorf		0.50	0.68	1.20	2.26		

Sector 7 (160° - 175°)		Tm02 (s)					
		0 - 2	2 - 4	4 - 6	6 - 8	8 - 10	10 - 12
Hm0 (m)	0.0 - 0.5	3	4723	160	0		
	0.5 - 1.0	0	2057	495	0		
	1.0 - 1.5	0	65	192	0		
	1.5 - 2.0	0	0	98	1		
	2.0 - 2.5	0	0	18	2		
	2.5 - 3.0	0	0	5	0		
	3.0 - 3.5	0	0	3	0		
	3.5 - 4.0						
	4.0 - 4.5						
	4.5 - 5.0						
	5.0 - 5.5						
	5.5 - 6.0						
	6.0 - 6.5						
	6.5 - 7.0						
	7.0 - 7.5						
	7.5 - 8.0						
Hmorf		0.50	0.70	1.26	2.35		

Sector 8 (175° - 190°)		Tm02 (s)					
		0 - 2	2 - 4	4 - 6	6 - 8	8 - 10	10 - 12
Hm0 (m)	0.0 - 0.5	4	4485	70	0		
	0.5 - 1.0	0	2762	961	0		
	1.0 - 1.5	0	107	464	0		
	1.5 - 2.0	0	0	155	0		
	2.0 - 2.5	0	0	64	1		
	2.5 - 3.0	0	0	11	0		
	3.0 - 3.5	0	0	3	0		
	3.5 - 4.0	0	0	0	1		
	4.0 - 4.5						
	4.5 - 5.0						
	5.0 - 5.5						
	5.5 - 6.0						
	6.0 - 6.5						
	6.5 - 7.0						
	7.0 - 7.5						
	7.5 - 8.0						
Hmorf		0.50	0.75	1.36	3.34		

H Frequency of occurrence table for sectors 1-8

	Sectors 1-8							
Directional Range (°)	70 - 85	85 - 100	100 - 115	115 - 130	130 - 145	145 - 160	160 - 175	175 - 190
Frequency (%)	8.5	8.7	7.5	5.7	4.8	5.1	7.2	8.4